Fabrication and Evaluation of Custom Scaffolds for Craniofacial Surgery and Tissue Engineering

Atra Malayeri

A thesis submitted toward the degree of Doctor of Philosophy

School of Clinical Dentistry

September 2016

Supervisors: Professor Paul Hatton
Dr Frederik Claeyssens
Dr Ilida Ortega Asencio

ABSTRACT

Facial congenital disorders or injuries may compromise the integrity and function of craniofacial tissue and these conditions frequently require correction via facial reconstructive surgery. Numerous techniques have been suggested to overcome challenges involved in reconstructing large defects, however currently the "gold" standard approach is the use of autologous bone grafts. Despite advances made, the main drawbacks of this technique include donor site morbidity and challenges in contouring. The research described herein is aimed at investigating composite polymeric materials fabricated via solid freeform fabrication technologies such as stereolithography in order to prepare a synthetic device or scaffold that is a custom shape for the planned surgery. This approach has the potential to overcome existing drawbacks associated with the repair of appropriate bone defects during maxillofacial reconstructive surgery. One key challenge is the absence of a biomaterial that is ideally suited to the preparation of such custom implants via additive manufacturing. Poly High Internal Phase Emulsions (polyHIPEs) are known to have inherited interconnected porous micro-structures that have the potential to enhance biocompatibility. However, only relatively recently these materials were discovered to have potential as biomaterials, and they have not yet been explored widely as a material to be used with solid free form fabrication technologies. Consequently, these materials may show great promise for bone tissue engineering as the fabricated scaffold comprises of random micro scaled porosity inherited by polyHIPE material as well as the pre-designed macro porosity introduced by stereolithography technology which is essential to contour the exact shape of the defect. Initially, the suitability of stereolithography to fabricate polyHIPE material was investigated using a well-developed acrylate-based non-degradable polyHIPE material. Upon its success, the study was later concentrated on developing biodegradable PCL based polyHIPE materials as a potential biomaterial for craniofacial defects.

ACKNOWLEDGMENTS

Firstly, I would like to acknowledge the generous financial support from my sponsors, the EPSRC who funded the White Rose Doctoral Training College in Tissue Engineering and Regenerative Medicine (EPSRC DTC TERM). This PhD was also associated with MeDe Innovation, the EPSRC Centre for Manufacturing in Medical Devices (EP/K029592/1).

I would like to express my sincere gratitude to my supervisors Professor Paul Hatton, Dr Frederik Claeyssens and Dr Ilida Ortega Asencio for their immense knowledge, guidance and encouragement. In addition, I am grateful to Dr Keith Smith and his clinical team, especially Dr Abdurahman for the opportunity to visit the operating theatre for orthognathic surgery observation and their time for discussion on the subject. With respect to this, I also thank Dr Nastaran Barkhi for providing an example of an orthopantomogram. Professor Neil Cameron and his team, especially Caitlin Langford, are gratefully acknowledged for the training during my placement at Durham University, essential for the key discoveries of polyHIPEs as biomaterials for additive manufacturing.

Many thanks to all my colleagues and friends at the Kroto institute for their immense support including Dr Colin Sherborne for teaching me the art of stereolithography and fabricating many scaffolds for me, also Mr Thomas Paterson for his support and assistance in confocal microscopy. I would like to thank Dr Caroline Wilcock for teaching me the synthesis of hydroxyapatite. Finally, I would like to acknowledge Caroline Gabbot who worked on related studies as a part of her undergraduate dissertation. Where her data has been used to illustrate a point, this is made clear in the accompanying text and figure legends.

A very special thank you goes to my parent-in-laws for their never-ending support and motivation. To my parents and my brother for the unwavering support, encouragement and love during every step of my life without them I would not have been where I am today. Finally, a massive thank you to my darling husband, Danyal for his endless love, understanding and support throughout my PhD.

This thesis is dedicated to Paridokht and Ahmad, my grandparents.

TABLE OF CONTENTS

Publications Arising From This PhD

Published Articles:

Malayeri, A., Sherborne, C., Paterson, T., Mittar, S., Asencio, I., Hatton, P., Claeyssens, F., 2016., Osteosarcoma growth on trabecular bone mimicking structures manufactured via laser direct write. *International Journal of Bioprinting,* vol.2 (2):67-77. http://dx.doi.org/10.18063/IJB.2016.02.005

Manuscripts in Preparation:

Malayeri, A., Langford, C., Paterson, T., Mittar, S., Asencio, I., Hatton, P., Cameron, N., Claeyssens, F. Developing biodegradable and biocompatible PCL based PolyHIPEs. *In preparation for submission to Biofabrication*

Poster Presentations:

Malayeri, A., Gabbott, C., Reilly, G., Ghassemieh, E., Hatton, PV., Claeyssens, F. **Feasibility of 3D printing and stereolithography for fabrication of custom-shaped poly (lactic acid)**, Journal of Tissue Engineering and Regenerative Medicine 2012, volume 6, supplement 1, 1-429, Vienna.

Malayeri, A., Claeyssens, F., Gabbott, C., Reilly, G., Hatton, PV. **Preparation of Poly(Lactic acid) – Hydroxyapatite Scaffolds for Bone Surgery** Manufacturing the Future Conference, Cranfield.

Malayeri, A., Claeyssens, F., Hatton, PV. **Fabrication and Evaluation of Complex or Custom Scaffolds For Skeletal Tissue Engineering**, Industry day 2013, Leeds

Malayeri, A., Claeyssens, F., Hatton, PV. **Fabrication and Evaluation of Complex or Custom Scaffolds For Skeletal Tissue Engineering**, Doctoral Centre in Tissue Engineering and Regenerative Medicine joint conference 2013, Sheffield.

Malayeri, A., Hatton, PV., Ortega, I., Claeyssens, F. ***In Vitro* Biocompatibility of a Poly(High Internal Phase Emulsion) Biomaterial**, Journal of Tissue Engineering and Regenerative Medicine, 2014, volume 8, supplement 1, 267-2518, Genoa.

Malayeri, A., Ortega, I., Claeyssens, F., Sherborne, C., Cameron, N., Hatton, PV. **Biocompatibility of Poly High Internal Phase Emulsion Scaffolds prepared using Stereolithography**, European Conference on Biomaterials 2014, Liverpool.

LIST OF ABBREVIATIONS

BA	Butyl Acrylate
CAD	Computer-aided Design
DAPI	4',6-diamidino-2-phenylindole
DIC	Differential Interface Contrast
DMD	Digital Micromirror Device
DMEM	Dulbecco's Modified Eagle Medium
DMSO	Dimethyl Sulfoxide
DPEHA	Dipentaerythritol Penta-/hexa-acrylate
EHA	2-Ethylhexyl Acrylate
EHMA	Methacrylate
ESC	Embryonic Stem Cell
EtOH	Ethanol
F	Amphotericin B
FCS	Fetal Calf Serum
FDM	Fused Deposition Modeling
FTIR	Fourier Transform Infrared Spectroscopy
GPC	Gel Permeation Chromatography
HA	Hydroxyapatite
hES-MPs	Human Embryonic Stem-cell Derived Mesenchymal Progenitor
HIPE	High Internal Phase Emulsion
HMDS	Hexamethyldisilazane
IBOA	Isobornyl Acrylate

LG	L-Glutamine
MAPTMS	Methacryloxypropyltrimethoxysilane
MFD	Melting Fused Deposition
MG63	Human Osteosarcome Cell Line
mL	Mililitre
mm	Millimetre
MSC	Mesenchymal Stem Cells
MSTL	Microstereolithography
MTT	3-(4,5)-dimethylthiahiazo (-z-y1)-3,5-di-phenytetrazoliumromide)
NC	Non-Coated
nHA	Nano Hydroxyapatite
nm	Nanometre
NSTL	Nanostereolithography
P/S	Penicillin / Streptomycin
PBS	Phosphate Buffered Saline
PCBM	Particulate Cancellous Bone and Marrow]
PCL	Poly (ϵ-caprolactone)
PCLMA	Methacrylated Poly (ε-caprolactone)
PED	Precision Extrusion Deposition
PEG	Polyethylene Glycol
PGA	Polyglycolic Acid
FITC-phalloidin	Phalloidin-fluorescein Isothiocyanate Labeled
TRITC-phalloidin	Phalloidin-Tetramethylrhodamine B Isothiocyanate
PLGA	Poly (lactic-co-glycolic) Acid
PLA	Polylactic Acid

PLLA	Poly-L-lactide
PRP	Platelet Rich Plasma
PTFE	Polytetrafluoroethylene
s	Seconds
SEM	Scanning Electron Microscopy
SFF	Solid Freeform Fabrication
SL	Stereolithography
SLM	Selective Laser Melting
SLS	Selective Laser Sintering
TCP	Tissue Culture Plastic
TE	Tissue Engineering
TEM	Transmission Electron Microscopy
Ti	Titanium
TMPTA	Trimethylolpropane Triacrylate
TMPTMA	Trimethylolpropane Trimethacrylate
Trithiol	Trimethylolpropane Tris(3-mercaptopropionate)
UV	Ultraviolet
LG	L-Glutamine
W/O	Water-in-Oil
XRD	X-ray Diffraction
µL	Micrometre

LIST OF FIGURES

LIST OF TABLES

1 INTRODUCTION

Healthy craniofacial bone and connective tissues contribute significantly to many aspects of human health including nutrition, communication, respiration, vision and aesthetics. The shape and anatomical structure of bones in the head, neck and face invariably plays a crucial role in supporting important functions. Therefore, it is not surprising that damage to these tissues is frequently associated with loss of functionality and pain, often with other problems including disfigurement and a loss of life quality.

Bone injuries in cranio-maxillofacial region may arise due to congenital disorders, injuries, tumor excisions as well as advanced resorption of alveolar bone tissue after tooth loss. The restoration of such large bone defects still plays a main challenge for maxillofacial surgeons. Traditionally, major bone losses have been treated with autografts, allografts or artificial bone substitutes. Nevertheless, these procedures have their own limitations including a limited supply of bone autografts and the associated risk of morbidity with the second surgical site. Allografts and xenografts do not generally perform as well, and has additional risks of immune response and disease transmission. Artificial biomaterials are therefore employed widely and often successfully. However existing biomaterials suffer from an inconsistent tissue response particularly in the ageing population or compromised patients.

Clinical success is generally achieved despite the limitations associated with current materials and arguably because of high surgical skill, complex procedures, and lengthy operations. None of existing interventions or technologies is designed specifically for the repair of a complex, custom defect as frequently encountered in craniofacial surgery. There is therefore arguably more than in any other region of the body, a significant opportunity to apply modern additive manufacturing methods to develop new therapeutic strategies to treat these complex defects associated with reconstructive surgery of facial bone.

With respect to the preparation of custom devices, some successes have been reported using metallic prostheses fabricated using advanced manufacturing technologies such as selective laser melting (SLM). The devices are often designed using radiographic data from the patient and these *in silico* models have also been employed in surgical planning. While this pioneering work has shown the potential for advanced manufacturing in craniofacial and other musculoskeletal fields, it is noteworthy that commonly used metallic materials do not assist bone regeneration at the surgical site and in many situations it may not be desirable to implant a permanent implant with associated risks of infection or rejection. More widely, while a range of advanced manufacturing technologies are now available to produce custom shapes, the biomaterials associated with these systems are relatively crude and not always suited to human implantation. Even potentially biocompatible materials such as starch are "bioinert" and contribute nothing to the regeneration of a bone tissue defect.

To summarise, advanced manufacturing and associated technologies related to the acquisition and processing of 3D musculoskeletal data are evolving rapidly, and progress has been made in preparation of metallic devices for facial reconstructive surgery. There is more recent work suggesting that a wider range of biomaterials may be processed to shape, and knowledge of so-called "bioactive" alloplastic materials is also increasing. The aim of this research was therefore to investigate promising biomaterials systems that could be processed to form complex or complex shapes, and determine how these could be modified to enhance their osteoconductive properties. On completion, this research will have opened up new opportunities to make significant advances in craniofacial surgery.

2 LITERATURE REVIEW

2.1 Basic Bone Biology and Function

Bone is a fundamental tissue within the human body and the assembly of chemical, mechanical and hematological functions of bone makes this tissue a highly complex form of connective tissue which experiences subtle and continues remodeling to correspond to its function [1]. It provides structural support and protection for internal organs as well as being the main reservoir for minerals and growth factors. Furthermore, it supports muscular contraction that results in motion. Overall, the diversity of its function imitates in its architecture, which is highly complex vascularised tissue that requires constant supply of nutrients and oxygen.

Hutmacher *et al*. described bone tissue as a composite construct in many aspects such as porosity, polymer-ceramic, lamellar and fibre-matrix [1]. Due to this characteristic of bone tissue, the mechanical properties of bone depends highly on the composition and structure [1]. Its composition is made of both organic and inorganic components, the organic component is composed of collagen-containing matrix that embeds mineral salt known as hydroxyapatites [2]. The deposition of calcium hydroxyapatite complex minerals, which is composed of calcium, phosphorus, sodium magnesium, fluoride and others ions is responsible for the hardness of bone tissue that can withstand exceptionally high loads. Overall, the macro- and nano-hierarchical structure of bone provides mechanical support and transmits mechanical and physiological signals [3]. Although the functional characteristic of bone in the skeleton varies in different sites, overall it provides mechanical strength and support.

Adult skeleton is composed of two different bone structures: cortical (or compact) bone and trabecular (or cancellous) bone. Cortical bone is relatively dense and compact, its porosity is less than 5% which can be found in the shafts of long bones, as well as in short and flat bones. The main purpose of cortical bone is to deliver stability and guard the underlying tissue as it has high tensile and ultimate strength.

The cancellous bone has a highly porous spongy-like structure (50-90%) with trabeculae that are aligned accurately alongside lines of stress to maintain the resistance against stress, therefore it has a high compressive strength (see Table 1) [4]. The mineral content of this type of tissue is around 15-25% and the rest is consist of an extremely vascularised network which contains bone marrow.

Table 1: Mechanical properties of bone component including collagen and hydroxyapatite [1].

	Young's Modulus (GPa)	**Ultimate Tensile Strength (MPa)**
Collagen	1-2	50-1000
Hydroxyapatite	130	100

2.1.1 Bone Development

Bone formation occurs through ossification and osteogenesis, which starts during fetal period in pregnancy (week 8 of development) [4]. The whole process involves two distinctive ossifications process, which are intramembranous and endochondral ossification. Intramembranous ossification results in the formation of flat bones, which are commonly present in craniofacial bones such as skull (frontal, parietal and temporal bones), cranium, mandible, clavicles and palate [4]. This type of ossification refers to mesenchymal stem cell differentiation succeeding in capillary ingrowth within a mesenchymal area. The process begins with centrally located mesenchymal cells cluster that differentiate directly into osteoblasts resulting in an ossification centre that lays the foundation of bone matrix. On the other hand, endochondral ossification forms all other bones in body such as long bones. This type of ossification is more complex, it involves forming bone collar which is resulted from osteoblasts secreting bone matrix on cartilage model [4]. Finally after formation of cartilaginous template, the periosteum surrounding the template starts to revascularise and bone matrix is produced [4]. The type of bone development and its relevance to craniofacial bone repair is discussed further in section 2.5.

2.2 Craniofacial Bone

2.2.1 Craniofacial Anatomy

The skull has arguably the most complex bony structure within the body that is comprised of cranial and facial bones and is mainly comprised of four tissues which are: cartilage, bone, mucosa and skin tissue [4]. The cranium encases and protects the brain while the facial bones protect the sense organs such as sight, taste and smell. Overall, the craniofacial bone has a vital role in supporting the surrounding soft tissues as well as offering anchoring for dental structures [5]. The facial bones on the other hand are consist of 14 bones of which the mandible and vomer are unpaired [4]. As it was mentioned previously in section 2.1.1, the cranial bones are formed via intramembranous ossification with mesenchymal cells condense and differentiate into osteoblasts.

The mandible is the lower jaw and it is the strongest bone in the craniofacial region which is made up of the chin and two upright rami that connects the mandible to the posterior region [4]. The mandible foramen is responsible for lower jaw dental nerves to pass through, on the other hand the mental foramina is responsible for the passage way of the nerves for the chin and lower lip [4]. The alveoli region is responsible for teeth socks, on the other hand the coronoid and condyle processes are responsible for articulation and muscle insertion. After the removal of mandible, the rest of the skull signifies as a lopsided hollow bony sphere.

The maxillary bone consist of the upper jaw and the central portion of the facial skeleton including: hard palate, orbits and nasal cavity walls [4]. All of facial bones including zygomatics, nasals, lacrimals and palatines articulate with maxillae except mandible [4]. Blood vessels and maxillofacial nerves (infraorbital, cranial and zygomatic) are passed through the bone structure via infraorbital foramen, fissure and incisive fossa [4]. The alveolar maxilla region is responsible for anchoring upper teeth

and the quality of bone varies as they move toward posterior, which is discussed further in the following section.

2.2.2 Craniofacial Bone Biology

Bone biology was previously described in detail in section 2.1.1, however in this section the classification for cranial bone is discussed. Overall, the difference in bone quality in upper and lower jaw can be associated with different areas of anatomy in maxilla and mandible. Overall the mandible is more densely corticated than maxilla. However, both lower and upper jaws tend to have a decrease in their cortical thickness and increase in trabecular porosity as they move toward posterior. Gamble *et al.* [6] investigated bone density variation in maxillae and mandible by using an original classification first introduced by Lekholm & Zarb [7]. The study concluded that: Anterior mandible is quality 1, posterior mandible / anterior maxilla is quality 2 and 3 while posterior maxilla is quality 4 and tuberosity region is quality 4*. The description of each classification is explained in the following table (Table 2).

Table 2: Bone quality categories established by Zerb *et al.* [7].

Quality 1	Approximately the whole jaw is encompassed of uniform compact bone
Quality 2	A thick layer of cortical bone surroundings a dense trabecular bone centre
Quality 3	A thin layer of compact bone surrounding a dense trabecular bone centre
Quality 4	A thin layer of compact bone surrounding low density trabecular bone centre
Quality 4*	Failure region where the implant would fail due to surface contact with bone marrow

Despite the extraordinary strength and mechanical properties of bone including craniofacial bone, this tissue is still prone to trauma. Craniofacial defects can be as result of trauma or congenital disorders, which will be discussed in more detail in the following section 2.3.

2.3 Craniofacial Clinical Challenges and Surgical Approaches

Bone is a very unique tissue due to its ability to repair via the development of new bone rather than forming a connective tissue scar. However, in some cases the tissue is unable to heal completely and is in need of some surgical intervention for example in case of critical sized bone defects. A critical size bone defect in orthopedic field is referred to a defect that would not heal naturally during the life time hence requires an intervention [8]. However, in some cases the bone defect does not heal due to the pathological process and would cause a non-union defect. Overall, these types of cranio-maxillofacial bone defects / injuries may be caused by congenital disorders, traumas, osteotomy, infection and oncologic excisions as well as advanced resorption of alveolar bone tissue after teeth loss [9]. These conditions can compromise the function and architecture of craniofacial bone, which means that both of these must be restored during the reconstructive. Overall, the success of the grafts depends highly on its survival after transplantation, which requires blood supply or soft tissue envelope[10]. Currently the conventional therapeutic strategies for critical-sized craniofacial bone defects within these conditions involve employing various types of bone grafts such as re-vascularised autografts, allografts or xenografts however the modalities depend highly on the type of the disease causing the defect as well as the defect's morphology and characters [10]. Even though that the ultimate surgical strategies for craniofacial reconstruction is yet not definite, the ideal strategy must deliver the utmost anticipated method to renovate function and form with preferably no second site of morbidity. The drawbacks of current technique are explained further in the following paragraphs.

Autografts are known to be the 'gold standard' benchmark treatment for critical-sized bone defect. This type of graft is harvested from the same individual during the surgical procedure and it is desired to have the graft originate from a distant area to the site of surgery such as fibula, iliac crest or rib bone [11]. The main advantages of autogenous bone grafts are its osteoconductive and osteoinductive properties that result in a more conventional bone healing. These grafts contain living cells,

osteoconductive and resorbable properties together with several human growth factors that ultimately offer the current "gold standard" bone substitute material. However, employing autogenous bone grafts are associated with disadvantages such as donor site morbidity, the risk of wound infection, limited availability, necrosis and resorption which is limited by harvesting difficulty and the surgeon's ability to contour a subtle 3D shape [12–14].

Allografts are known to overcome the major drawback associated with autografts, which are its limited availability and its second site of morbidity. These grafts are both osteoconductive and osteoinductive, however they lack osteogenic properties due to the lack of viable cells. Nevertheless, there is high risk of cross-contamination disease such as HIV and hepatitis as well as the possibility of immune rejection. In order to minimise the risks, allografts are usually sterilised and processed prior to the implantation, which includes freeze-drying, demineralisation and irradiation that ultimately may affect the osteoconductivity and mechanical properties of the graft. Bone tissue allografts are mainly sourced from a cadaveric bone or hip replacement surgical procedures. The current allogeneic bone grafts are available in many shapes, sizes and forms such as cancellous chips, demineralised bone matrix and cortical grafts [15]. Maxgraft® (Botissdental GmbH, Germany) is a commercialised allogeneic bone substitute in forms of either granules or blocks which is harvested from femoral head in living donors. The graft is tested extensively for any transmitted diseases prior to multi-step chemical cleaning process and finally gamma-sterilisation [16]. Alternative commercialised (cadaver sourced) allografts are such as Puros® and Tutoplast® (Zimmer Dental Inc, Germany) [17]. In general, the craniofacial bone defects treated with allografts suffer from a high rate of non-union healing with the neighboring tissues as well as high risk of infection.

Xenografts are another type of tissue grafts that may be employed during the treatment of critical-sized bone defects. These types of grafts are obtained from dissimilar species, which consequently have high risks of immune response that can be reduced via de-proteinisation treatment. However, this vital pre-treatment step will eventually destroy the osteoconductive protein thus affecting the quality of the

transplanted graft. One of the major xenogeneic commercialised products is BioOss® (Geistlich, Switzerland) which is consist of inorganic components of bovine bone that is achieved by undergoing process of removing organic phase through stepwise annealing process, followed by chemical treatment that ultimately results in a porous hydroxyapatite bone material [15,18]. Other bovine-based commercialised bone grafts are OsteoGraf® (Dentsply Friadent, Germany) and Cerabone® (Botissdental GmbH, Germany).

Bone healing requires constant supply of oxygen and nutrients, thus not all bone defects can be repaired via natural bone self-repair pathways. In adults, only minor defects are capable of self-healing, on the other hand critical-sized bone defects resulted from trauma, osteotomy, infection, or congenital disorders are incapable of achieving successful natural bone healing. Currently, autogenous bone grafts are using widely in restoration of maxillofacial skeleton. Despite the successful clinical outcomes, this graft has its own limitation that is mainly its limited availability, and the requirements for the additional surgery to harvest the graft, which may be associated with further patient's complications such as infection, pain and hematoma. As the result of all limitations associated with different bone grafts, there has been an increasing demand for development of alternative bone substitutes. The ideal graft must offer osteoconductivity to enhance ingrowth of new blood vessels and recruitment of osteogenic cells as well as osteoinductivity to encourage osteogenesis. As such, there is a high demand for designing and developing biocompatible materials that can be employed as 3D bone substitute to fill and enhance the regeneration process of critical-sized bone defect. Bone tissue engineering is a relatively new concept that aims to address current disadvantages associated with conventional bone therapies. In order to investigate the concept of bone cranio-maxillofacial tissue engineering, orthognathic surgery has been chosen as the model to study different biomaterials and fabrication techniques to evaluate its suitability. Orthognathic surgery will be discussed in more detail in the following section 2.3.1

2.3.1 Model Clinical Challenges in Orthognathic Surgery

Having an ideal facial convexity is desirable, indeed lack or excessive convexity may cause breathing problems and open bite problems, speech difficulties as well as pathological alternation in muscle fibers and masticatory function. In addition, these individuals are commonly suffering from at least one of the following conditions: temporomandibular disorders, protruded mandible, retruded mandible, protruded maxilla or retruded maxilla. Thus a maxillofacial surgical intervention is required to correct congenital and acquired dentofacial discrepancies, which is known as orthognathic surgery.

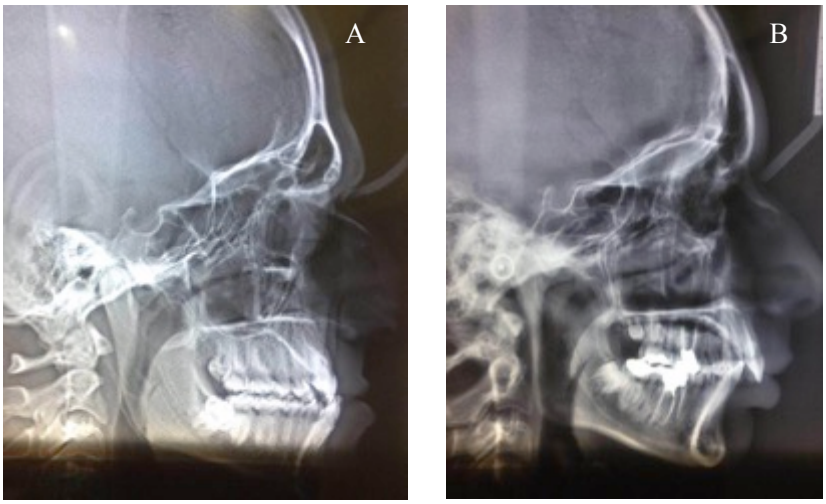

Figure 1: Showing different facial convexity A) excess and B) lack of facial convexity.

During the orthognathic surgical procedure, there are three main important tissues that need to be considered; they are facial soft tissue (skin, connective tissues, fat and muscles), facial skeleton (bone and cartilage) and dentition which Berge *et al*. refers to it as a triad [19]. It is known that the triad plays a crucial role in the planning of orthognathic and orthodontic procedures therefore its outcome [19]. The individuals with dysgnathic malformation are in need of precise and detailed assessment of soft tissue anatomy, interradicular distance, sinus and nerve location as well as bone quality prior to any the surgical procedure. Over the years, the pre-surgical assessment procedure have changed and developed considerably as it plays a crucial

role in the outcome of the surgery. In the following paragraphs, the conventional and recent advances in the pre-surgical assessment procedure will be looked at in more detail.

The first orthognathic surgery was carried out in late 19th century by Angle *et al.* [20]. In early 20th century, plaster casts were introduced as pre-operative planning models to predict the orthognathic and orthodontic outcomes which was welcomed as a 'gold standard' approach [21]. However in early 20th century, the pre-operative planning procedure was modified by introduction of dentals casts and anthropometry which is based on the study of the human body in relative to its variation in size and proportions [22]. Furthermore, the pre-operative planning procedure was revolutionised with the introduction of X-ray imaging, which is used widely in medicine to visualise the internal bone anatomy for orthognathic and orthodontics procedures. The concept of using cephalograms during surgery was first initiated by Broadbent in 1930s [23]. It was believed that the cephalograms offers the new 'gold standard' approach as it demonstrates the dentition in relation to facial skeleton. However, later on it was found out that the use of cephalograms only would result in a desirable functional dental occlusion and poor aesthetic outcome [19]. Thus the need of orthodontics procedure to achieve a desirable dental arch together with occlusion and repositioning of maxilla, mandible or both is needed in order to achieve a pleasing aesthetic features [19]. Due to the impact of aesthetic features on the outcome of the surgery, during the late 20th century the pre-surgery planning procedure was altered and the use of facial plaster casts, morphological data (e.g. CT and MRI) together with anthropometry was introduced. Currently this approach is being used widely even with great advances in virtual planning.

The conventional orthognathic surgery that comprise autogenous bone grafts, involves five main stages (see Figure 2). The initial stage involves obtaining the right morphological data and based on these information and patient consultation, the treatment procedure can be initiated which occasionally involves some level of orthodontic procedures to first straighten any dental displacements. Currently, the conventional orthognathic surgery procedure involves using dental

models/ articulators to physically visualise the surgical steps during orthognathic surgery such as the site and size of the sagittal split. With the assistance of accurate surgical planning, the treatment is preceded in theatre with the use of radiographs and articulators. The first actual invasive surgical procedure involved comprises of sagittal split osteotomy which depending on the patient's anatomy might be either a mandible osteotomy or maxilla osteotomy and in some cases both. However, during the osteotomy if the split created is a critical-sized bone defect, the surgeon will employ an autogenous bone graft ideally harvested from a region distant to the site of surgery such as rib. The graft is reshaped to contour a subtle 3D shape and implanted to the site of defect in mandible or maxilla.

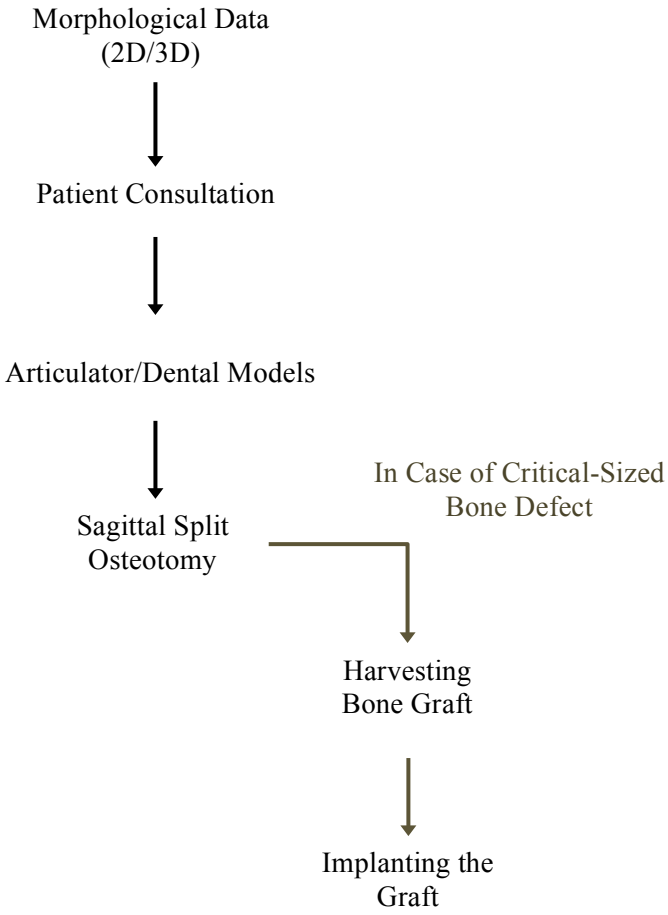

Figure 2: Different stages involved in the current strategy used in orthognathic surgery including 5 consecutive stages 1) obtaining morphological data (CT or MRI) 2) patient consultation 3) examining the articulator and dental models 4) performing sagittal split osteotomy by the surgeon during the surgery 5) harvesting autogenous bone graft from a distant site such as iliac crest 6) implanting the obtained graft into the bone defect.

The final objective of the cranio-maxillofacial bone reconstruction surgery is the successful regeneration of the physiological bone tissue that simultaneously accomplishes both morphological and functional restorations. Currently, there are various surgical mandibular and maxillae reconstruction surgeries technologies/ methods. However, there is no consensus on a definite reconstruction method [24]. Therefore, attaining three-dimensional stability after corrective bimaxillary mandibular and maxillae surgery remains a challenge [25]. The clarification, planning and execution of cranio-maxillofacial surgery is an inherently convoluted procedure due to the complex anatomy of craniofacial area as well as morphological variation encountered in each individual. Currently in the field of craniofacial surgery especially orthognathic surgery, surgeons can achieve up to 0.5 mm accuracy however there is a high risk of infection associated with this surgery in particular when there is more than one site of surgery during harvesting autographs. Overall, the current conventional orthognathic procedure is time-consuming and has other common associated issues that may go wrong during a surgery, which affects the outcome. Nevertheless even with the great existing successes in attaining surgical precisions, the mediation of computer-aided design and pre-surgical planning software can benefit the pre-surgical planning hence the outcome of the process greatly. Together with the great advances in tissue engineering, the ultimate goal for reconstruction of cranio-maxillofacial bone is closer to reality as it would offer the elimination of the major challenge hence the use of autogenous bone grafts as well as improving the accuracy and offering a time efficient approach. The basic concept of bone tissue engineering will be discussed in the following section 2.4.1, however the concept of orthognathic tissue engineering will be explained in detail in section 2.5.

In this study, the orthognathic surgery has been chosen as the main surgical challenge to study. This is because in terms of a clinical challenge, this surgical procedure offers a suitable ground for the proof of concept study to consider as it is elective (i.e. planned) as well as demand for bone tissue repair in predictable defect that will be created by the surgeon. However the following proposed concept could be adopted to use in design of any customised bone tissue engineered scaffold to be implanted at the site of critical-sized bone defect.

2.4 Innovative Technologies to Improve Craniofacial Bone Repair

2.4.1 Principles of Bone Tissue Engineering

The reconstruction and regeneration process of critical-sized bone defects can benefit greatly from bone tissue engineering due to its high demand as it is the second most common tissue to be transplanted after skin [26]. Particularly in craniofacial skeleton, there is a significant need for the substitution of bone tissue due to congenital malformations, disorders and injuries and a study by Scheller *et al.* also indicates more than 85% of the United States population is in need of reconstruction or replacement of a craniofacial structure including bone, tooth and temporomandibular joint which emphasises the need for craniofacial tissue engineering [27].

The success of adopting bone grafts during bone reconstructive surgery depends highly on the blood supply, consequently the lack of blood supply will result in absorption of avascular graft by the surrounding tissue. However to avoid the failure of the graft, the vascularisation process of the graft must be carried out which is a challenging task and requires microsurgery [28]. Due to all aforementioned drawbacks associated with conventional grafts, tissue engineering which is a discipline that was first introduced by Skalak *et al.* as "the application of the principles and methods of engineering and life sciences toward the fundamental understandings of structure-function relationship in normal and pathological mammalian tissues and the development of biological substitutes to restore, maintain or improve functions" bears great potential for regeneration of new tissue [29]. Later in 1993, Langer *et al.* introduced the fundamental ground of tissue engineering which was defined as 'an interdisciplinary field that applies the principles of engineering and the life sciences toward the development of biological substitutes that restore, maintain, or improve tissue function' [30]. Currently during the 21st century, most medical advances in regenerative medicine are closely associated with the progress in tissue engineering. Nowadays tissue engineering is based on the concept of restoring a tissue's function by supporting the natural healing process through enhancing

angiogenesis in the affected area [5]. To conclude, developing a successful bone tissue engineered grafts is now a closer and more realistic possibility due to all current advances in tissue engineering technologies. Generalised outline displaying the bone tissue engineering route is shown in Figure 3, which involves sourcing and harvesting a suitable cell source following *in vitro* cell expansion to obtain the adequate number of cells. The required numbers of cells are seeded on a suitable 3D scaffold with the appropriate tissue engineering scaffold properties, which is discussed in more details in section 2.4.1.2. In some cases, the resultant construct is required to culture *in vitro* to promote growth and tissue development in prior to defect implantation. However in other cases, the scaffold is embedded with cells just before the implantation in the theatre, which classifies the scaffold as a medical device.

Generally in tissue engineering, a highly porous artificial extracellular matrix is crucial to conduct the growth of mammalian cells and ultimately tissue engineering in three dimensions [31]. The 3D porous construct (scaffold) is expected to maintain cell colonisation, migration, growth/ differentiation and ultimately to direct the growth of the tissue [32]. In terms of bone tissue engineering, the concept aims to repair or reconstruct bone defects by employing a biodegradable scaffold seeded with autogenous osteogenic cells to create a scaffold-cell based hybrid to help the regeneration process. In the following sections, the choice of sourced cells, and the crucial properties required for 3D construct will be explained in more detail.

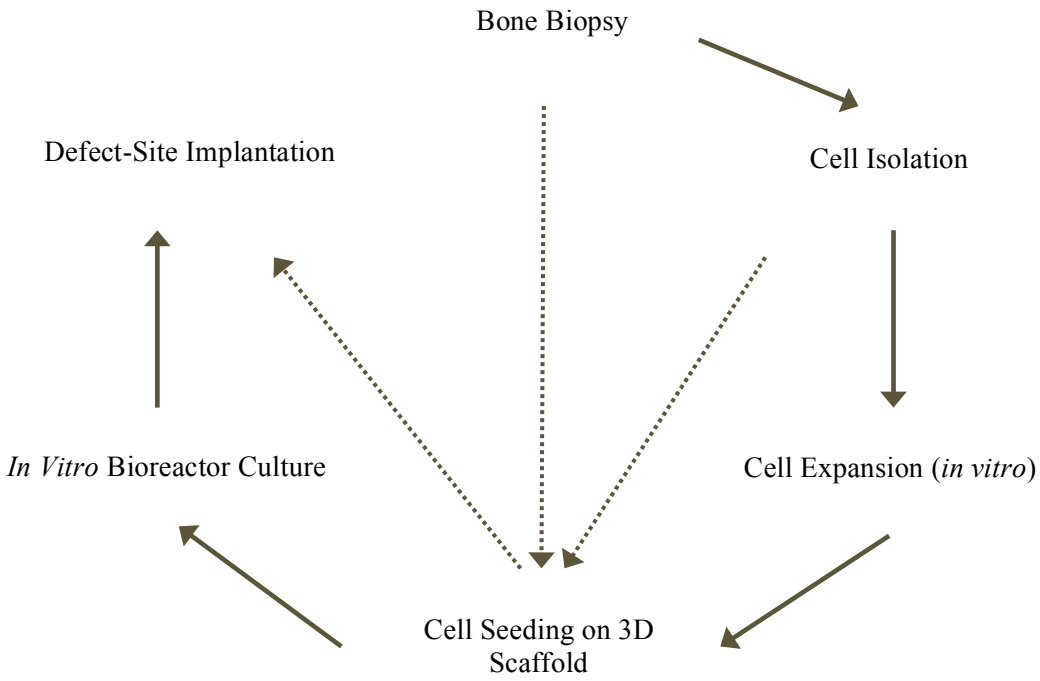

Figure 3: Bone tissue engineering diagram showing possible different routes to implant successful bone tissue engineered construct.

2.4.1.1 Cell Sources

One of the critical aspects of tissue engineering is having suitable source of autogenous cell line that is capable of tissue restoration. The ideal cell line must offer easy sourcing site with minimal side effects such as pain and infection. One of the main cell lines with advantageous properties is autogenous stem cell. Stem cells are capable of committing to multiple cell lineages. Human embryonic stem cells (ESC) are known to have high potential to differentiate, however these cell lines are very controversial due to moral and legal issues. Kahle *et al*. study showed successful differentiation of embryonic stem cells into osteogenic cells, hence achieving successful mineralised bone tissue formation in rats and Kuznetsov *et al.* also reported successful osteogenic behavior when co-culturing human ESC with osteoconductive materials (hydroxyapatite/ tricalcium phosphate) [33,34]. Xu *et al.* also reported promising results by combining calcium phosphate cement with bone marrow mesenchymal stem cells for treatment of critical sized bone defect in Beagle dogs [35].

Successful bone formation was also reported by Guo *et al.* by employing composite biomaterials (polyamide / hydroxyapatite) together with bone marrow stromal cells in treatment of *in vivo* rabbit mandibular defect [36].

Mesenchymal stem cells (MSCs) are the most studied stem cells in maxillofacial bone tissue regeneration [37]. Successful bone formation between the construct and the tissue was reported from the investigation in which porcine stem cells were seeded on $poly_{DL}$-lactic-coglycolic acid scaffolds and incubated for 10 days in osteogenic medium before implanting into critical-sized pig mandible [38].

Overall, there are many reports of using different sources of cells with tissue engineering scaffolds for treatment of critical sized bone defects. However, due to the associated challenges with clinical approval of such treatments, it is more desirable to develop a medical device scaffold that can be implanted into the critical sized bone defect in the operating room. There are three possible ways of employing these devices, they may be used alone or can be further modified to enhance bioactivity; for example by addition of bone chips or platelet rich plasma or in conjunction with cells. It could therefore be argued that, because the presence of the scaffold with or without PRP or cells may influence healing, there are all " tissue engineering" to craniofacial repair.

2.4.1.2 Scaffolds for Bone Tissue Engineering

The scaffold is a fundamental component in bone tissue engineering, acting as a carrier for cell delivery and mechanical support to the site of interest. The tissue-engineered structure is aimed to support angiogenesis within the affected area as well as retaining a consistent supply of cells all through the structure. Overall, a bone substitute material is expected to perform as extracellular matrix to support and later stabilise the formation process of the bone. The following characterisations are the main factors that have direct implications on the scaffold's functionality; therefore they play a crucial role in the outcome of the tissue's regeneration.

Biocompatibility – The biocompatibility characteristic of the graft ensure the absence of any toxic, teratogenicity, antigenicity or carcinogenicity effects of the bone substitute materials.

Osteoconductivity - The osteoconductive property of the bone substitute materials ensure the attachment of the osteoblasts and osteoprogenitor cells to ultimately differentiate and migrate within the porous structure and form the new blood vessels.

Osteoinductivity – the osteoinductivity characteristic of the material would induce the differentiation of undifferentiated and pluripotent cells into osteoblastic (osteogenesis) cells where the process is not expected to take place naturally.

Porosity – The scaffolds must be a highly porous macro-structure with completely open interconnected structure to facilitate the transport of nutrients, metabolic waste removals, cell proliferation and the process of angiogenesis during the regeneration process of tissue [39]. On the other hand, the level of porosity has a direct effect on the mechanical properties of the structure. Even though higher-level porosity may advantage the process of nutrient exchange and cell ingrowth but the mechanical

properties of the structure will be compromised caused by the large amount of void volumes. Hence, a balance between the mechanical properties and the level of porosity needed for the cell migration must be met in order to optimise the outcome of bone tissue regeneration process.

Pore size - In terms of nanostructures, the porous interconnecting structure must have a desirable pore sizes with usually the pore sizes of 5 to 10 times larger than the average cell size for the cells to penetrate and attach within the interconnected structure [40]. However, the minimum pore size necessary for angiogenesis procedure is 300 μm.

Mechanical properties – The mechanical properties of the scaffold must represent the native mechanical characterisation of the bone (see Table 1). The structure must provide the mechanical support during tissue regeneration in order to gradually transform the load applied to the structure to the surrounding regenerated tissue *in vivo*. However as for designing a bone tissue engineered constructs for cranio-maxillofacial bone defect, the mechanical properties of the structure plays a less crucial role; as the craniofacial bones are non-load bearing unlike long bones. As it was previously mentioned, a balance between the mechanical properties and the level of porosity must be met, however by choosing a biomaterial with the right innate mechanical properties the compromise may be overcome.

Biodegradability - It is crucial to understand the fundamental difference between biodegradability and bioresorbability of biopolymers. The concept of bioresorbability suggests the total elimination of degradation products from the body with no side effects [41]. In contrast, biodegradation reflects the decomposition of the material by the natural metabolic activity of body. Degradation pathway may occur via surface degradation pathway or bulk degradation pathway. Bulk degradation occurs when water penetrates the whole structure resulting in the whole structure to degrade simultaneously. During bulk degradation mechanism, hydrolytic chain cleavage takes place randomly which results in molecular weight reduction [41]. The water penetrates

within the polymer bulk and hydrolyses the chain that results in monomers and oligomers to diffuse out, thus the degradation takes place gradually and equilibrium for the diffusion-reaction phenomenon would be accomplished [41]. If the equilibrium is disturbed, the carboxyl and hydroxyl end groups initiates the internal autocatalysis mechanism [41]. Therefore, the degradation mechanism results in a bimodal molecular weight distribution. A higher molecular weight equates a longer chain which requires a greater number of ester bonds to be cleaved in order to create water soluble monomers and oligomers for degradation to proceed [41].

Overall, the 3D structure must offer an appropriate nutritional and spatial environment for the harvested cells to proliferate, attach and generate extracellular matrix. A highly complex tissue such as bone with extremely complex micro-structure and extensive vascular networks require a more detailed specialised scaffold micro-structure compare to the constructs manufactured by the conventional fabrication technologies. The overall success of an engineered bone graft depends highly on its mechanical properties and the ability of cells to make tissue-specific proteins which emphasises the need for the control over designing the macro-structure of the scaffold [42]. Also, the anatomical precision and accuracy of the bone graft is highly crucial for the craniofacial defects as its functionality depends highly on the overall geometry [43]. To summarise in order to design an effective bone tissue engineered substitute, there are several main factors to be considered which are "function", "formation", "form" and "fixation" [44]. "Form" implies to the ability of the construct to reform into the 3D shape of the defect. "Function" refers to the ability of the construct to match the tissue's function to the construct, by matching the mechanical properties of the constructs to the native bone and transmit mechanical stimuli which ultimately regulates cell and matrix biology and stimulate remodeling and regeneration [3]. "Formation" refers to the ability of the structure to encourage osteoconductivity that is a function of porosity, diffusivity and the combination of cells or bioactive factors [3]. Finally, the term "fixation" refers to the ability of structure to incorporate into the surrounding tissue [3].

A variety of different scaffolds have been developed and used as biodegradable bone fillers as well as supporting the structure to enhance attachment and proliferation of seeded cells. However, currently there are no scaffolds for bone tissue engineering with high clinical satisfaction depending on the conditions of the bone defects. Therefore it is crucial to develop a more functional bone tissue engineered scaffolds, which can be applied to cranio-maxillofacial bone defects. In order to achieve this goal the first step involves selecting appropriate biomaterials. In the following section (2.4.1.3) the biomaterials used in bone tissue engineering will be discussed in more details.

2.4.1.3 Biomaterials for Bone Tissue Engineering

The regeneration process of a tissue is a complex procedure therefore appropriate biomaterials must meet various requirements such as bioactivity, biodegradation, mechanical properties and biocompatibility characteristics. Generally, a bone tissue engineering scaffold should not result in immunological and foreign body reaction and the degradation product must exert from the body through a body's natural metabolic reaction [45]. As the degradation of the biomaterial takes place, the mechanical properties and functional stability of the biomaterial varies. Generally, the selection of materials and the chosen fabrication technology can affect the chemical, physical, mechanical and cellular detection characteristics of the biomaterials [3]. Therefore, the scaffold material selection is one of the main factors of the process. The essential mechanical characteristics required in bone tissue engineering scaffold includes stiffness, strength and appropriate degradation kinetics during the regeneration of the tissue while the scaffold degrades [46]. An appropriate biomaterial should result in a structure where stresses are evenly distributed [1]. In prior to any mechanical characterisation of the biomaterials, there is the biological interaction of materials such as protein and peptide adhesion, cell adhesion, migration, proliferation and differentiation [1].

Metal implants such as titanium alloys and stainless steel have been used widely for fixation of bone defects. However due to the low degradation rate of metals and the lack of its osteoconductivity properties, the metal graft is implanted permanently in the body which can cause hypersensitivity or immune reaction [47]. In contrast, other materials such as ceramics are known to have osteoconductive properties as 90% of the inorganic constituent of bone matrix is based on hydroxyapatite. Bio-ceramics are inorganic materials, which have a crystalline assembly formed by high temperature and comprise of calcium phosphate, calcium sulfate and hydroxyapatite. Overall, the mechanical properties of ceramics are not favorable for load bearing bone tissue engineering applications due to the brittle nature of the material as well as their low resorption rate.

Polymeric scaffolds have been used widely in bone tissue engineering. Polymeric bone tissue engineered scaffolds can be classified into two categories, natural and synthetic polymers. Poly (α-hydroxy acids) such as poly (glycolic acid), poly (lactic-acid) and their copolymers poly (lactic-co-glycolic acid) are the most common synthetic polymers used in bone tissue engineering. These polymers are FDA approved and have a well-known history of bone tissue engineered biomaterials [45]. Poly (α-hydroxy acids) based polymers degrade through hydrolysis and typically produce a non-toxic, natural metabolite product that can be eliminated through the Krebs cycle in form of water and carbon dioxide [45]. The mechanical characteristics of a polymeric scaffold depend highly on the molecular weight of the polymer matrix. In general, the molecular weight and mechanical integrity of the scaffold material decreases as the biomaterial degrades [48]. However, the degradation rate of the synthetic polymers can be tailored by alternating crystallinity, molecular weight and the chemical composition of the polymer [45]. For example successful use of 3D poly (ϵ-caprolactone) polymeric scaffolds treated with platelet-rich plasma and rhBMP-2 for treatment of mandibular defects was reported by Schuckert *et al.* [49]. On the other hand natural biomaterials such as collagen have been used extensively in medicine as a device, and has been reported for use as in scaffolds. Despite advances in collagen processing, and some evidence that collagen gels may be used to produce custom shapes, issues related to risks of disease transmission have reduced the popularity of this versatile natural material [50,51].

Recently, High Internal Phase Emulsions (HIPEs) polymers have attracted many interests due to their inherited porous morphology, which is beneficial for tissue engineering and other biomedical applications. PolyHIPE is a highly porous; emulsion template polymers which can be synthesised from biodegradable monomers, hence can be employed as tissue engineering biomaterials. Porous polymer materials have shown to be functional in wide range of applications. These polymers are in demand due to their application in microelectronics, biomedical devices and membrane processes [52]. Generally two different approaches have been made for manufacturing highly porous polymeric materials; the fabrication technologies are based on either templating processes or non-templating techniques. The templating

process involves having the precursor to the porous materials in two phases, where one of the precursors is removable and consequently pore-forming [53]. The non-templating technique create porous materials from one phase such as solvent-casting and gas foaming [53]. High Internal Phase Emulsions (HIPEs) are an emulsion-templated porous polymers, which are used as a templates to produce highly porous materials (polyHIPEs). PolyHIPEs were first patented in the 1980's by Unilever and since then they are very well-known in food preparation, fuels and oil recovery fields [54].

A polyHIPE is manufactured by curing a non-homogenous emulsion of two immiscible liquids. The polymerisation process takes place by curing the continuous phase of the emulsion, monomers polymerise around the emulsion droplets with the help of crosslinkers and results in creating pores/ voids in the resulting material. PolyHIPE materials inherit complex morphology comprising of spherical cavities known as voids and windows that interconnect the adjacent voids (see Figure 4). When the ratio of non-continuous phase of emulsion/ droplets (internal phase volume ratio Φ) exceeds 74% of total volume, the emulsion is known as a High Internal Phase Emulsion (HIPE), which can be increased to maximum 99%. At the droplet phase volume fraction Φ of 0.74, the emulsion droplets have spherical shape and are closely packed together (see Figure 5). Greater value of Φ will result in a system packed with polyhedral shaped droplets rather than spherical morphology. The continuous phase formed around this packed droplets, which contain monomers and crosslinkers, will be polymerised by radical initiation and form a porous structure.

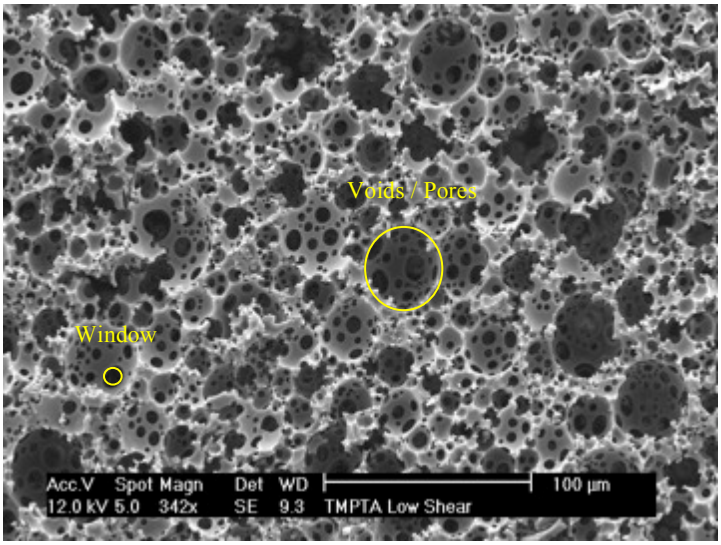

Figure 4: Typical porous morphology inherited by polyHIPE materials showing the voids and the windows.

The internal structure of polyHIPEs, such as the pore morphology and the degree of interconnectivity can be affected/ adjusted during the emulsion process of the material by altering the ratio of crosslinker, monomers and emulsifiers/ surfactant. Overall, pore diameter/ void size of between 1-100 µm can be achieved [55]. On the other hand, the mechanical property of the polyHIPE material can be controlled by using different crosslinkers as well as monomers such as 2-ethylhexyl acrylate to produce flexible materials or monomers such as isobornyl acrylate to produce stiff polymers [53]. The main advantage of polyHIPEs is the level of control over the porous macro-structure of the material and how the inherent porous structure of the material can enhance the nutrient and waste transfer during the regeneration process of tissue.

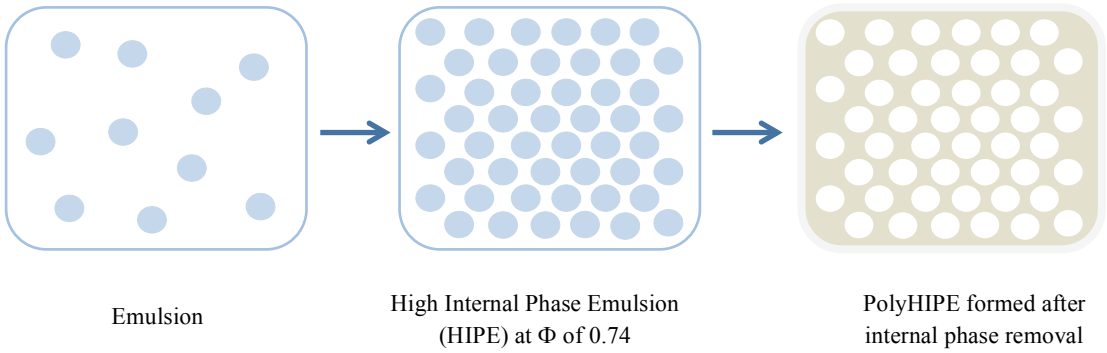

Figure 5: Stages involved during polyHIPE formation and stabilisation.

In some cases the internal, external phase or both phases of the emulsion contains monomers, which enables the polymerisation of monomers hence formation of polymer within the PolyHIPE structure. If the internal phase contains monomers, the polyHIPE will be formed in shape of concentrated latex. On the other hand if the external phase contains the monomers, a polyHIPE in form of a continuous polymer phase surrounding the emulsified droplets of the internal phase is formed e.g. water-in-oil emulsion. The most critical property of monomers in water-in-oil emulsion polyHIPEs is its hydrophobic properties. Greater hydrophobicity is more favorable as it increases the stability of two immiscible liquids used for two-phase emulsions. Styrene is one of the most common hydrophobic monomers which are water-immiscible, therefore polystyrene HIPEs can be formed via w/o emulsion [52]. Other hydrophobic monomers such as 2-ethylhexyl acrylate (EHA), methacrylate (MA), butyl acrylate (BA) and isobornyl acrylate (IBOA) are also used to create polyHIPEs from w/o emulsions. The aforementioned monomers cannot be employed in tissue engineering (TE) field for regeneration of the tissue, as they are not biodegradable. Many studies in the field of employing polyHIPEs for fabrication of TE scaffolds have focused on using biodegradable poly (ε-caprolactone) (PCL)

oligomers by incorporating with styrene based polyHIPEs with assistance of divinyl terminated PCL for polyHIPE crosslinking. However, PCL has more hydrophilic properties and that has resulted in less stable polyHIPE structure and thus large pores were formed.

Use of surfactants play a crucial role in achieving a stable emulsion as the molecules are adsorbed at the interface of two immiscible liquids to provide stability and maintain their separations. These molecules inherit both hydrophilic and hydrophobic properties/ groups, which can be classified into anionic, cationic, or amphiphilic according to the charge on the side chain of the molecule that adsorb to the interface. Based on Bancroft theory, the liquid in which the surfactant is mainly dissolved will form the external or continuous phase of an emulsion. The surfactant must be dissolvable in one of the phases that will diffuse out of this phase and adsorb at the interface of the two liquids, thus enhancing formation of HIPEs. The concentration of surfactants used in a HIPE emulsion affects the nature of voids/ pores as well as interconnecting windows between the voids as it affects the interfacial tension hence the resulting droplet diameter. A lower concentration of surfactant will result in closed voids while higher concentration will cause thinning of the wall around the droplets. At a critical wall thickness, windows between adjacent droplets will be formed upon curing. Generally, achieving a greater stability will result in formation of smaller droplets and on the other hand larger droplets are formed in a less stable emulsion as a result of smaller droplets diffusing together.

Overall, during the last decade the application of polyHIPE materials for tissue engineering purposes has been investigated. Busby *et al*. investigated the preparation of polyHIPE foams containing poly (ϵ-caprolactone) either on its own or with comonomer (styrene or methyl methacrylate), however the study lacked a long term biocompatibility analysis [56]. Later on in 2002, the same group studied the behavior of poly (lactic acid) HIPE foams as tissue engineering matrixes [55]. The study investigated the adherence of cells to PCL-based materials compare to the PLA-based materials and concluded that the cells tend to adhere more rapidly to PCL compare to PLA [55]. However, both studied carried by Jahoda *et al.* lacked long-term

biocompatibility analysis and also the use of styrene or methyl-methacrylate is not very desirable in tissue engineering constructs [55,56]. Overall, these constructs lack micro- and nano- structural physical and chemical signals of natural regeneration of bones and are non-degradable.

Recently, thiol-ene chemistry has attracted many attentions due to its ease and versatility in formation of wide range of photocurable polyHIPE [57,58]. This reaction involves adding thiyl radicals to an alkene and has been used widely as a route for preparation of polymers by reacting the reaction between thiols and alkenes, which recently drawn many interests because of the ease and versatility. Overall, thiol-ene and thiol-yne reaction differs in terms of crosslinking intensity as thiol-yne reaction involves reaction of two thiols to alkyne. Initially studies by Prasath *et al.* and Gong *et al.* reported employing thiol-ene and thiol-yne reaction in fabrication of porous microfluidic particles via photopolymerisation which can be employed in many fields such as ion exchange and high performance liquid chromatography [59,60]. Polymerising polyHIPEs via photopolymerisation is very rapid in compare to the conventional methods, which widens the choice of emulsions, as curing less stable emulsions is possible. Hence studies investigated preparation of less hydrophobic emulsions to be used for tissue engineering applications. As it was previously mentioned, the use of more hydrophobic monomers in emulsion formation is desirable as it forms more stable emulsions, however hydrophobic properties are not anticipated for tissue engineering applications. Further surface chemical modifications can be used to improve attachment of cells on porous materials after formation of stable emulsion hence developing polyHIPEs [61]. Employing thiol-ene or thiol-yne reactions for manufacturing polyHIPE structures via photopolymerisation to be used in tissue engineering purpose means the necessity of biodegradability of polyHIPEs. Preparation of degradable porous polyHIPE materials based on trithiol and acrylate monomers by UV-initiated thiol-ene “click” chemistry was previously reported by Lovelady *et al* [58]. The monomers investigated included trimethylolpropane triacrylate (TMPTA), trimethylolpropane tris(3-mercaptopropionate) (trithiol), dipentaerythritol penta/hexa-acrylate (DPEHA). Later Caldwell *et al.* investigated the two different degradable acrylate:thiol based

polyHIPEs (DPEHA:thiol and TMPTA:thiol) for tissue engineering applications and reported higher modulus for DPEHA polyHIPEs compared to the TMPTA due to higher crosslinking. The biocompatibility of DPEHA:thiol polyHIPE was then investigated using human keratinocyte cell line (HaCaTs) for hard tissue applications such as bone and showed good biocompatibility. Furthermore, preparation of thiol-ene based polyHIPEs consist of divinyl adipate and pentaerythritol tetrakis (3-mercaptopropionate) was reported by Sušec *et al.* and primary biocompatibility analysis with murine derived osteoblast cell line (MC3T3-E1) showed promising results for tissue engineering applications [62].

Recently, Johnson *et al.* showed successful preparation of trithiol and triacrylate-PCL based polyHIPE by photopolymerisation via thiol-ene "click" chemistry which resulted in a fully degradable polyHIPE material (90% and 95% nominal porosity) with 60 μm void diameter [63]. The successful formation of PCL based polyHIPE material via photopolymerisation is very promising for tissue engineering applications as it shows promising approach to selectively photopolymerised to manufacture customised scaffolds via UV-based SFF technologies such as stereolithography. The biocompatibility of the resultant material was assessed with fibroblast cells (L929) cultured for 7 days and MTT assay was carried at day 3 and 7 which was found to be capable of supporting cell growth [63]. The scaffolds were also found to hydrolyse successfully in NaOH(aq) proving its biodegradability [63].

Upon the successful reports on developing degradable polyHIPE materials via thiol-ene chemistry photopolymerisation, the fabrication of polyHIPE materials via laser-based solid free form fabrication technology applicable for tissue engineering is considerably promising. Only recently our group investigated fabrication of polyHIPEs using stereolithography which concluded the successful fabrication of micro structured 3D polyHIPE scaffold through stereolithography [53]. The fabrication of polyHIPEs through photostereolithography has been done through agitating two immiscible liquids in which one of them is photocurable. The photocurable polyHIPEs can be described as having photocurable continuous phase surrounding droplets as non-continuous phase.

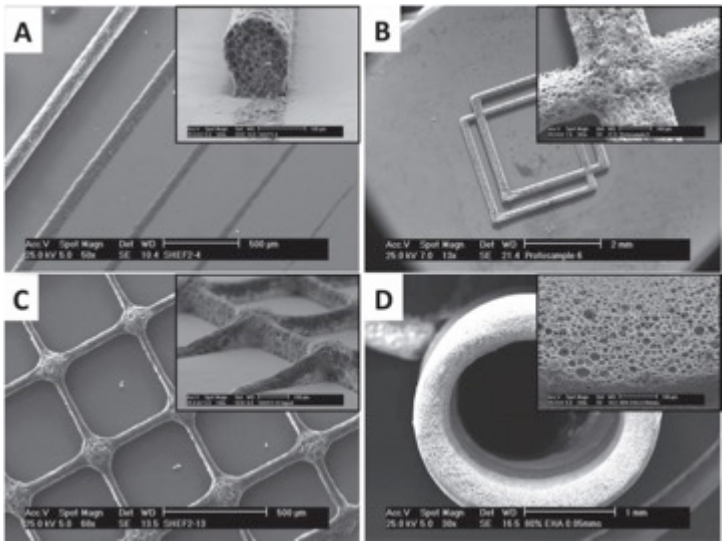

Figure 6: SEM images of polyHIPE structures manufactured by stereolithography [permission to reuse the image granted from Advanced Materials] [53].

Following that study Owen *et al.* carried an extensive study on fabricating 2-ethylhexyl acrylate and isobornyl acrylate based polyHIPE woodpile structures (non-biodegradable) with different monomer ratios via single-photon direct-write stereolithography technique and investigated its suitability for bone tissue engineering applications [64]. The fabricated woodpile structures were plasma coated with air and acrylic acid in prior to cell culture with human embryonic stem cell derived mesenchymal progenitor cells. The metabolic activity of cells were higher on polyHIPE woodpile structures with higher composition of EHA monomer [64]. However, the osteogenic differentiation hence the alkaline phosphatase activity of the structures with the highest IBOA composition treated with acrylic acid was significantly higher than other scaffolds showing the effect of the mechanical properties of the scaffolds on the osteogenic differentiation of cells [64].

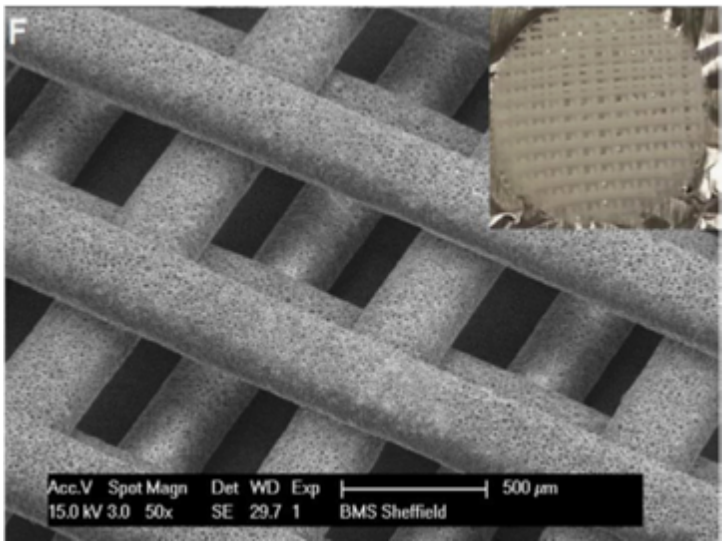

Figure 7: EHA/IBOA based woodpile polyHIPE scaffold fabricated by Owen *et al.* via single-photon direct-write stereolithography [64].

To summarise, all previously mentioned grafts and biomaterials suffer from some serious drawbacks such as the lack of osteoconductivity and undesirable mechanical properties [3,15]. Therefore a more comprehensive research study would focus on developing hybrid biomaterials to maximise osteogenic advantages. Hybrid biomaterials will have improved mechanical properties compared to the individual organic/ inorganic components as well as improved osteoconductive properties [65,66]. Therefore, it is very desirable and demanding to design biodegradable and biocompatible biomaterials to enhance the regeneration process of bone tissues to replace the use of the current gold standard bone defect treatment e.g. autografts. Since polymers can be tailored in terms of its biological, mechanical and chemical properties; they present convincing future opportunity together with ceramics as composite bone tissue engineered biomaterials. In other words the biomaterials and the constructs designed are desired to have osteoconductive and osteoinductive properties to regenerate critical-sized bone defects while degrading. Currently, there are reports of employing commercialised hybrid medical device

(OSTEOTRANS MX, Takiron Co, Ltd, Japan) consist of hydroxyapatite and poly-L-lactide for fixation of craniofacial bone defect due to its osteoconductive properties [67]. However, recently our group determined successful selective photopolymerisation of nano-scale hydroxyapatite composite acrylate based polyHIPE via stereolithography, which demonstrates possibility of fabricating composite polyHIPE materials [68]. The advantage of polyHIPE composite materials may be advantageous to bone tissue engineering, as the nano-scale hydroxyapatite particles are surfaced in the surface area of the pores hence improving the attachment and differentiation of cells. Therefore, due to all aforementioned advantages of polyHIPEs such as the tunable mechanical properties and inherited porous structure of the material together with the recent advances in fabrication of polyHIPEs using stereolithography, polyHIPE materials are a promising technique to fabricate complex composite bone scaffolds.

Generally, fabrication of biomaterials via SFF technologies for applications in craniofacial tissue engineering has been reported widely [69], however SFF technologies will be discussed and explained in more details in the following section 2.4.2.

2.4.2 Scaffold Fabrication Technology

Many studies have been carried out on developing and analysing different fabrication technology for manufacturing porous scaffolds for the past three decades. The conventional fabrication technologies in tissue engineering are such as particulate leaching/ solvent casting, gas foaming, electrospinning and emulsion freeze-drying. These technologies have been used widely in bone tissue engineering as an attempt to manufacture porous constructs to support the regeneration process of the tissue [70–73]. However, the conventional 3D scaffolds for tissue engineering proved fewer ideals for implantation applications as they failed to promote complete interconnected channels, having low mechanical properties, use of toxic solvents as well as failing to offer great control over macro- and micro- features. However, the main breakthrough happened in 1990s with development of solid freeform fabrication technology (SFF) and rapid prototyping (RP).

Solid free form fabrication technology was developed over years to circumvent the problems associated with the conventional fabrication technologies in terms of accuracy and control over the macro- and micro-structure of the construct. In other words, SFF technology is a fabrication technique that permits the accurate fabrication of complex 3D customised scaffolds designed by computer-generated image-based design technique, using a layer-by-layer manufacturing approach based on liquid, or powder [74]. This technology offers great control over pore size, macro- and micro-architecture, porosity, permeability that may enhance cell behaviors such as nutrient and waste transport, attachment and infiltration within the structure. The main advantage of SFF and RP technology over the conventional fabrication technology is by selectively adding materials layer-by-layer rather than removal of materials [32]. Therefore, solid free form and rapid prototyping technologies are a convenient platform for fabrication of pre-designed customised scaffolds as well as offering highly reproducible architecture.

Solid free form fabrication technology cover a wide range of techniques, which can be further divide into three major categories introduced by Hollister *et al.* based on how the materials is laid for each layer [75]. The first category is based on laser and UV light sources where the material is photopolymerised and cured or sintered powdered materials. The next category is nozzle-based systems, where the material is processed chemically or thermally while extruding via nozzle. The final category involves fabrication techniques where the material is directly printed. Each of these systems again cover a range of other technologies, which are fundamentally same but vary in how each layer of structure is laid.

As it was mentioned earlier in section 2.4.1.3 biocompatible polyHIPEs are exciting materials that have great potential for bone tissue engineering as they have inherited hierarchical microporous architecture similar to natural bone. It is now possible to fabricate photocurable polyHIPEs using laser and UV based SFF fabrication technologies. Therefore, in the following section a more intensive literature review on these systems is conveyed in compare to other SFF technologies, as the UV and laser-based technologies are more relevant to polyHIPE fabrications.

2.4.2.1 Additive and Advanced Manufacturing

2.4.2.1.1 Systems Based on Laser and UV Light Sources

Stereolithography

The initial commercialised rapid prototyping systems were based on selective photocuring of a photocurable resin, generally labeled as stereolithography (SL) [76]. Stereolithography (SL) SFF technology fabricates scaffolds using selective photocuring of a photopolymer. The solidification of the photocurable ink is caused by ultraviolet (UV) laser irradiation, which is done layer-by-layer and lowered into the photopolymerised bath which then photocuring of the next layer takes place. The pattern that the laser strikes represents the CAD designs and the ultimate 3D structure is achieved by stacking the solidified 2D patterns together. The laser penetrates into the resin covering a short distance which represent the layer thickness [76]. Once the 3D structure is fabricated completely, the platform is risen out of the resin bath, which makes the excess resin to drain. The final stage, the structure is removed from the platform and washed of excess resin and then positioned in a UV oven for a final curing [32]. SL technology is sometimes further divided into microstereolithography (MSTL) and nanostereolithography (NSTL) [77]. Through MSTL technology a more precise micro-structure can be fabricated compared to the conventional technologies. On the other hand, NSTL technology has been used to manufacture bi-pore scaffolds with extremely precise pores as well as global pores which enhance cell adhesion and proliferation compare to the scaffolds with global pores characterisations only [78]. The generally stereolithography approach may differ, for example in projection stereolithography the proposed pattern is projected using a digital micromirror device (DMD) into photocurable resin where the 3D structure is made layer-by-layer, each pattern corresponds to each layer of 3D structure. On the other hand, scanning stereolithography approach involves scanning the focal point of laser across the photocurable resin, which its movement corresponds to design of each layer. Overall, stereolithography technique is the most accurate and advanced technology among the SFF technologies. The technique is highly dependent on appropriate liquid photocurable resin that has well-defined

viscosity properties. However, the main drawback associated with this technique is the limited choice of photocurable biomaterials and their cost [77].

The conventional photocrosslinkable resins are combination of low molecular weight monomers capable of long chain reacting to result in solid polymers when activated by radiant energy within specific wavelength range. The conventional photopolymer resins used in industry are such as epoxy-based and acrylate-based resins which have strong, durable and accurate parts/ models characteristics [32]. However, only a limited number of these materials are biodegradable. Overall, the conventional photopolymerised materials cannot be used in tissue engineering and regenerative medicine due to the lack of biocompatibility. Due to limited choice of photocurable biomaterials approved by Food and Drug Administration (FDA), many research studies were focused on developing FDA approved biomaterials such as poly (propylene fumarate) (PPF), trimethylene carbonate (TMC) and poly (ε-caprolactone) based biomaterials [78,79].

Poly (ε-caprolactone) is a FDA approved biodegradable material with CE Mark registration. This polymer is semi-crystalline with glass transition (T_g) value of -60°C and low melting temperature. It has slow degradation kinetics, which can be tailored further by copolymerising with other polymers or integrating more labile bonds into its backbone [80]. PCL is less expensive in compare to other biocompatible polymers and is readily available. The versatility of PCL encouraged studies to investigate and develop successful photocurable PCL and PCL-based photocurable polymers with different molecular weight were synthesised by incorporating methacrylic anhydride to end-functions [81]. The success development of photocurable PCL resins have widens the possibilities of employing FDA approved polymers to fabricated tissue engineered constructs via laser-based SFF technologies. For example, a study by Makitie *et al.* showed successful fabrication of PCL based trachea scaffold fabricated via 3D photocuring technology [82]. Other biocompatible photocurable polymers have also been investigated. For example, Claeyssens *et al*. manufactured poly-lactide based (PLA) 3D scaffolds for neural tissue engineering application [83]. The study showed that the photocurable PLA can be photopolymerised

via direct laser write with a femtosecond Ti:sapphire laser and resolution of nearly 800 nm was achieved [83]. The biocompatibility assay on the scaffold indicated good cell viability and proliferation which raises the possibility of photocurable PLA being a suitable biomaterial (photocurable PLA is not currently FDA approved) [83]. Also successful fabrication of patient specific composite scaffolds (acrylic monomers and hydroxyapatite) via stereolithography was previously reported by Popov *et al.* [84].

Selective Laser Sintering

Selective laser sintering SFF technology is derived from using CO_2 laser to selectively heat up and sinter the biomaterials under their melting point [77]. Each cross-section shape of the 3D structure is scanned by the laser onto a power bed surface [77]. A roller lays each new layer of powder after completion of the previous layer. The parameters involved in SLS technology are such as scan speed, part bed temperature and laser power [85]. These parameters control the quality of sintering achieved through SLS fabrication.

Williams *et al*. study showed successful fabrication of PCL condoyle bone scaffolds via SLS technology [86]. The technology was proved to be highly useful for fabrication of scaffolds with specialised exterior derived architecture, which can be derived from CT or MRI data. Overall, SLS is a more favorable manufacturing process for fabrication of ceramic based scaffolds [77]. However, SLS technology is limited for fabrication of polymers as it is only suitable for thermally stable polymers [77]. SLS processing for polymer scaffolds benefits from the absences of any organic solvents as it eliminates any contamination risks [85]. Liu *et al.* carried a detailed study to fabricate tissue engineering based scaffold for mandibular defect via SLS technology, the study covered the initial aspects of manufacturing the scaffold including processing defect image from CT or MRI scan and applying Boolean subtraction to introduce macroporosity, however overall the study shows the suitability of SLS technology for fabrication of custom designed craniofacial scaffolds [28].

2.4.2.1.2 Systems Based on Extrusion and Direct Writing

Fused Deposition Modelling

Fused Deposition Modeling (FDM) is an additive manufacturing technology, which is mainly used for fabrication of models and prototypes used in different fields. Overall, FDM technology is based on extrusion of materials, which is fed through a heated nozzle and melts inside the feed chamber. S. Scott Crump first invented the technology in the late 1980s [87], which was commercialised during 1990 as Stratasys®.

The morphology of each layer can be predesigned and varied by altering the angle of deposition, the diameter of printed rods and the spacing between the rods. In other words, the morphology of each layer can be altered to attain different localised pore morphologies within a 3D scaffolds can be fabricated for the regeneration of multiple types of tissues such as bone and cartilage interface. Nevertheless, fused deposition modeling is limited to thermoplastic polymers with suitable melt viscosities. As this technology depends highly on depositing melted materials on a substrate, the need of a support structure is crucial which is needed to support the overhanging features and avoid the structure to collapse. Generally, FDM systems employ a filament from liquefied material by two roller which requires additional fabrication timing [77]. However, other fabrication technologies were developed to overcome disadvantages associated with FDM. Precision extrusion deposition (PED) is an alternative SFF technology where the bulk granulated materials is used compare to FDM where toxic organic solvents are needed [77]. For manufacturing complex 3D structures using PED technique, fabrication of a supporting structure alongside the scaffold is required. The presence of supporting structure may cause undesirable materials contamination [88].

As it was mentioned previously, PCL has low glass transition and melting temperature as well as its flexibility toward environmental factor such as moisture and temperature [89]. Due to the lack of accessibility medical graded PCL filaments, the filaments must be fabricated in advance by using extruders, which melt PCL pellets, and extrudes filaments of PCL polymers with known thickness suitable to be fed through FDM machines. A study by Zein *et al*. showed the successful process of manufacturing PCL scaffolds via FDM technology, which involved filament fabrication, scaffold design and finally fabrication [89]. Also, Arafat *et al. and* Hutmacher *et al.* reported on fabrication of composite PCL/ tri-calcium phosphate scaffolds via screw extrusion system, despite promising biocompatibility the scaffolds were further investigated for the effect of different laydown pattern of each layer for cranial bone healing; the study emphasised the importance of scaffold architecture in achieving desirable clinical outcome [90,91].

Generally, FDM technology is limited over the choices of thermoplastic polymers and their availability in the medical grade polymer market. Even though there are many different types of established biocompatible thermoplastic polymers exist, the availability of such polymers in form of feeding wires suitable for FDM with right specifications is limited.

Robocasting

Three dimensional printing or robocasting is based on incorporating computer-aided design with ink jet printing technology (x-, y- and z- axis control). The jet head moves in accordance to the CAD model cross-sectional data to form three-dimensional structures at room temperature [92]. Initially, robocasting has been used to fabricate ceramics inks where consolidation of the scaffold is attained through a fluid-gel transition during deposition [93]. SFF technique has the potential to be used to manufacture scaffolds with global pores, which in other words mean that the micro-structure of the scaffold is controlled and monitored completely to prevent any non-uniform micro-structure unlike other available fabrication techniques.

As a reference, Zhang *et al*. analysed the micro-structure of PLLA scaffold using phase separation technique and aimed to achieve a complete uniform global pores throughout the scaffold which is only possible by using SFF technique [94]. Russias *et al*. investigated PLA/HA (70 wt % HA) scaffold manufactured by robocasting technique [65]. The technique is very versatile, which is an advantage in combining bio-ceramics and polymers for orthopedic applications [78]. In another recent study, Tomsia *et al*. manufactured highly porous glass scaffolds using direct ink writing technique [78]. The mechanical properties of the scaffolds were investigated, and glass scaffolds exhibited compressive strength (136 ± 22 MPa) comparable to human' cortical bone (100-150 MPa) which is as a result of the ability to manufacture porous and strong structures using direct ink writing technique [78]. The ability to fabricate porous and strong scaffolds for load-bearing bone defects repair is crucial.

The parameters of robocasting techniques are such as printing speed, flow rate and the viscosity of the polymer solution. One of the disadvantages of robocasting is the use of organic toxic solvents such as dichloromethane to form polymer solution. The simplicity and flexibility of this technology allow the fabrication of range of biomaterials such as ceramics, polymers and metal [65,78]. On the other hand, robocasting is carried out at room temperature which means temperature sensitive biomaterials can be used.

2.4.2.1.3 Systems Based on Printing

3D Printing

3D printing technology was first developed by MIT University for selective fabrication of ceramics and metals. The technology is based on selectively printing binders onto layers of powders where each layer is laid using a roller. The binders aggravate the binding procedure between powder granules. This procedure is repeated until the complete fabrication of the 3D structure and latterly the remaining powder is aspirated. Similar to the other SFF technologies, morphology of each layer is directed by a CAD file. The main parameters considered in these technologies are such as powder wettability, binder droplet volume, intensity of powder, powder layer depth as well as the ability of powder spreading evenly each layer. This fabrication technology has been used for fabrication of bone tissue engineering ceramic scaffolds (calcium phosphate, hydroxyapatite) as well as composite materials (PLGA/calcium phosphate) [95–99]. Lee *et al.* showed successful fabrication of patient specific polycaprolactone and chitosan mandibular condyle via 3D printing for potential application of osteochondral tissue engineering directly from CT scans [100].

This technology is cost effective, and it can be used with a wide range of materials and there is no need for structural support materials, however the main disadvantage associated with this technology is the use of organic solvent as binders as they may also dissolve the binder head [101].

2.5 Scaffold-Enhanced Orthognathic Surgery

As it was previously explained in section 2.4.1, tissue engineering offers an alternative modality permitting reduced morbidity of donor site and lowers the risk of rejection for less compatible alloplastic tissue. Due to the nature of orthognathic surgery or any other cranio-maxillofacial surgery, surgeons are forever searching for improvements in reconstruction technologies or pre-operative form and function to ultimately achieve a minimise operative morbidity and recovery time, additionally eliminating any associated drawbacks with the use of autogenous bone grafts. A medical surgical procedure is a matter-of-fact art. Conventionally, the pre-surgery planning procedure depends highly on surgeon's expertise as well as employing simple models and mental visualisation of the procedure [102]. Overall to execute the physical surgical procedure, the surgeon requires having high understanding of the precise morphology of the defect as well as its interaction with the surrounding tissues, which has been made possible by the evolution of medical technologies such as medical imaging. Further, advances in manufacturing techniques have enabled the surgeons to adopt custom physical models of patient anatomy during pre-surgery planning to assist the pre-procedural planning. For example, physicians involved in complicated medical interventions such as cranial reconstruction surgeries rely heavily on physical models, e.g. articulators [102].

Cranial bones unlike long bones do not experience the daily loadings; therefore its capability to withstand repeated high maximal loads is more flexible for cranial scaffolds compare to the long bone scaffolds. Cranial bones are known to develop predominantly by intramembranous ossification unlike endochondral ossification of long bones [103]. Intramembranous ossification process of cranial bones refers to mesenchymal stem cell differentiation succeeding capillary ingrowth inside a mesenchymal area [103]. Consequently, a cranial tissue engineered scaffold must facilitate the migration, proliferation, and direct osteoblastic differentiation of local mesenchymal stem cell [103]. In order to design/ produce a desirable cranial tissue engineered scaffold, the architecture of the construct must be well designed.

Craniofacial scaffolds unlike other bone scaffolds for appendicular skeletons must fit perfectly to the complex 3D defect area due to its aesthetic outcomes. Therefore, the basic requirements for craniofacial skeletal scaffolds are [104]:

- Fit completely to the complex 3D area of the defect
- Provide temporary load bearing support to the surrounding tissue
- Enhance the bone healing/ regeneration process

A main component of bone tissue engineering is the scaffold that provides a template for cell interaction and development of extracellular matrix for relatively new-formed tissue as well as providing structural support. To conclude, the construct must have adequate porosity to provide chemical and biological support for the regeneration while also supporting the process mechanically. As mentioned previously, currently the autogenous bone grafts are known as the gold standards for reconstruction of bone defects. Based on that, the ideal tissue engineered bone graft must be osteoconductive, osteoinductive and osteogenic. Tissue engineered construct with osteoinductive characteristics enhance bone tissue regeneration process through delivery of biofactors which includes cell, gene and proteins. In order for the craniofacial scaffold to enhance the regeneration process via the delivery of biofactors, the construct must exhibit a highly porous characteristics while it must be capable of mechanically support the surrounding tissue [104].

The macro- and micro-structure of the scaffold must be optimised in terms of percentage of porosity and pore size to ensure the most effective bone ingrowth and ultimately bone regeneration. Many studies have emphasised on the effect of the pore size of tissue-engineered construct and how it play a crucial role in bone regeneration process [103,105]. Aronin *et al.* study mentioned on how the pore size may influence the type of osteogenesis that may occur during the regeneration process [103]. Smaller pore sizes ranged between 90-120 μm have showed to result in chondrogenesis in advance to osteogenesis although constructs with larger pore sizes (350 μm) result in direct

osteogenesis. Overall, large pore sizes encourage vascularisation and oxygenation while constructs with smaller pore sizes undergo osteochondral ossification.

In terms of the macro-structure of the construct, it must be precise and accurate to fit well into the bone defect in order to initiate bone regeneration. These specifications for the orthognathic bone tissue engineered scaffold emphasize the need for a well accurate, CAD/CAM based fabrication technology. The engineering scaffold fabrication technology chosen for the fabrication craniofacial constructs must be able to fulfill all aforementioned basic requirement and in order to achieve that, the fabrication process must be able to offer high accuracy and control over the macro- and nano-architectural design. The only current fabrication technology, which is capable of offering great control over the macro- and micro-structure design of the scaffold, is the rapid freeform fabrication technique (SFF), which was previously explained in more details in section 2.4.2.1. With the recent advances in image processing and SSF technologies, the TE concept used for regeneration of critical-sized defects can be used along with image processing techniques and SFF to digitalize the whole process of pre-surgical planning can be considered as a realistic goal. It is believed that the modern digitalised surgery will benefit the process by eliminating any unexpected event as well as moving toward a more minimally invasive surgery [106].

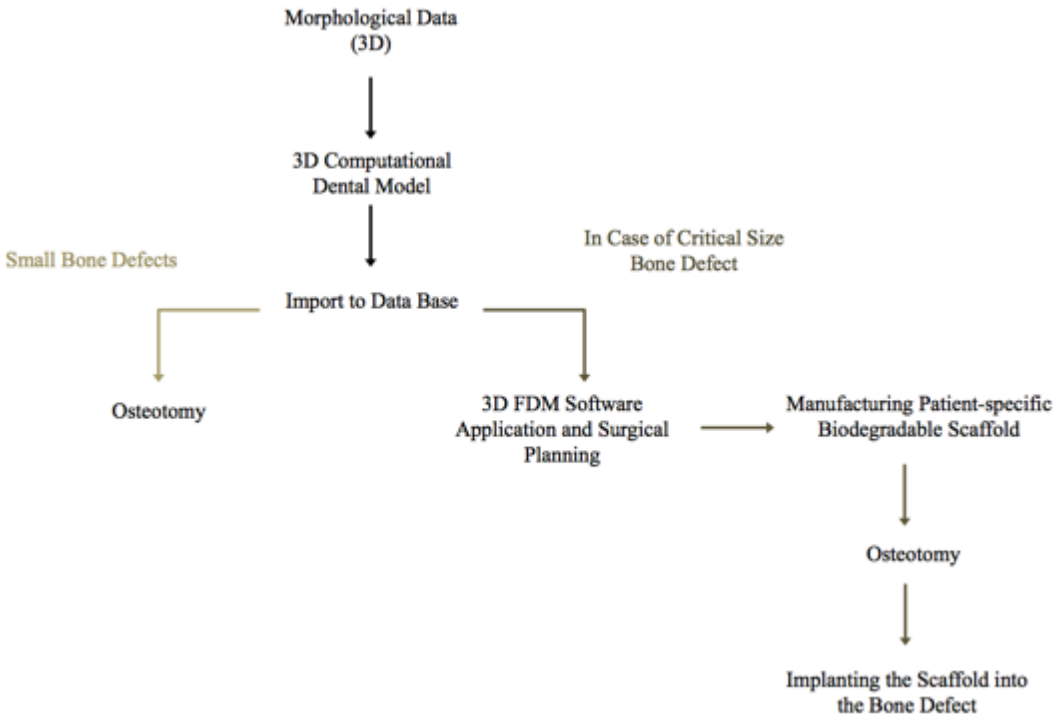

Figure 8: A novel tissue engineered approach toward orthognathic surgery with critical s bone defects involving four consecutive stages including obtaining morphological data (CT scan, MRI), 3D software application and surgical planning, fabrication of customised scaffold and finally implantation of customised scaffold in operation room.

Despite the great progress in virtual pre-procedural craniofacial surgery, most of the virtual representations are based in 2D, which consequently provides no 3D understanding of the challenge. Using computer-aided design together with manufacturing (CAD/CAM) technology is a standard process in manufacturing industry that can be adopted in the medical field. However, 3D imaging enables the physicians to interpret the data more precisely as well being able to adopt employing 3D models of the biological structure in a solid substance manufactured by rapid prototyping technique. The main advantage of using such a technology is the predictable outcome and increased productivity [107]. In today's world, the digital morphological data can be taken from CT scans or other 3D medical images which can be used along with medical image analysis software and rapid prototyping to transform the clinical practice in cranio-maxillofacial surgeries such as orthognathic surgery. To conclude, with the great advances in manufacturing technology for medical applications as well as medical imaging techniques; it is now possible to

maximise therapeutic success with minimizing operative morbidity as well as mortality by tailoring the surgical strategies to each individual. This change in the clinical practice will enable the surgeons to be able to fabricate customised biocompatible tissue engineered scaffolds to be implanted into the defects and eliminate any disadvantages associated with autogenous bone graft to regenerate the bone defects. Figure 8 illustrates the proposed novel tissue engineering approach to revolutionise orthognathic surgery to overcome the associated risks with autogenous bone grafts and optimise the outcome of healing cranio-maxillofacial bone defects by introducing novel materials such as biodegradable and biocompatible polyHIPE material.

3 AIMS AND OBJECTIVES

Chapter Two demonstrated that there was now a clear opportunity to develop biomaterials systems that were optimised for both advanced manufacturing methods and bone tissue regeneration. Despite this, there has been relatively little progress in the fabrication of custom scaffolds or medical devices for craniofacial reconstructive surgery. The aim of this PhD research was therefore to develop new biocompatible biomaterials and fabricate custom-made scaffolds to be used in orthognathic surgery as an example here to illustrate for feasibility. Therefore, specific objectives of the work reported during the PhD were:

- To evaluate a number of biomaterials and advanced manufacturing techniques and to determine which were best suited to offer opportunities for fabrication of custom-made scaffolds.

- Investigate the opportunity of employing of the biomaterials and techniques considered in the initial objective above, laser-based SFF technology combined with polyHIPE materials approved to hold considerable promise. The objective here was therefore to investigate this combination in more detail.

- While the conventional polyHIPEs will be seen to have potential, there are considerable benefits in developing biocompatible resorbable polyHIPEs. Therefore future objective will be to develop biodegradable and biocompatible polyHIPE materials including PCL based polyHIPEs.

- To investigate the *in vitro* biocompatibility of the most promising polyHIPE biomaterials used for bone tissue engineering applications.

- To consider the incorporation of nanoscale HA particles into polyHIPEs composite materials due to its osteoconductive properties to enhance the regeneration process of bone tissue.

On completion of this work, this thesis will provide a new opportunity to apply modern additive manufacturing methods to produce devices or scaffolds for a regenerative "tissue engineering" solution. The work will also have addressed the need for polymeric biomaterials that may be processed via SFF technologies to fabricate scaffolds or devices to enhance local healing and regeneration. Here the morphology and precision manufacture of the scaffolds will play a crucial role in the outcome of the procedure.

4 MATERIALS AND METHODS

4.1 Fused Deposition Modeling

4.1.1 Manufacturing PCL Rods by Extruder

Poly (ϵ-caprolactone) (Sigma-Aldrich) with molecular mass of M_n= 80000 g/mol was fed into Rondol® twin-screw extruder (Lab Twin) and the melting temperature was set as 75 °C. Rondol® extruder has 4 zones, where zone 4 is toward the extrusion point and zone 1 is the nearest zone to the feeding point of polymer granules. Zone 1 is usually set at a lower temperature compare to other zones, and zone 2 at a highest temperature. The PCL rods were collected from collection point (10 mm) at the end of the zone 4. In total 250 g of PCL granules were fed into the extruder and the resulting filaments were collected. The filament thickness was measured at 10 cm interval using a micrometer caliper.

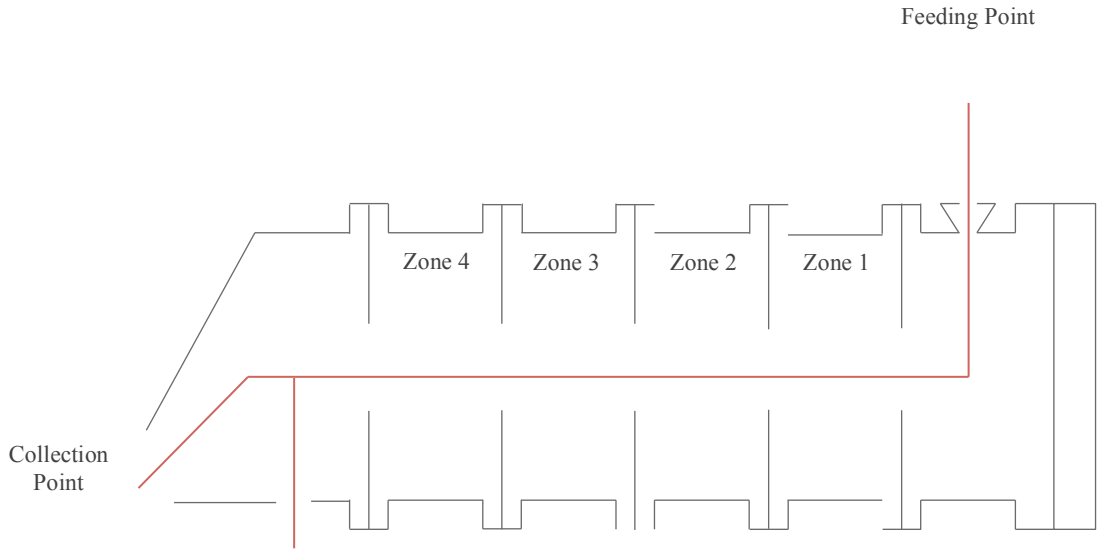

Figure 9: Image of Rondol® extrusion instrument used for manufacturing PCL rods.

4.2 Robocasting

Poly (ϵ-caprolactone) (Sigma-Aldrich, UK) with molecular mass of M_n= 80000 g/mol was dissolved with 15 mL of dichloromethane (99+%, Fisher Scientific, UK) wrapped in parafilm using a magnetic stirrer at room temperature. Further organic solvent (ethanol 7 mL (99+%, Fisher Scientific, UK) was used to ensure appropriate viscosity for dispensing which also would affect the drying rate of printed ink. The robocasting dispensing set-up shown in Figure 10 was made of a high precision translational stage (ATS100 XYZ, Aerotech, UK) controlled by a multi-axis controller (A3200, Aerotech, UK) attached to a fluid dispenser (EFD Ultimus, Nordson Ltd, UK). The dispensing nozzle size used was 0.10 mm inner diameter with printing speed of 4 μm/s for first layer and 3 μm/s for second layer. The fluid dispensing parameters are shown in Table 3. The G-code used to assess feasibility of robocasting technology was developed manually on A3200 program provided with the set-up. The generated G-code represented a woodpile structure with 400 μm rod spacing and 150 μm rod thickness, which represents 81% porosity based on Equation 1 mentioned in section 5.1.

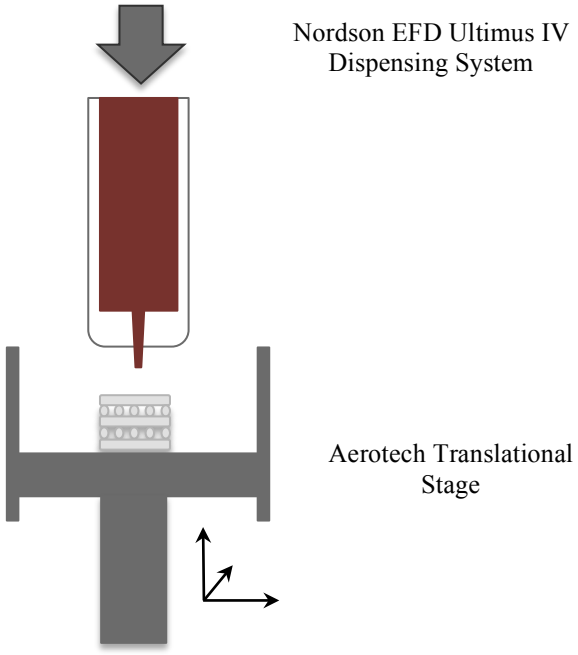

Figure 10: The schematic representation of robocasting set-up.

Table 3: Fluid dispenser parameters used for fabrication of woodpile structures.

Level [a]	102.0%
Dispense Rate [b]	0.0018 cc/s
Shot count/ Deposit volume [c]	0.0017 cc
Steps [d]	30

[a] *Level shows the syringe barrel volume (3 cc syringe barrel)*

[b] *Dispense rate (cc's per second)*

[c] *Shot count shows and tracks the number of deposit cycles (cc)*

[d] *Forward steps (with 3cc barrel, two steps will displace 0.0001 cc)*

4.3 Digital Micromirror Device Stereolithography

4.3.1 Preparation of Photocurable Materials

For preliminary photocuring trials using DMD stereolithography, poly (ethyleneglycol) diacrylate (Sigma-Aldrich, UK) with average molecular weight M_n= 258 g/mol was used. In order to prepare photocurable PEG, the photoinitiator camphorquinone (97%, Sigma-Aldrich, UK) (2% w/w) and light absorber Eosin Y (Sigma-Aldrich, UK) (0.1% w/w) was added which was therefore sonicated in water bath at room temperature to ensure complete mixture of powder with resins.

For preparation of photocurable 4-arm PLA (with the aimed molecular weight of 1200 g/mol), the hydroxyl terminated oligomers were synthesised by addition of (3S)-cis-3,6-dimethyl-1,4-dioxane-2,5-dione (98%, Sigma-Aldrich, UK) (0.1 mol, 8 molar equivalent) to pentaerythritol (>98%, Sigma-Aldrich, UK) (0.0125 mol, 1 molar equivalent) via refluxing procedure under nitrogen atmosphere and at 160 °C in presence of 100 mL of toluene (99.8%, anhydrous, Sigma-Aldrich, UK) and 1 drop of catalyst tin 2-ethylhexanonate (95%, Sigma-Aldrich, UK). The synthesising procedure was left stirring for 8 hours at 160 °C and finally cooled down to room temperature. The mixture was purified and filtered to remove any uncreative pentaerythritol, following vacuum distillation process to achieve a clear resin. The follow-on hydroxyl terminated PLA oligomers (0.01 moles, 1 molar equivalent) was dissolved in dichloromethane (>99.8%, anhydrous, Sigma-Aldrich, UK) and cooled in an ice bath following the addition of triethylamine (>99%, Sigma-Aldrich, UK) (0.16 moles, 16 molar equivalent). Finally, methacrylic anhydride (94%, Sigma-Aldrich, UK) (0.08 moles, 8 molar equivalent) was carefully added via a funnel to the and the reaction and were left at room temperature under the absence of light for 24 hours. Afterward, the solvent was removed by rotary evaporation yielding a crude product. The crude product was purified by three times by precipitation from isopropanol (99.5%, anhydrous, Sigma-Aldrich, UK) at -80°C. Further the produced tetramethacrylated PLA was mixed with photoinitiator camphorquinone (2% w/w).

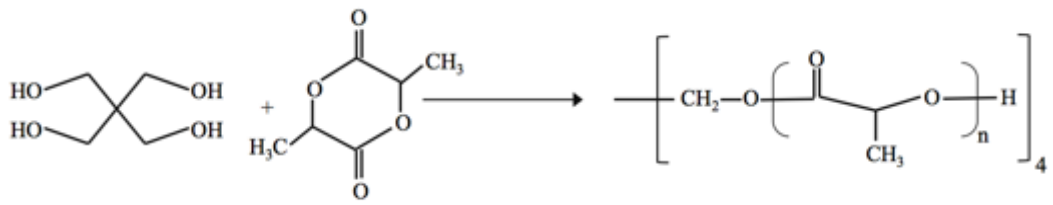

Figure 11: Synthesis process of 4 armed polylactic acid.

In order to incorporate hydroxyapatite particles (Captal® 30 D50, UK) (average particle size of 30 μm) with photocurable PLA, HA (20% w/w) with camphorquinone (2% w/w) was added together with dichloromethane to PLA. The amount of DCM differs to achieve an appropriate viscosity. The resulting mixture was mixed further via water bath sonication for 5 minutes.

4.3.2 Digital Micromirror Device Stereolithography Fabrication Process

In order to assess DMD stereolithography system reliability, the following bitmap design 2 and 3 (Figure 12 and Figure 13) was studied which was generated using Paint software.

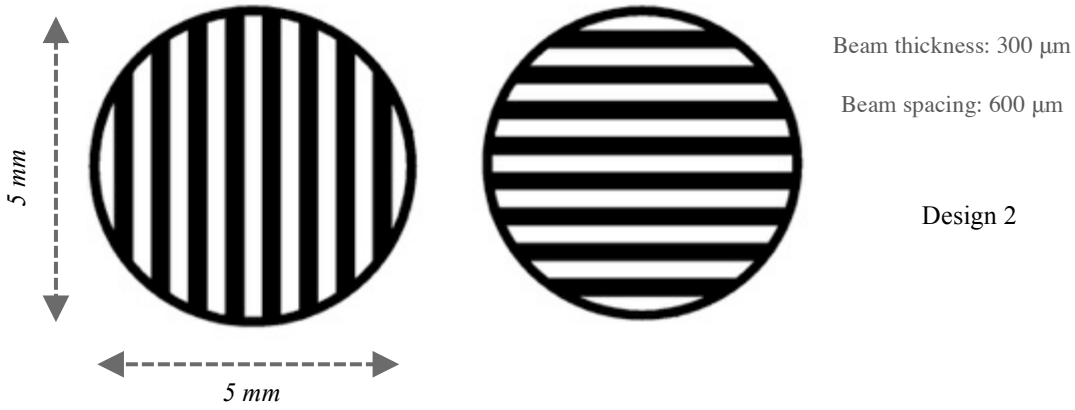

Figure 12: DMD design used for fabrication of Design 2.

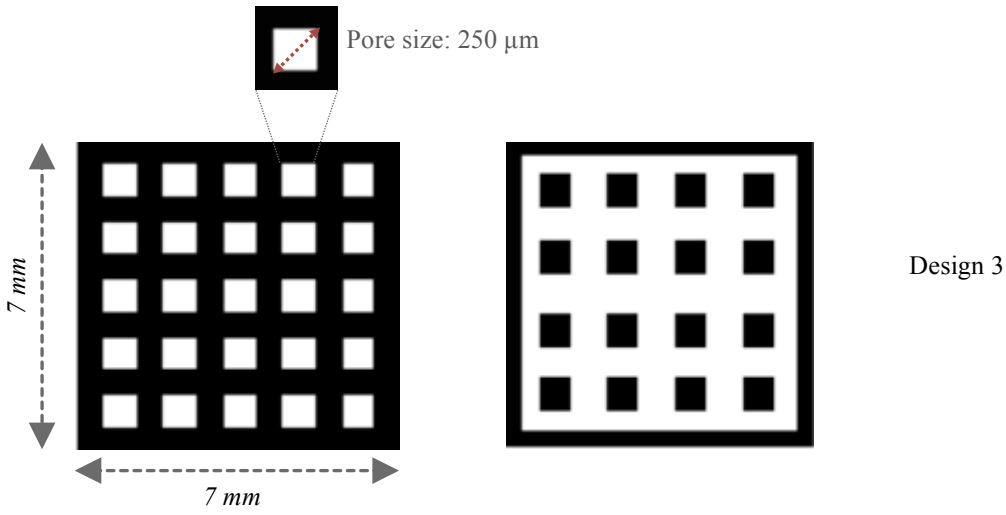

Figure 13: DMD design used to fabricate 3D structures (Design 3) [Images courtesy of Gabbott].

The DMD stereolithography system used in this study consisted of a blue laser source (MB-473, CNI Laser) with 150 mW power (473 nm), beam forming lens, digital micromirror device (Texas Instruments), image focusing lens and a (*x,y,z*) translational stage (PT3 Translational Stage, Thorlabs) where the sample holder is mounted on. The system was mounted on an anodised aluminium optical breadboard (Thorlabs) with a black matte finish to eliminate unsupervised laser reflection, which was further secured with using a protective box shield. In order to expand the emitted beam by the laser, a telescopic lens set-up was used to ensure successful laser coverage over the DMD surface. The focal length of lenses was varied for each design to ensure adequate beam diameter expansion required for fabrication of each structure. After an appropriate resolution and size of image was achieved, the proposed image was reflected onto the photocurable resin, and consecutively the 3D structure was formed by curing each layer onto a surface and lowered into photocurable resin assisted by a linear translational stage. A basic representation of DMD stereolithography system is elaborated in Figure 14.

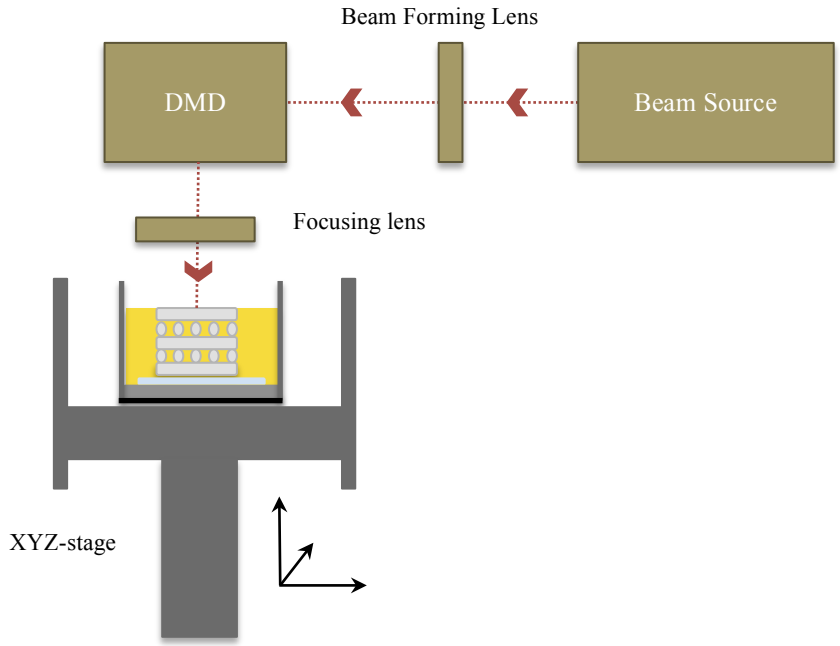

Figure 14: Schematic presentation of DMD stereolithography system used to fabricate 3D structures. The laser is emitted which is passed through an optical lens to produce a suitable beam, which is reflected by a DMD device. The resulting beam is then focused into a photocurable resin where the image is cured according to its design.

The system was used to fabricate the proposed structures (Design 2 and 3) single layer-by-layer to consecutively create the three-dimensional structures. The resulting structures were imaged using light microscopy.

4.4 Cell Preparation

4.4.1 General Cell Culture Condition

The standard culture medium used in this study was Dulbecco's modified Eagles media (DMEM, Invitrogen, UK) supplemented with 10% (v/v) fetal calf serum (FCS, Sigma-Aldrich, UK), 1% L-glutamine (LG, 2 mM, Sigma-Aldrich, UK), 1% penicillin and streptomycin (P/S, 0.1 mg/mL, Sigma-Aldrich, UK) and 0.25% amphotericin B (Sigma-Aldrich, UK). Human osteosarcoma cell line was cultured in T-75 flasks (VWR International, UK) with the use of standard culture media at 37°C and 5% CO_2 and passaged at density of 5×10^5 between passages of 69-72. All cells were examined daily and observed under light microscope for healthy cell morphology and density, and the media was changed every 3 days until 70-80% confluency was reached. To passage cells the media was removed gently and cells were washed with phosphate buffered saline (Oxoid Ltd, UK), 1.5 mL of trypsin-EDTA solution (Sigma-Aldrich, UK) was added and incubated for 2-3 minutes. The activity of enzyme was therefore immobilised by adding media and the cell suspensions were centrifuged (CL10, Thermo Scientific, UK) at 200 g for 5 minutes. The supernatant was removed and resuspended in 2-5 mL of media. The cell count was carried (at least twice) using a haemocytometer (AC1000, Hawksley, UK), and known numbers of cells were transferred into a new T-75 flask filled with appropriate culture media. Cells for future experiments were cryopreserved by suspending the cells in 10% dimethyl sulphoxide (DMSO, Sigma-Aldrich, UK) in FCS solution. Finally, the cells were stored at -80 ° C for 24 hours before being stored at -196 ° C for long-term storage.

4.5 Non-Degradable Acrylate-Based Elastic PolyHIPE

4.5.1 Glass Slide Functionalisation

The glass slide used as a substrate to fabricate the polyHIPEs. The substrates or the glass slides (Φ13 mm, Deckgläser, Germany) were functionalised in advance to optimise the attachment of polyHIPEs. The functionalisation process involves removing any organic residues on the substrate which may have been left from the manufacturing stages as well as exposing the methacrylate groups onto the glass slides to ultimately enhance the attachment of the materials onto the substrate. The functionalisation process was carried out by preparing piranha solution using mixture of 3:1 sulphuric acid (Sigma-Aldrich, UK) and hydrogen peroxide (Sigma-Aldrich, UK), which was used to wash the substrates for 30 minutes. The substrates were then rinsed in deionised water and dried in prior to soaking in a 10% MAPTMS solution (Polysciences Inc, Germany) in toluene for at least 24 hours. Finally, the substrates are washed with 70% isopropanol in prior to drying.

4.5.2 PolyHIPE Preparation

Monomers isobornyl acrylate (IBOA, Sigma-Aldrich, UK) and 2-ethylhexyl acrylate (EHA, Sigma-Aldrich, UK) were mixed together with crosslinker trimethylolpropane triacrylate (TMPTA, Sigma-Aldrich, UK) at room temperature. Surfactant hypermer B246 (Croda Ltd, UK) (3% w/w organic phase) was added to the organic phase and stirred continuously to ensure the complete dissolvent before adding the photoinitiator to minimise the light exposure. Finally, the photoinitiator (diphenyl(2,4,6-trimethylbenzoyl)phosphineoxide/2-hydroxy-2methylpropiophenone) (Sigma-Aldrich, UK) is added (5 v/v% of organic volume) to the organic phase, which is then subjected to gentle agitation (Pro40 SciQuip, UK) at 350 rpm for 5 minutes before adding the distilled water (28 mL) drop by drop to the mixture. The resulting mixture was stirred for further 5 minutes before removing from the stirrer.

PolyHIPE	EHA[a]/*g*	IBOA[b]/*g*	TMPTA[c]/*g*	PI[d]/ *g*	Surfactant[e]/*g*	Water/*mL*
EHA80	3.66	1.56	1.4	0.34	0.199	28

Table 4: Composition of EHA80 polyHIPE.

[a] 2-Ethylhexyl Acrylate

[b] Isobornyl Acrylate

[c] Trimethylolpropane Triacrylate

[d] Photoinitiator (Diphenyl(2,4, 6-trimethylbenzoyl) phosphine oxide/ 2-hydroxy-2-methylpropiophenone)

[e] Hypermer B246

4.5.3 Bulk Polymerisation

The bulk photopolymerisation was carried in form of 13 mm round disks on a functionalised round glass slides under UV belt curer (GEW mini, GEW engineering UV, UK) with a 100 W cm^{-2} UV bulb. The samples were exposed to UV light several times at speed of 5 $m.min^{-1}$ on both sides to maximise successful photopolymerisation. The resulting monoliths were washed with in 100 mL acetone (Sigma-Aldrich, UK) for 24 hours before drying in vacuum oven until constant mass is achieved.

4.5.4 Woodpile Fabrication

Woodpile structures with fibre spacing of 1.1 mm were fabricated via single-photon direct laser write. The set-up used for single-photon direct-write is shown in Figure 15. The single-photon direct lasers write set-up included the light source (passively Q-switched DPSS microchip laser, PULSELAS®-P355-300, Alphalas, Germany), which emits both 532 and 355 nm wavelengths. The 355 nm UV light is diffracted via a Pellin-Broca prism (ADB-10, Thorlabs, UK), which then is expanded via a Galilean beam expander to achieve diameter of roughly 8 mm. A uniform circular UV beam is achieved by using an adjustable pinhole in prior to entering the microscope objective (EC-Plan Neofluar 10×, Carl Zeiss Ltd, UK), which is used to focus the beam onto the object. The beam is controlled via a shutter (Uniblitz LS6, Vincent Associates, Canada) that is controlled via a shutter driver (VCM-D1, Vincent Associates, Canada). The object is affixed onto a high precision xy stage (ANT130-XY, Aerotech, UK) with assisted with z stage (PRO115, Aerotech, UK), which is controlled via motion control software (Aerotech, UK) to translate the stage in xyz direction to maximise focal spot. A silicon mould is placed on top of a functionalised glass slide to avoid spillage and 120 µL of HIPE solution is pipetted for first layer and 50 µL for consecutive layers. Finally, the structured were rinsed in acetone for 24 hours in prior to drying procedure in vacuum oven.

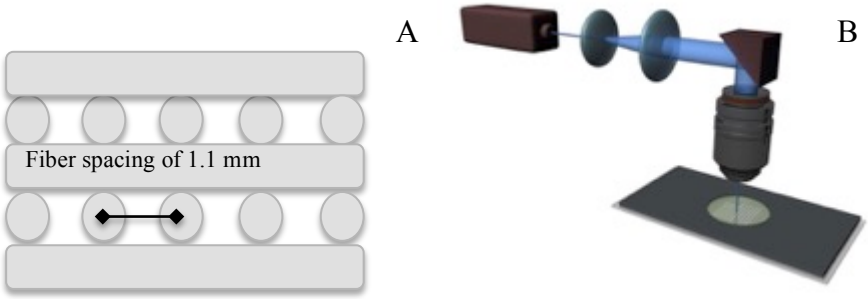

Figure 15: A) Schematic representation of 3D woodpile structure B) Schematic representation of single-photon laser set-up used to fabricated 3D woodpile structures.

4.5.5 Acrylic Acid Plasma Polymerisation

The EHA80 polyHIPE disks and woodpile structures were sterilised in 70% methanol or ethanol for between 45 to 60 minutes and washed with PBS for at least 3 times to minimise contamination. The samples were air-dried to ensure complete removal of alcohols in prior to plasma polymerisation process. The in-house plasma polymerisation rig consists of cylindrical plasma chamber with stainless steel endplates enclosed with cupper coil connected to frequency generator (Coaxial power systems Ltd, UK) at 13.56 MHz. An active Pirani gauge (APG-L-NW25, Edwards, Irelands) was used to detect the chamber pressure, which is controlled via a needle valve (LV10K, Edwards, Irelands). The samples were placed inside the chamber and pressure of 3.0×10^{-3} mbar was achieved in prior to opening acrylic acid (Sigma-Aldrich, UK) inlet and adjusting the pressure to 3.0×10^{-2} mbar. The plasma was then generated at power of 15 W for 20 minutes with flow rate of 2.4 cm^3/min.

4.5.6 *In Vitro* Biocompatibility of EHA80 PolyHIPEs

4.5.6.1 Sample Sterilisation

The EHA80 polyHIPE disks and woodpile structures were immersed in 70% ethanol or methanol (Fisher Scientific, UK) for approximately 50 minutes. Consequently, the samples were washed with PBS for 5 minutes and repeated 3 times. Finally, disks are air dried in a sterilised environment for at least 48 hours. After sterilisation, the disks were placed in 12-well plate and were secured using a steel ring with internal diameter of 1cm inner diameter and soaked in culture medium for at least 24 hours in prior to cell seeding

4.5.6.2 EHA80 PolyHIPE Disk Cell Seeding

Human osteosarcoma cell line (MG63) was used as representation of cell's proliferation and attachment to the EHA80 polyHIPE disk materials. MG-63 cells (P70) were seeded in T75 culture flask (VWR International, UK) in standard expansion medium (see 4.4.1). During polyHIPE disk cell seeding, two different approaches were made to ensure successful seeding. Ring confinement approach (Marine grade stainless steel rings, Sheffield NHS medical workshop, UK) using stainless steel rings with outer diameter of 2 cm and inner diameter of 1 cm and low volume seeding approach were made to minimise disk floatation and maximise number of cell seeded on the materials rather than tissue culture plastic. The disks were seeded with MG-63 at density of 20,000 cells in 10 μL of cell suspension, which was placed on top of the centre of the disk (n=6 of each sample type per day). The disks were placed in incubator for approximately 30 minutes to maximise attachment of cells to structure, hence minimise cell floatation while adding cell medium. Finally, 990 μL of culture medium is added slowly from the outside of the ring to avoid cells flowing outside the ring and all samples were incubated at 37 °C and 5% CO_2 for periods of 1, 3 and 7 days. The controls used in this study was 12 well plate tissue culture plastic seeded with MG63 containing the standard

medium. The medium was changed every 2 days and the experiment was repeated twice.

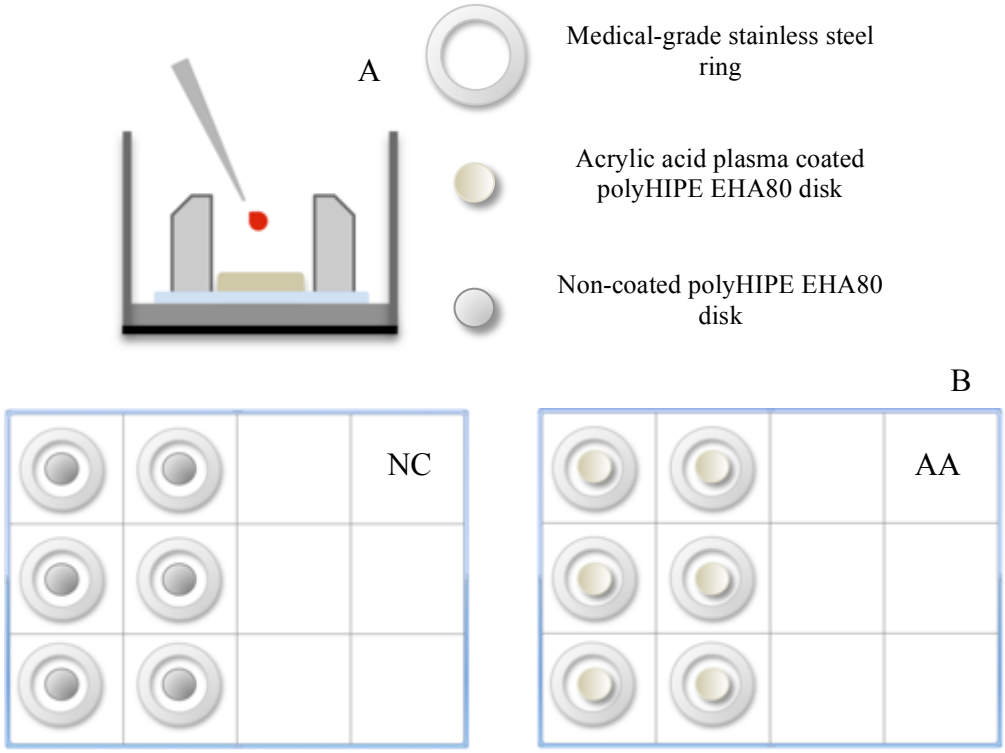

Figure 16: A) Schematic representation (side view) of ring confinement used for EHA80 disks seeded via low volume cell seeding approach (10 µL) B) Schematic presentation of 12-well plate including the metal rings and disks.

4.5.6.3 EHA80 PolyHIPE Woodpile Structure Cell Seeding

The cell seeding approaches used for woodpile structures were same as previous section (4.5.6.2). A total number of cells seeded per structure were 100,000 cells (n=6), which were seeded in 10 µL cell suspension and incubated for approximately 30 minutes in prior to adding 990 µL of culture medium. The structures were incubated at 37 °C and 5% CO_2 for period of 1 day, 3 and 7 days.

4.5.6.4 Assessment of Cell Viability

4.5.6.4.1 MTT Assay

MTT (3-[4,5-Dimethyl-2-thiazolyl]-2,5-diphenyltetrazolium bromide) assay (Sigma-Aldrich, UK) is a quantitative indicator of cell viability via metabolic activity. Metabolically active cells alter yellow MTT dye into purple formazan crystals/ salts. Ethoxyethanol solution (Sigma-Aldrich, UK) is used to dissolve formazan salts which then the intensity of the purple color can be measured using an absorbance reader (ELx800, Biotek, UK). Therefore, the quantity of purple formazan crystals produced is related to the quantity of viable cells present in the culture. The assay was carried out on day 1, 3 and 7 on untreated polyHIPEs as well as acrylic acid coated polyHIPEs (n=6). MTT solution was prepared in advance at concentration of 0.5 mg/mL and 1 mL of solution was added to each disk and incubated for 40 minutes. The cell-seeded disks were washed slowly with PBS to reduce accidental dismiss of produced formazan salts. 500 µL of ethoxyethanol solvent was added to each disk and mixed rigorously on a mechanical rocker for 24 hours in prior to the pipetting 150 µL of MTT solution (triplicates readings) from each disk into a 96-well plate (Thermo Scientific, UK). The absorbance of the solution was measured using Biotek absorbance reader at single wavelength of 562 nm.

4.5.6.5 Characterisation of Cultured EHA80 PolyHIPEs

4.5.6.5.1 Scanning Electron Microscopy

The EHA80 polyHIPE samples were prepared in advance by drying thoroughly as the SEM chamber operates under high vacuum. The living cell samples were washed with PBS 3 times (approximately 4 minutes each) following being removed from cell culture medium. Subsequently samples were fixed with 2.5% glutaraldehyde (Sigma-Aldrich, UK) at room temperature for 60 minutes to preserve cell structure. Each sample was rinsed with PBS for 15 minutes (3 times), and then soaked in distilled water for further 5 minutes. Finally the samples were dehydrated in series of ethanol solution with 35%, 60%, 80%, 90% and 100% concentration (15 minutes for each concentration). The samples were subsequently treated with drying agent (1:1 EtOH:HMDS) for 1 hour following rinsing with 100% HMDS (Sigma-Aldrich, UK) for 5 minutes (repeated 2 times). The drying procedure was carried to air dry the samples for at least 1 hour in prior to sputter coating (Emscope SC500, Philips, UK) with gold. The samples were imaged using a Philips XL-20 scanning electron microscope with accelerating voltage of 10.0 kV.

4.5.6.5.2 Image Processing

Images collected from SEM and confocal microscopy were analysed using image analysis software Image J 1.48. An average of 25 random voids were selected from each SEM micrographs (n=2) were observed and used to determine the average void diameter of polyHIPE structures, also statistical correction factor was applied [108]. Z-stack images obtained from confocal microscopy were converted to single plane images using Image J software via max intensity setting.

4.5.7 Immunofluorescence Microscopy to Image Cell Nucleus and Cytoskeleton

4.5.7.1 EHA80 PolyHIPE Disks and Woodpile structures Stained with DAPI and FITC-Phalloidin

In order to observe the morphology of attached cells to the EHA80 polyHIPE disks, the cytoskeleton of cells were stained with fluorescence dyes. DAPI (Sigma-Aldrich, UK) is a fluorescence dye that has been used widely to establish the existence of cell nuclei hence presence of DNA. The nuclei dye (DAPI) was excited using a tunable Ti-Sapphire two-photon laser with 800 nm wavelength and the emission was detected in range of 435 nm and 485 nm wavelengths. Cytoskeleton staining was carried by selectively labeling F-actin in cells. Phalloidin is a fungal toxin derived from Amanita phalloidin, which is a type of poisonous mushroom, it can bind to actin filaments and its fluorescent conjugates are used to visualise the structure under fluorescence microscope such as FITC-phalloidin (Life Technologies, UK) excited via a single-photon laser at 495 nm and emitted at 513 nm.

Due to the high porosity nature of the polyHIPE disks, its proven difficult to stain the disks with any dyes as the penetration of liquid into the porous structures in obstructed. Therefore, it was decided to cryo-section the samples in prior to any immunofluorescence staining. The samples were removed from media and washed with PBS once. The samples were fixed by soaking in 3.7% formaldehyde (Sigma-Aldrich, UK) at room temperature for 30 minutes. Following this, the disks were washed with PBS (3 times) to ensure complete removal of any fixing agent in prior to cryosectioning the samples. The samples were then frozen in freezing media and cryosectioned. Afterward, the sectioned samples were soaked in 0.1% Triton-X100 (Fisher Scientific, UK) in PBS to permeabilise the cells following washing procedure with PBS (3 times) and then FITC-phalloidin (1 μg/mL in PBS) and DAPI (1 μg/mL in PBS) were added at room temperature and were left for 30 minutes in prior to the final wash in PBS to remove any unbound phalloidin

conjugate. The samples were wrapped in foil, as they are light sensitive in prior to the imaging. Fluorescence microscope was used to assess the surface topography of the cell-seeded disks.

In order to visualise attached cells to the 3D EHA80 woodpile structures, the attached cells were visualised using confocal microscopy. The samples were prepared by initially fixing samples with 3.7% formaldehyde (approximately 30 minutes) at room temperature and permeabilised using Triton-X100 (1%) for 3 minutes. Samples were washed with PBS for 3 times (5 minutes each). Afterwards, the cells were stained with DAPI (1 μg/mL in PBS) and FITC-phalloidin (1 μg/mL in PBS). Following this, the samples were washed with PBS (3 times) to ensure complete removal of any unbound DAPI and phalloidin conjugates. An 800 nm laser (11% transmission) was used to excite DAPI and emission was detected between 435 and 485 nm and 488 nm was used to excite with 4% transmission (λ_{em} of above 505 nm). Also, in order to produce contrast of scaffold in the images, a 543 nm laser with 21.8% transmission was used to produce differential interference contrast (DIC). The samples were imaged using Zeiss LSM Meta upright confocal microscope (Carl Zeiss Ltd, UK), single plane images with properties of 1024 × 1024 pixels and Z-stack images (512 × 512 pixels) were attained with same setting as single plane images but translated in Z direction (11 μm each time).

4.6 Degradable PolyHIPE Materials

4.6.1 Thiol-ene PolyHIPEs

4.6.1.1 Trithiol-Penta/Hexa-Acrylate PolyHIPEs

In this study, the procedure for preparing thiol-ene based polyHIPE was based on the work by Lovelady *et al*. [57,58]. The monomers trimethylolpropane tris (3-mercaptopropionate) (Trithiol, Sigma-Aldrich, UK), dipentaerythritol penta-/hexa-acrylate (DPEHA, Sigma-Aldrich, UK), photoinitiator diphenyl(2,4,6-trimethylbenzoyl)phosphine oxide/2-hydroxy-2-methylpropiophenone (Sigma-Aldrich, UK) and surfactant Hypermer B246 (Croda Ltd, UK) were the main constitutes of the oil phase. Initially, the monomers and the surfactant were dissolved in dichloroethane (≥99%, Sigma-Aldrich, UK) and added to a flat bottom beaker wrapped in foil. Afterward the photoinitiator is added to the oil phase to minimise unnecessary light exposure. Finally, the known volume of aqueous phase at right (deionised water) is added drop by drop at room temperature. Once the water was added completely, the mixture is left to be mixed for further 2-3 minutes to ensure even distribution of water phase within the oil phase. The whole procedure was carried at room temperature using a high shear stirrer (1000 rpm) shown in Figure 18. Finally the emulsion is poured into a PTFE mould secured with two glass sheets at each side and cured for several times (approximately 4 times each side) at each side under UV curing system (Light Hammer®, Fusion UV systems Inc, UK) assisted with bench top conveyor (LC6E, Fusion UV systems Inc, UK) set-up at power output of 200 W cm^{-2}. The resulting materials was washed in acetone for overnight and placed between filter sheets to air dry.

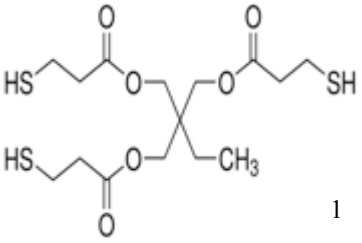

1

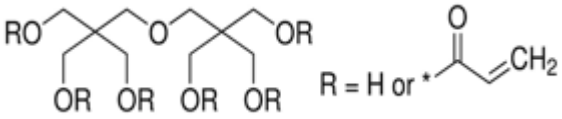

2

Figure 17: Monomers used in preparation of thiol-ene polyHIPE materials
1) trimethylolpropane tris (3-mercaptopropionate) 2) dipentaerythritol penta-/hexa-acrylate.

Figure 18: Schematic representation of polyHIPE preparation set-up using a high shear stirrer (1000 rpm).

Table 5: Compositions of thiol-penta/hexa-acrylate HIPEs prepared using a high shear stirrer at 1000 rpm.

Nominal Porosity	Trithiol/*g*	DPEHA/*g*	DCE /*mL*	Organic Phase/*mL*	Water/*mL*	Y/N
80%	1.61	1.16	2.5	4.84	19	Yes
85%	1.61	1.16	2.5	4.84	27	Yes
90%	1.61	1.16	2.5	4.84	44	No

[a] *Photo-initiator diphenyl(2,4,6-trimethylbenzoyl)phosphine oxide/2-hydroxy-2-methylpropiophenone with 5% (v/v) with respect to organic phase.*

[*] *Surfactant Hypermer B246 with 3% (w/w) of organic phase.*

Y= Successful emulsion *N= Unsuccessful emulsion*

4.6.1.2 Trithiol-Trimethylolpropane Triacrylate PolyHIPE

The procedure was carried as it was explained in section 4.6.1.1. The stirrer used for this emulsion was an over-head stirrer (Eurostar digital IKA, Germany). The monomers were mixed in a two-necked round bottom flask as shown in Figure 20. The photoinitiator is added to the oil phase just before the addition of water. Following that, the deionised water is added drop by drop through pressure equalising funnels attached to the two-necked round bottom flask. Finally, the monolith was cured via Light Hammer® UV curing system assisted with bench top conveyor set-up at power output of 200 W cm^{-2}. The resulting materials was washed in acetone for overnight and placed between filter sheets to air dry for at least an overnight. In total three trithiol:TMPTA emulsion formulation was attempted, 85% porosity emulsion was stirred at 330 rpm and 90% porosity emulsion was stirred at two different speeds of 250 and 300 rpm.

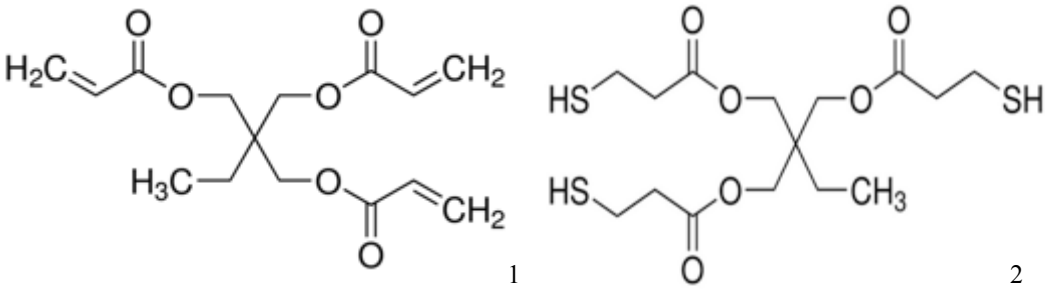

Figure 19: Monomers used in preparation of thiol-ene based polyHIPEs
1) trimethylolpropane triacrylate 2) trimethylolpropane tris (3-mercaptopropionate).

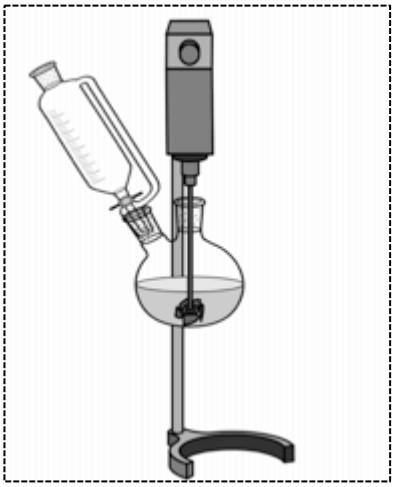

Figure 20: Schematic representation of polyHIPE preparation set-up using an overhead stirred with round bottom flask and pressure equalising funnel emulsion set-up.

Table 6: Shows composition of thiol-trimethylolpropane triacrylate based HIPEs.

Nominal Porosity	Trithiol /*g*	TMPTA/*g*	DCE/*mL*	Organic Phase /*mL*	Water /*mL*	Y/N*
85%	1.33	0.99	2.5	4.5	25	Yes
90% [a]	1.33	0.99	2.5	4.5	39	No

[a] *90% trithiol:TMPTA formulation was attempted using two different stirring speed (250 and 300 rpm).*

Photo-initiator diphenyl (2,4,6-trimethylbenzoyl)phosphine oxide/2-hydroxy-2-methylpropiophenone with 5% (v/v) with respect to organic phase.

Surfactant Hypermer B246 with 3% (w/w) of organic phase.

**Y= Successful emulsion* *N= Unsuccessful emulsion*

4.6.1.3 Thiol – Triacrylated Poly (ε -Caprolactone) PolyHIPEs

The known mass of monomers triacrylate-PCL (900 g/mol), trithiol, surfactant (Hypermer B246) and crosslinker (trimethylolpropane triacrylate) were weighted in separate glass vials (based on Table 7 formulations), which were dissolved in small amount of dichloroethane. Consequently, each of mentioned components were added to a round bottom flask and was stirred continuously with a half-moon shaped PTFE stirrer head attached to an overhead stirrer at approximately 300 rpm. Afterward, the crosslinker were added to the flask following the addition of photoinitiator while covered with foil to avoid light exposure. The final step involves the addition of deionised water that added very slowly to the continuous phase through pressure equalizing funnels attached to the round bottom flask (shown in Figure 20). After complete addition of deionised water, the resulting emulsion was left to stir for further 3 minutes to ensure complete mixture of emulsion. The resulting emulsion was poured into a PTFE mould which was placed in between two glass sheets and were cured under Light Hammer® UV curing system assisted with bench top conveyor set-up at power output of 200 W cm^{-2} and washed in acetone for overnight following air drying for at least an over night.

Table 7: Thiol-Triacrylate PCL polyHIPEs formulation.

Molar Ratio Thiol:Acrylate	Porosity [a]	Trithiol/*g*	PCLA/*g*	TMPTA/*g*	DCE/*mL*	Water/*mL*	Yes/No*
50:50	80	1.61	1.818	0.6	3	24	Yes
50:50	85	1.61	1.818	0.6	2	34	No
60:40	85	1.61	0.88	0.6	2.5	24	Yes
70:30	80	1.61	2.72	0.299	3	28	Yes

[a] *Nominal Porosity*

Photo-initiator diphenyl (2,4,6-trimethylbenzoyl) phosphine oxide/2-hydroxy-2- methylpropiophenone with 5% (v/v) with respect to organic phase.

Surfactant Hypermer B246 with 3% (w/w) of organic phase.

*Y= Successful emulsion N= Unsuccessful emulsion

4.6.1.4 Thiol-ene Methacrylated Poly (ε-caprolactone) PolyHIPE

4.6.1.4.1 Preparation of Methacrylate Poly (ε-caprolactone)

Two different methacrylated poly (ε-caprolactone) was prepared and used during this study, poly (ε-caprolactone) -tetramethacrylated (1200 g/mol) and poly (ε-caprolactone) -tetramethacrylated (20000 g/mol). The required amount of ε-caprolactone (97%, Sigma-Aldrich, UK) and a multifunctional alcohol initiator molecule pentaerythritol (>98%, Sigma-Aldrich, UK) were added to a round-bottomed flask with toluene (99.8%, anhydrous, Sigma- Aldrich, UK). The solution was degassed with nitrogen. Following that, the reaction was allowed to continue for 6 hours at 130 °C under nitrogen while stirring while 1 drop of tin 2-ethylhexanoate catalyst (95%, Sigma-Aldrich, UK) was added. The reaction mixture was allowed to cool to room temperature before removing the solvent by rotary evaporation. The resulting hydroxyl terminated PCL polymer was re-dissolved in dichloromethane (>99.8%, anhydrous, Sigma-Aldrich, UK) and cooled in an ice bath following the addition of triethylamine (>99%, Sigma-Aldrich, UK). Methacrylic anhydride (94%, Sigma-Aldrich, UK) was added drop wise whilst maintaining a low temperature (below 10 °C). The reaction was allowed to warm to room temperature and continued under nitrogen gas, in the absence of light while stirring for 24 hours. Finally, the solvent was removed by rotary evaporation yielding a crude product. The crude product was purified by three times by precipitation from methanol at -80 °C.

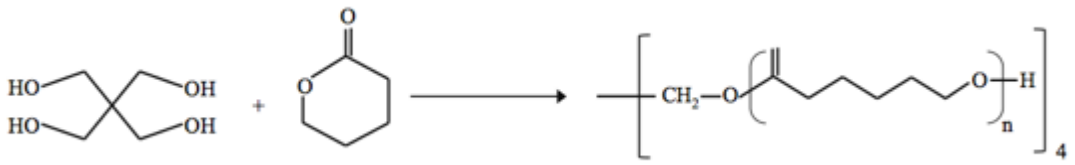

Figure 21: Synthesis process of 4 armed poly (ε -caprolactone) via ring opening polymerisation.

4.6.1.4.2 Polymer Characterisation

The PCL based oligomers were analysed via Gel Permeation Chromatography (data in Appendix).

4.6.1.4.3 Preparation of 1200 and 20000 g/mol Thiol-Tetramethacrylated PCL via Thiol-ene Chemistry

The known mass of tetra-methacrylated PCL, hypermer B246 surfactant and trithiol was weighted and added to separate glass vials and were dissolved in small amount of dichloroethane. Following complete dissolvent of components, they were added to a round bottom flask and was stirred continuously with a half-moonshaped PTFE stirrer shaft using an overhead stirrer at 300 rpm for PT2 samples and 400 rpm for PT1 samples. Afterward, the crosslinker trimethylolpropane trimethacrylate (Sigma-Aldrich, UK) were added to the flask. The flask is covered with foil to avoid light exposure. The last step was the addition of photoinitiator as it is important to minimise the light exposure. Finally, the known volume of deionised water was added very slowly to the continuous phase through pressure equalising funnels attached to the round bottom flask. The process set-up used in this experiment was based on section 4.6.1.1, and the formulations are shown in Table 8.

The resulting material was transferred into a PTFE mould which was placed in between two glass sheets and were cured under Light Hammer® UV curing system assisted with bench top conveyor set-up at power output of 200 W cm^{-2}. The resulting monolith was washed in acetone for overnight and placed between filter sheets to air dry for 2 days.

Table 8: Tetramethacrylated (1200 g/mol) PCL:Thiol polyHIPE formulations.

	Porosity [a]	PCLMA [b]/*g*	Trithiol [b]/*g*	Surfactant [c]/*g*	TMPTMA/*g*	DCE/*mL*	Photoinitiator [d]/*mL*	T [e]/°C	Water/*mL*	Y/N [*]
PT2	80%	1.82	1.61	3%	0.683	3	0.25	23	25	Y
PT2a	80%	1.818	1.61	3%	0.683	3	0.25	40	25	Y
PT2b	80%	1.818	1.61	3%	0.683	3	0.25	80	25	Y
PT2c	80%	1.82	1.61	6%	0.683	3.5	0.25	40	25	N
PT2d	80%	1.82	1.61	6%	0.683	3.5	0.25	23	25	Y
PT2e	80%	1.82	1.61	12%	0.683	4	0.25	23	25	Y
PT2f	80%	1.82	1.61	12%	0.683	5	0.25	23	25	N

[a] *Nominal porosity percentage* [c] *Percentage of organic phase* [e] *Temperature of deionised water*

Table 9: Tetramethacrylated (20000 g/mol) PCL:Thiol polyHIPE formulation.

	Porosity [a]	PCLMA [a]/*g*	Trithiol [b]/*g*	Surfactant [c]/*g*	TMPTMA/*g*	DCE/*mL*	Photoinitiator [d]/*mL*	T [e]/°C	Water/*mL*	Y/N *
PT1	80%	5	3.22	3%	2.5	9	0.5	23	35	Y

[a] *Nominal porosity percentage*

[b] *50:50 methacrylate:thiol molar ratio*

[c] *Percentage of organic phase*

[d] *5% of organic phase*

[e] *Temperature of deionised water*

* *Successful emulsion=Y, Unsuccessful emulsion= N*

4.6.2 *In vitro* Biocompatibility of PCL : Thiol PolyHIPEs

4.6.2.1 PCL : Thiol PolyHIPE Disk Cell Seeding

In order to assess *in vitro* biocompatibility of PCL:Thiol polyHIPE disks (PT1 and PT2 samples) were sterilised and washed as described in section 4.5.6.1. As it was mentioned earlier in section 4.5.6.1, the polyHIPE disks were then transferred into a 12-well plate filled with cell culture medium and were left to be soaked for an overnight. Due to the high porosity nature of polyHIPE disks, the samples tended to float within media, which should be avoided as it can affect the cell seeding procedure. In order to prevent sample floatation, the sterilised samples were transferred into sterilised bottle fitted with air filter as shown in Figure 22 and placed into a vacuum oven to remove trapped air. Following the treatment, the samples were transferred into a 12 well plate in prior to cell seeding procedure.

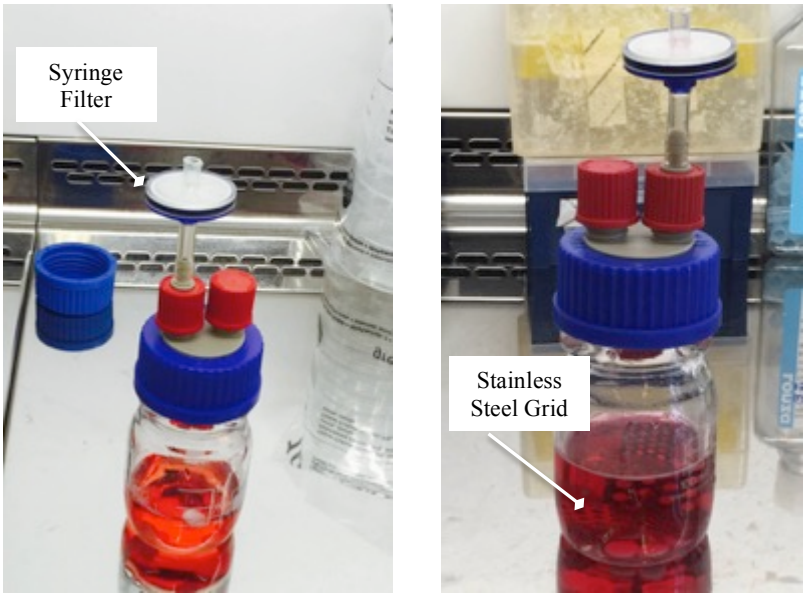

Figure 22: Post sterilisation process used to avoid polyHIPE disk floatation.

Human osteosarcoma cell line (MG63) was used as representation of cell's proliferation and attachment to the PT1 and PT2 polyHIPE disk materials. MG-63 cells (P69-P72) were seeded in culture flask in standard expansion medium (see section 4.4.1). The disks were seeded with MG-63 at density of 20,000 cells in a small quantity of cell suspension (10 μL), which was seeded on the centre of the samples (n=3) in same approach as section 4.5.6.2. The samples were incubated for 7 days in total and the medium was changed every 2 days. The controls used in this study was tissue culture plastic seeded with MG63 containing the standard medium. The experiment was repeated 2 times for each type of polyHIPE disks.

4.6.2.2 DNA Quantitation Assay

Cell proliferation was assessed using PicoGreen® dsDNA quantitation assay (Life Technologies, UK). The samples were removed from media following PBS washes repeated three times. Afterward, the disks were treated with 500 µL cell assay buffer (1:10 Tris-EDTA (TE) buffer (1.5 M Tris-HCL, 1 mM $ZnCl_2$, 1 mM $MgCl_2$) in deionised water and 1% triton-X100) at time points of day 3 and 7 for 30 minutes at room temperature and the samples were placed in freezer at 4 °C for overnight. Following three times freeze-thaw cycle (-80°C, 10 minutes) and vortex for 15 seconds at 37°C, 180 µL of supernatant was taken and added to 180 µL of PicoGreen® reagent (diluted in 1:20 TE buffer (10 mM Tris-HCL, 1 mM EDTA, pH 7.5), 1:200 PicoGreen in deionised water). The samples were incubated at room temperature for 10 minutes in darkness in prior to fluorescence reading at λ_{ex} of 485 nm and λ_{em} of 528 nm.

4.6.2.3 LIVE/ DEAD® Staining

LIVE/ DEAD® staining (Life Technologies, UK) was performed to determine cell viability. Media was removed from sample and fresh media was added containing Calcein AM (2 µM) and ethidium homodimer-1 (4 µM) and incubated for 30 minutes. Media removed and washed once with PBS before adding fresh media. Samples imaged under a Zeiss LSMMeta upright confocal microscope with ×10 and ×40 water dipping W-N-Achroplan objectives. Calcein AM was detected using λ_{ex} = 488 nm (12.0% transmission), λ_{em} = 505 nm and ethidium homodimer-1 using λ_{ex} = 543 nm (30.7% transmission), λ_{em} = 560 nm.

4.6.2.4 Degradation

The degradation of PT1 and PT2 samples were analysed via accelerated and non-accelerated degradation routes. The non-accelerated degradation was carried by using Lipase (Sigma-Aldrich, UK) from thermomcyes lanuginosus as a catalyst. The samples were weighted and measured, in total of 3 samples per type were used. Lipase solution was prepared with concentration of 2000 U/mL in PBS. The samples were soaked in the lipase solution and placed on an orbital shaker and incubated at 37 °C for 4 days. On the final day, the samples are washed with PBS and air-dried as well as drying procedure in vacuum oven in prior to weighting the samples.

The accelerated degradation protocol was adopted from Caldwell *et al.*[57] study. The samples were dried and weighted in prior to soaking in 0.1 M NaOH(aq) (Sigma-Aldrich, UK) solution. The samples were placed in a dried incubator at 37 °C for 57 days.

4.6.2.5 Characterisation of PCL : Thiol PolyHIPE Disks

4.6.2.5.1 Scanning Electron Microscopy Analysis with Image J Software.

The morphology of PT1 and PT2 polyHIPE disks were analysed using Philips XL-20 scanning electron microscope operating at 10.0 kV. The polyHIPE disks were cut through cross-section and sputter-coated (Emscope SC500, Philips, UK) with gold in prior to be attached on carbon pads adhered to aluminium stubs. The image processing was carried as it was explained in section 4.5.6.5.2 and 90 measurements in total were made and statistical correction factor was applied to the average void diameter [108].

4.6.2.5.2 Confocal Microscopy

DAPI and TRITC-phalloidin or FITC-phalloidin stained specimens were prepared by diluting the stains (1 μg/mL in PBS) and incubated at room temperature for 30 minutes in darkness. Single plane images (1024 × 1024 pixels) were taken via an upright confocal microscope (Zeiss LSM510-META, UK) assisted with ×10 objective (W-N-Achroplan 10×/0.3, Zeiss ltd, UK). DAPI stain was excited using an 800 nm two photon Ti-Sapphire laser set to 358 nm λ_{ex}, 461 nm λ_{em}. TRITC and FITC-phalloidin (F-actin) was determined via single-photon laser set to λ_{ex} = 495 nm, λ_{em} = 515 nm (FITC) and λ_{ex} = 545 nm, λ_{em} = 573 nm (TRITC). Z-stacks were converted to single images using Image J's Z-project feature via the max intensity blend setting.

4.7 Preparation of nHA Particles

Hydroxyapatite particles were produced via Prakash *et al.* method [109]. nHA particles were precipitated via the following reaction:

$$5Ca(OH)_2 + 3H_3PO_4 \rightarrow Ca_5(PO_4)_3(OH) + 9H_2O$$

Calcium hydroxide $Ca(OH)_2$ solution (50 mmol, 3.7045 g) was prepared by dissolving calcium hydroxide powder (Sigma-Aldrich, UK) in deionised water (500 mL) and stirred for 1 hour with speed of 400 rpm. Meanwhile, phosphoric acid solution (85%, (Sigma-Aldrich, UK) (30 mmol) was prepared by slurring in deionised water (250 mL) and stirred for a few minutes. Following the complete dissolvent, the phosphoric acid solutions was mixed with calcium solution and were left to stir (400 rpm) for further one hour. The resulting solution was left to settle to allow precipitates phase separation, following filtering and washing procedures with distilled water. The filtering and washing procedures were repeated until the reached conductivity was below 15 µS/cm (typically three washes) and dried in oven at 60 °C. The dried powder was grinded in agate motor and pestle. A portion of nHA powders were sintered at 1000 °C for further characterisation. The resulting hydroxyapatite materials were stored in a vacuum desiccator.

4.7.1 nHA Particles Characterisation

The characterisations of nHA particles were carried using X-ray diffraction (STOE IP, Philips), transmitted electron microscopy (FEI Tecnai G2 Spirit, UK) and fourier transform infrared spectroscopy (Thermo Scientific Nikolet Spectrmeter, Unicam Ltd, UK). TEM samples were prepared by ultrasonic dispersion (15 minutes) of unsintered nHA powders in ethanol following pipetting onto a 400 mesh copper grid with a permeable thin carbon film (Agar Scientific). The images were taken at accelerating voltage of 80 kV.

Samples were prepared for X-ray diffraction via depositing small amount of nHA powder onto an acetate film using PVA glue. The samples were dried by hot air gun in prior to the reading. The micrographs were taken with Cu $K_{\alpha 1}$ radiation, $\lambda = 0.15406$ nm, which was operated at 40 kV and 35 mA. Finally, the results were analysed via ICDD PDF 4^{+} software.

FTIR-ATR analysis was carried by placing and compressing small amount of the sample onto the diamond. FTIR-ATR readings were taken between 500 – 4000 cm^{-1} and resolution of 4 cm^{-1} with 32 scans and 64 background scans which was deducted from the following scans.

4.7.2 Incorporation of nHA Particles With PT1 PolyHIPE Sample

The protocol for preparation of nHA-PT1 samples was according to the protocol used in section 4.6.1.4.3. The nHA particles (1 g nHA in 15 mL deionised water/ stock solution) were added to the aqueous phase and were precipitate in prior to adding to the oil phase. The oil phase was stirred with overhead stirrer at speed of 400 rpm for 400 seconds while the aqueous phase was added drop by drop via funnel. The formulations used are explained in the following table. The successful emulsions were washed with acetone for an overnight.

Table 10: PolyHIPE formulation of thiol:PCLMA polyHIPEs incorporated with nHA particles.

	Porosity [a]	PCLMA [b]/*g*	Trithiol [b]/*g*	Surfactant [c]/*g*	TMPTMA/*g*	DCE/*mL*	Photoinitiator [d]/*mL*	nHA/*mL*	Water/*mL*	Y/N *
3PT1H5	80%	5	3.22	3%	2.5	9	0.5	1.75	33.25	N
1.5PT1H10	80%	5	3.22	1.5%	2.5	9	0.5	3.5	31.5	N
3PT1H10	80%	5	3.22	3%	2.5	9	0.5	3.5	31.5	N

[a] *Nominal porosity percentage*

[b] *50:50 methacrylate:thiol molar ratio*

[c] *Percentage of organic phase*

[d] *5% of organic phase*

* *Successful emulsion=Y, Unsuccessful emulsion= N*

5 RESULTS

5.1 Process of Choosing Scaffold Micro-Designs

In 2012, Chantarapanich *et al*. carried a study to develop a scaffold library for tissue engineering: a geometric evaluation [110]. The group categorised the design into two different criteria: 1) open cellular tissue engineering scaffold 2) close-cellular tissue engineering structures [110]. A highly porous interconnected construct is crucial as it facilitates the nutrient and waste diffusion during bone regeneration process to avoid formation of necrotic tissue in center of scaffold as well as allowing the growth of connected bone growth. As mentioned previously, it is crucial to achieve a well-interconnected porous structure within a craniofacial bone scaffold. The following structural designs are the potential open-cellular units that can be used in developing completely interconnected structure for craniofacial scaffolds [110]:

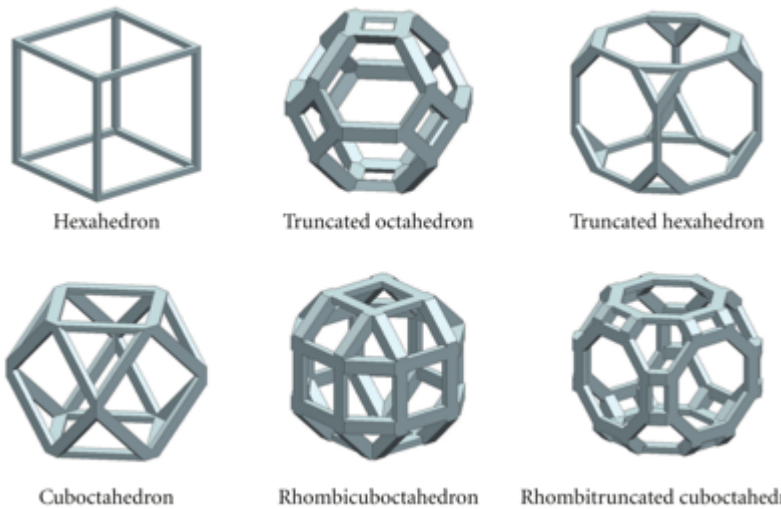

Figure 23: Potential open-cellular unit library adopted from Chantarapanich *et al*. [110].

Hexahedron design is the simplest form of open-cellular cell unit, which was used to assess the liability of SFF technologies to reproduce the digital designs.

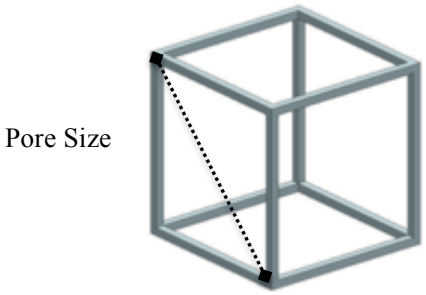

Figure 24: Open-cellular hexahedron unit cell adopted from Chantarapanich *et al*. [110].

The important factor is that the percentage of porosity does affect the bone ingrowth, therefore it is crucial to have accurate calculations of porosity. However, different research groups have different methods of calculating the porosity, the following formulas have been adopted from the study by Chantarapanich *et al*. [110]. The porosity value obtained from this formula will be ranged from 0 to 1, where 0 indicates that the scaffold is dense / no porosity and 1 indicates a well porous structure [110]. The ratio between the pore size and the beam thickness in hexahedron affects the percentage of porosity, and the relation is described by the following equation [110]:

$$y = \frac{1.01}{(1 + (\frac{x}{1.02})^{-1.50})}$$

Equation 1 Formulation adopted from study by Chantarapanich *et al*. which determines the ratio between the pore size and beam thickness where y is porosity and *x* is the ratio of pore size to the beam thickness [110].

The pore size of a tissue-engineered construct is a key factor in the quantity and characteristics of regenerated tissue. As stated previously, the cranial ossification takes place via intramembranous ossification succeeding in capillary ingrowth. In order for vascularisation to occur during the process of bone regeneration, a minimum pore size of 300 μm is required [111]. On the other hand, large pore size may result in a structure with low mechanical strength properties and smaller pore sizes (100μm) may induce endochondral cartilage ossification prior to osteogenesis [111]. Overall, the pore size must be small enough to withstand the mechanical loadings and large enough to allow capillaries to grow as well as nutrient and waste. From the literature, it is desirable to have percentage porosity higher than 70% which corresponds to y=0.7. By using this, an appropriate beam thickness can be calculated. The following values have been calculated and chosen for this design:

Table 11: Pore size, beam thickness and percentage of porosity used for Design 1.

Design 1	
Pore Size	400 μm
Beam Thickness	200 μm
Percentage of Porosity	74%

The following design has been produced on Inventor professional (Autodesk, 2012):

Design 1

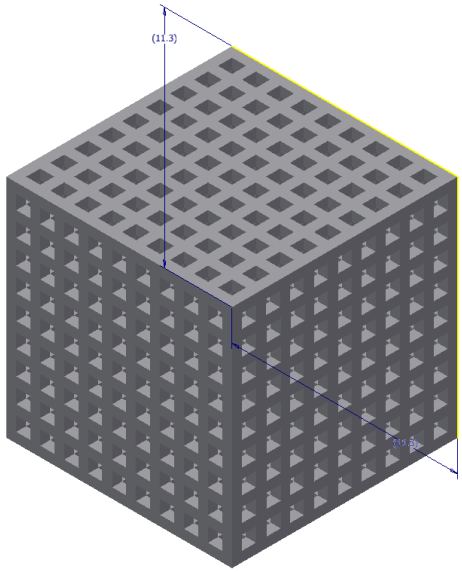

Figure 25: AutoCAD design of a cubic porous scaffold with 400 µm pore size and beam thickness of 200 µm.

Figure 25 (Design 1) was used as a primary prototype to study different rapid freeform fabrication techniques available at the University of Sheffield. Design 1 was exported as a STL file which needs to be converted to a G-code file format in prior to be imported to any SFF technology instrument. The G-code file is the interpreted file from a CAD model that represents the movement of print head layer-by-layer. The available programs for the conversion of STL file to G-code are such as Axon (Bits from Bytes, USA) or free online slicer software such as KISSlicer and Slic3r. The first SFF technology that was assessed for compatibility was Fused Deposition Modeling (FDM), which will be discussed in more details in the following section (Section 5.2).

5.2 Fused Deposition Modeling SFF Technology

RepRap pro Mendel® and RapMan® 3.1 are two types of FDM techniques available at the University of Sheffield. The technology was previously explained in more details in section 2.4.2.1.2. This technique requires the initial materials/ polymer to be fed into the machine in form of filaments with certain thickness specific to the model of FDM instruments. The rod thickness of each model differs which is shown in Table 12.

Table 12: The filament thickness specifications required for RapMan® 3.1 and RepRap Pro Mendel® FDM technologies.

	Filament Thickness (mm)	Nominal Thickness (mm)	Maximum Thickness (mm)
RapMan 3.1®	3	2.88	3
RepRap Pro Mendel®	1.75	1.75	1.75

As it was previously mentioned in section 5.1, Figure 25 was used as a prototype to assess the feasibility of each SFF technique to reproduce and print the design. In prior to fabrication via SFF technologies, the STL file, which is exported from AutoCAD software, must be converted to G-code. Axon 2 (Bits from Bytes, USA) is a free software provided with RapMan® 3.1 to convert STL files to G-code and stimulate its parameters such as the layer height. RapMan® 3.1 is only compatible with Axon 2 software in order to stimulate parameters within this model's limitations. However, after changing the parameters such as the layer height to 200 μm, the software distorts the original design of Figure 25 and refuses to process the design.

The error is due to the fact that the software has been set to only recognise the resolution higher than 1 mm.

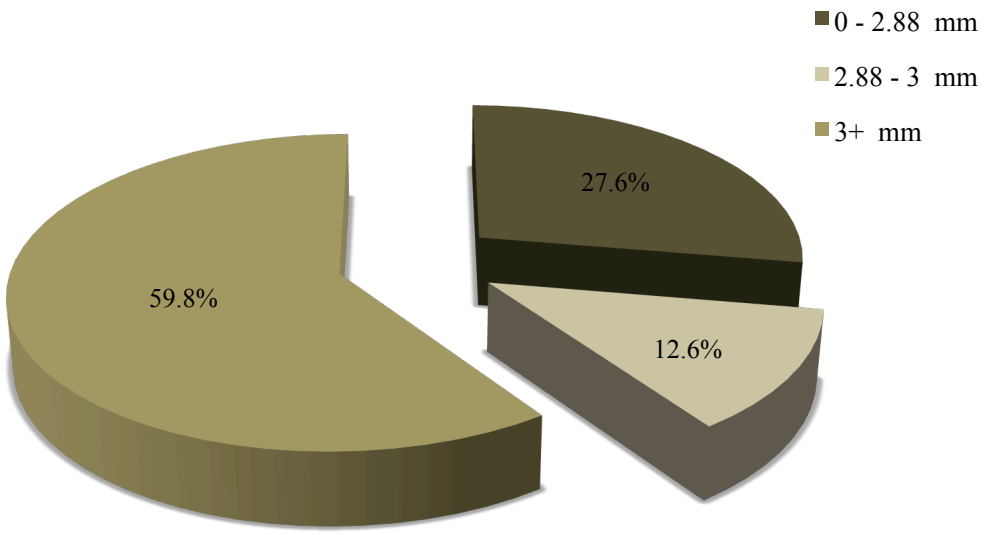

Figure 26: PCL filament thickness percentage distribution manufactured via polymer rod extruders.

The main limitation associated with this technique is the availability of the biocompatible medical-grade polymer filaments. The current filaments used for fabrication of 3D structures by FDM are non-biocompatible or medical-graded. In order to fabricate Design 1 using the mentioned FDM techniques, the first step involved manufacturing biocompatible polymer rods using medical grade biocompatible polymer granules via filament extruder instruments. As it was mentioned earlier, Table 12 specifies the filaments thickness required by each FDM machines; therefore the fabricated biodegradable filaments must have precise thickness within a certain range. An attempt was made to make medical grade PCL filaments with precise thickness required by each FDM technology using Rondol® twin-screw extruder (Rondol®, UK, diameter 10 mm) machine. The extruder technique focuses on melting thermoplastic polymers and extruding in form of polymer rods, which is fed to the extruder in from of polymer granules or powders.

The thickness of manufactured filaments is controlled by the diameter of extrusion point. However if the diameter of the extruder is not specifically accurate, the closest extrusion diameter is chosen and its thickness is further altered by other parameters such as the speed of collection. In other words, as the speed of collection increases the lower the thickness of collected filament would be. Due to the manufacturing limitations, the most appropriate extruder diameter was 10 mm, therefore in order to achieve a lower filament thickness (3 mm), the filaments were collected manually at the collection point and were pulled to produce thinner rods. However, it is very hard to maintain continuous and consistent thickness of filament.

Overall, the twin screw extruder available at the University of Sheffield (Rondol®, UK) was only compatible with 3 mm thickness filaments, which can only be used with RapMan® 3.1 model. In total 250 g of PCL was fed into the extruder which produced ~ 20 m of PCL filaments and only 12% (Figure 26) had the required thickness for RapMan® 3.1 FDM technology hence functional. However unfortunately this extruder is used for industrial applications and is contaminated with many non-biological polymers, which ultimately affects the biocompatibility of PCL rods extruded. The contamination of extruded filaments could not be resolved by sterilisation process as the contamination had penetrated within the filament, which would have only been released during degradation process and would result in immune reaction once implanted.

5.3 Robocasting SFF Technology

In order to assess the feasibility of robocasting SFF technology to fabricate pre-customised structure designs, the G-code was generated manually on the relevant software. The micro-structure of the woodpile structure was chosen in advance to meet the specifications for intramembranous ossification of craniofacial defects as it was mentioned previously in section 5.1. The macro-structure of woodpile design comprised of total dimensions of 11 × 11 mm with 400 μm spacing and 150 μm rod thickness. Based on this design and Equation 1, the proposed design had approximately 80% porosity, which offers open interconnected structure beneficial for nutrient and wastage diffusion of attached cells.

The robocasting fabrication ink was prepared via dissolution of PCL granules in dichloromethane and subsequently addition of ethanol to achieve more appropriate polymer ink viscosity hence rate of polymer ink drying. In order to print the designed lines, the consolidation of ink is accomplished via harmonising the speed of printing with the drying rate of the ink. It was founded that employing relatively lower printing speed (<4 μm/s) had resulted in initially achieving thicker printed lines, however later the ink would consolidate within the dispensing nozzle, hence blockage and discontinuous of printed ink. On the other hand, employing relatively higher printing speed (>4 μm/s) had resulted in thinner printed lines or in some cases discontinuous of printing (see Figure 29). The first 2 layers of the structures were printed and their thickness and spacing were investigated using Figure 27 and Figure 28, the findings are shown in Figure 30.

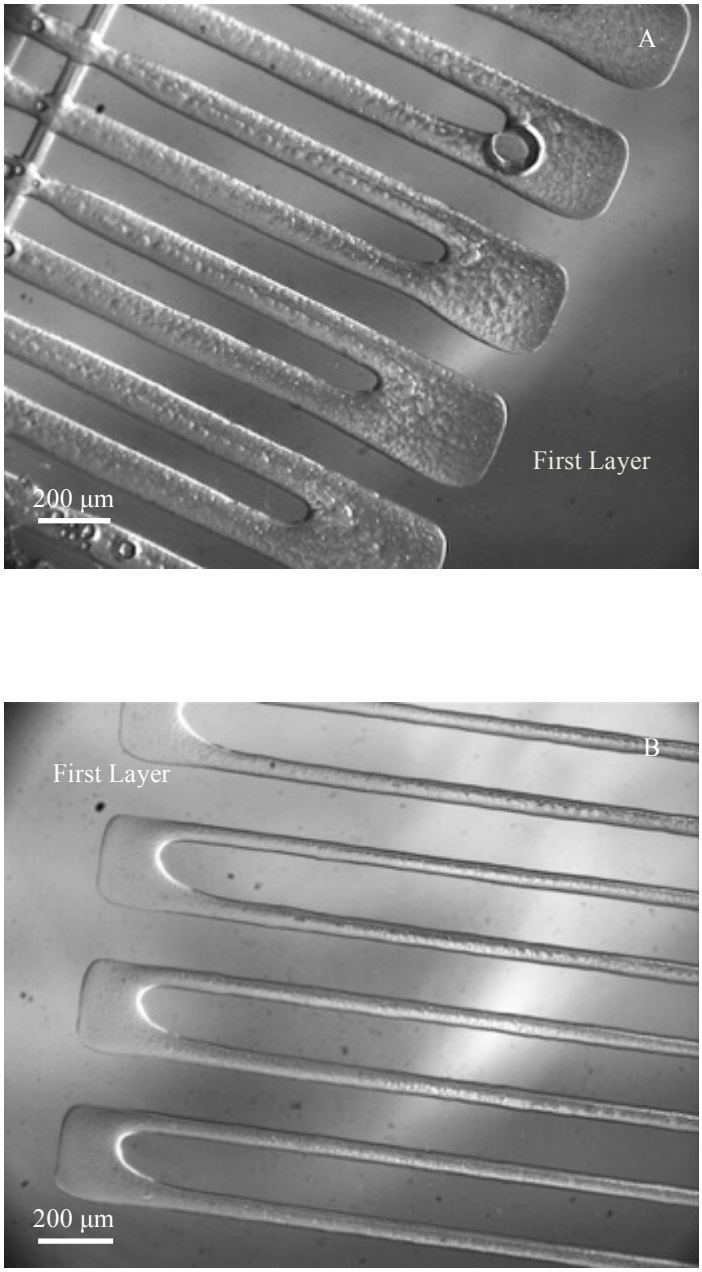

Figure 27: (A-B) Light microscopy micrographs of first layer printed PCL rods fabricated via robocasting technology, all the structures above have been printed with inner nozzle diameter of 0.10 mm.

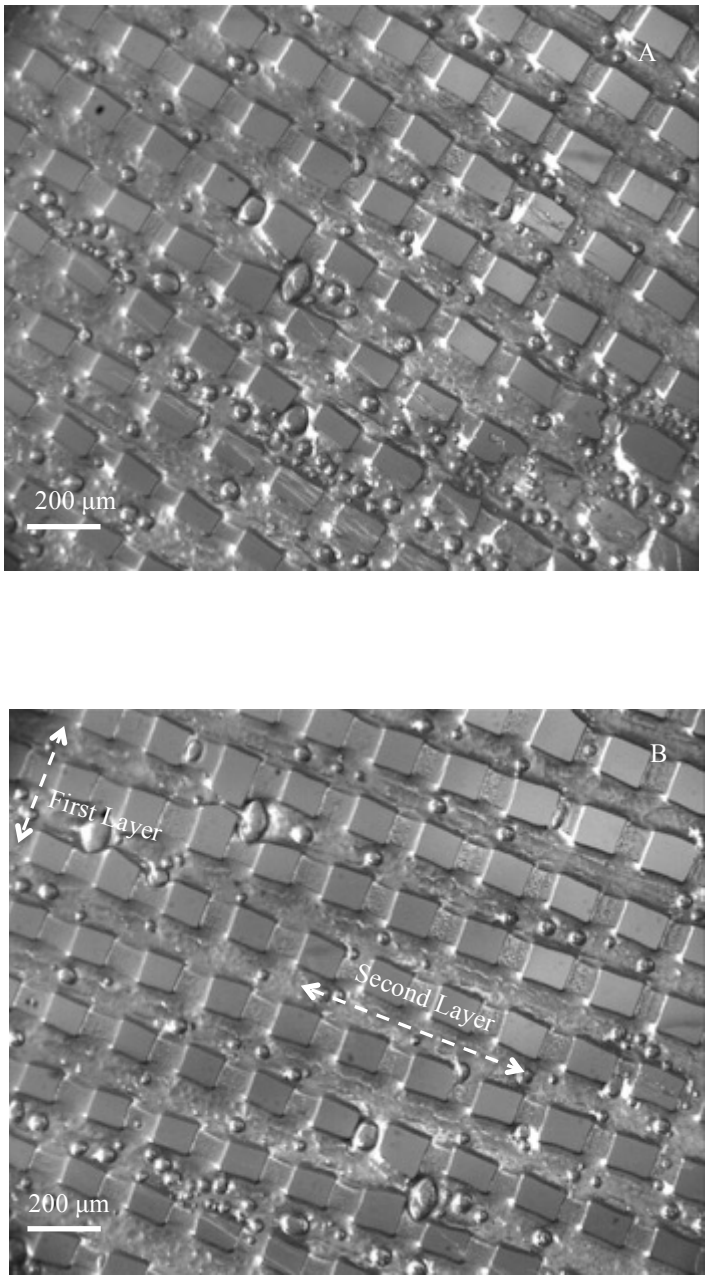

Figure 28: (A-B) Light microscopy micrographs of first and second layer of fabricated pure PCL rods printed via robocasting technology, all the structures above have been printed with inner nozzle diameter of 0.10 mm.

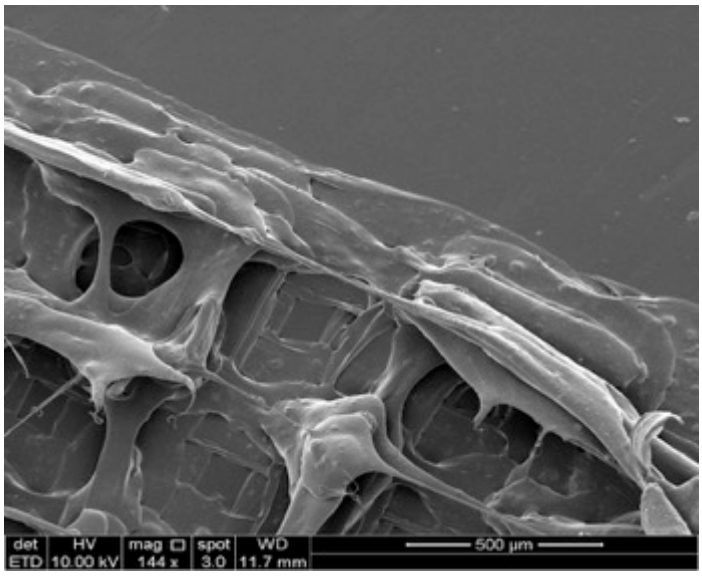

Figure 29 SEM micrograph of fabricated four successive layers manufactured via robocasting SFF technology (scale bar 500 µm).

As shown in Figure 27 and Figure 28, the first layer and second layers were reproduced successfully, resulting in a relatively precise structure. The thickness of fabricated lines were determined based on Figure 27 and Figure 28, which is approximately 76.4 µm for first layer and 100 µm for second layer. However, both printed layers exhibited lower line thickness compare to the proposed design. Fabrication of consecutive layers without changing the printing ink resulted in discontinuous of printed lines as the solvent evaporates over time and results in higher viscosity hence printing non-continuous lines.

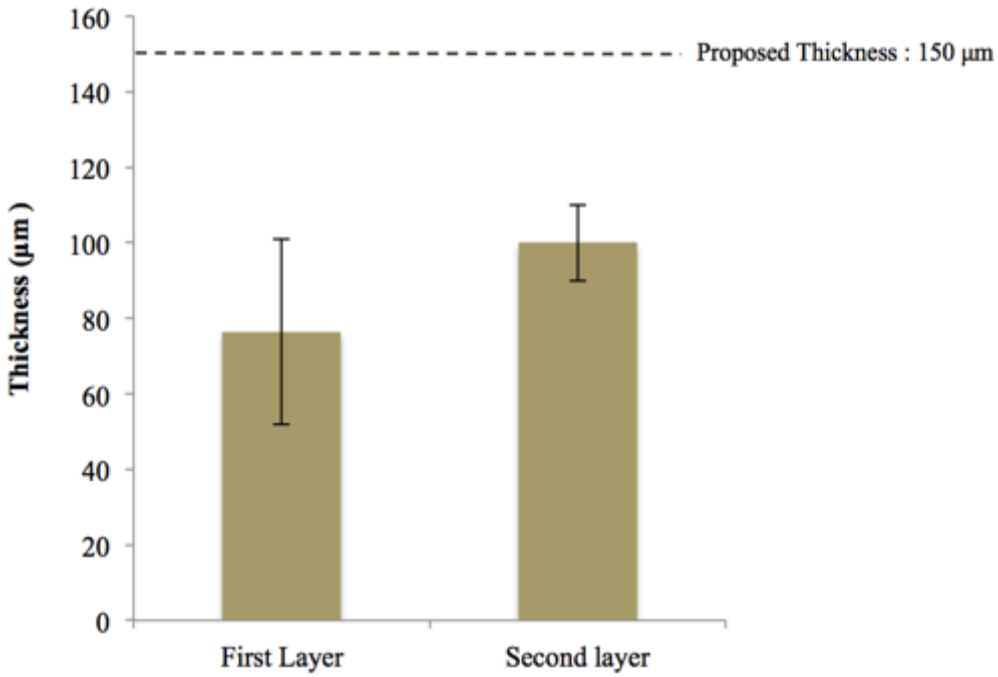

Figure 30: PCL printed rod thickness of first, second and proposed design (n=15).

In order to replicate the pre-customised designs in medical field, it is crucial to achieve the design in high accuracy. However, the robocasting SFF technology has shown less feasibility to meet the requirements essential for a reasonable SFF technology and this is due to the relatively high number of variable parameters such as liquid flow/ viscosity, dispensing pressure, dispensing nozzle size, translational stage movement's speed. One of the most important advantages of SFF technology is the ability of technology to replicate pre-customised designs in a time-efficient matter. However comparing robocasting technology to other SFF technology, robocasting has proven to be more time consuming with lower accuracy.

5.4 Laser-Based SFF Technology

5.4.1 Digital Micromirror Device Stereolithography

The DMD projection stereolithography system was used to fabricate patterned design (see Figure 12 and Figure 13) in order to reconstruct the proposed bitmap. The bitmap image representing the micro-structure of each layer was developed and loaded into relevant software. The image was then reflected on the resin using the DMD that consist of many small mirrors (768 rows of 1024 micromirrors) which each corresponds to a bitmap. Each micromirror represent a bitmap which turns "on" or "off" by rotating positive 12 ° or negative 12 °, in case of presence of bitmap the micromirror will turn "on" and reflects onto the focusing lens hence the resin. For fabrication of 3D structures, the subsequent layer bitmap is shown on DMD and the resin is lowered on a translational stage for curing following layers.

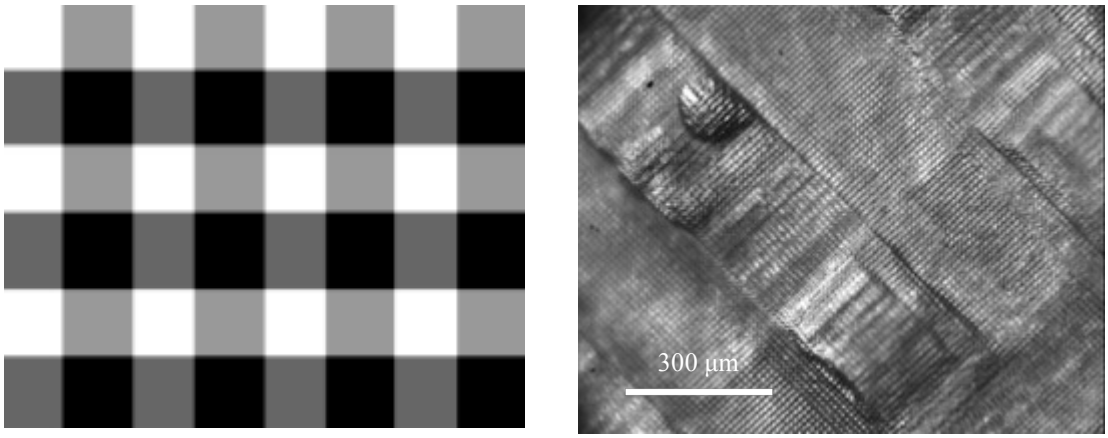

Figure 31: Bitmap input (873 × 710 pixels) used for fabrication of 3D structure (PEG) using DMD stereolithography and the resulting 3D structure fabricated (scale bar 300 µm).

In order to investigate the DMD stereolithography abilities further, supplementary attempts were made to recreate 3D structures based on design 3 (see Figure 13), initially with the non-bioresorbable photocurable PEG material and later biodegradable PLA. The 3D fabrication of the designed bitmap (Design 3, see Figure 13) was developed using a blue laser source. As shown in Figure 32, the resultant structure was fabricated successfully and was exposed to U.V lamp radiation in order to eliminate photoinitiator camphorquinone as it may affect the biocompatibility behaviour of scaffolds. The fabricated structure displayed relatively well-defined macro-structure, which could be improved further by varying intensity and curing situations such as exposure time as well as layer thickness.

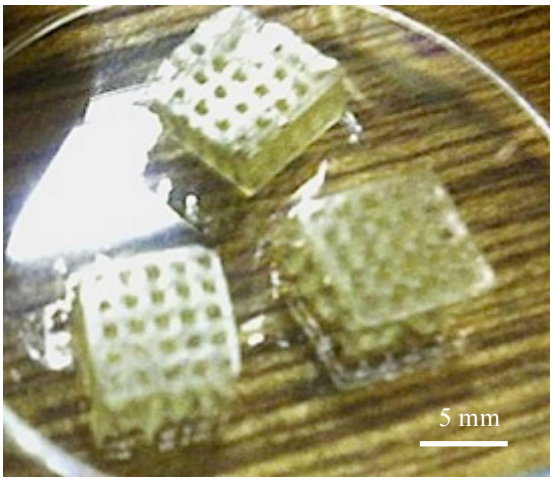

Figure 32: 3D PEG scaffolds fabricated via DMD stereolithography recreating the designed bitmap (see Figure 13) [Images courtesy of C.Gabbott].

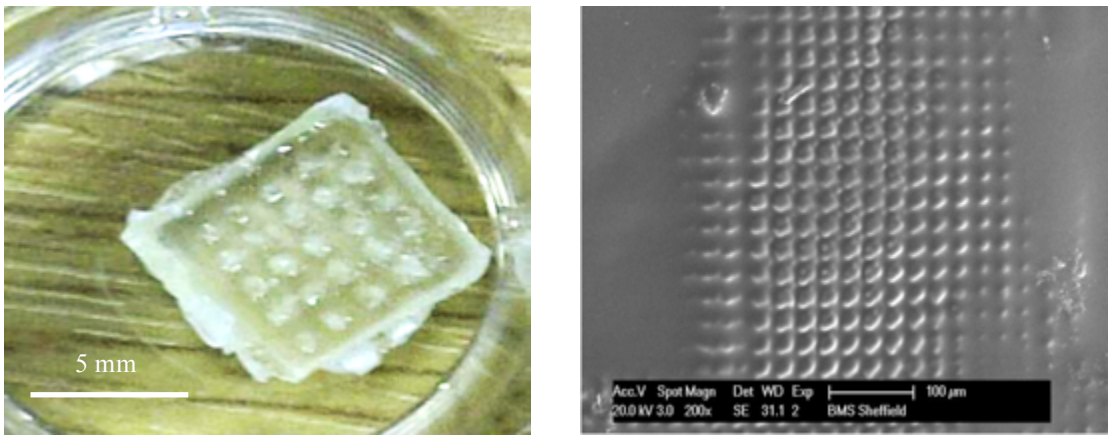

Figure 33: SEM micrographs of fabricated PLA micro-structure using DMD stereolithography [Images courtesy of C.Gabbott].

Upon the successful fabrication of 3D structures using DMD stereolithography, further attempts were made to recreate the bitmap from biodegradable and biocompatible photocurable PLA materials. Scaffold of photocurable PLA was produced recreating the bitmap design 3 (see Figure 13) with an exposure time of 4½ minutes for each layer. The structure was manufactured using layer-by-layer approach and Figure 33 shows the morphology of cured top surface of the 3D structure and it is evident that the structure was recreated accurately, however the morphology of the pores is less accurate and well defined toward the right hand side, which can be improved further by achieving a better balance between curing exposure and intensity of curing. However, this may also be due to excessive curing exposure.

To investigate DMD technology further, the incorporation of HA particles into photocurable PLA was carried out to recreate the user defined 3D structure and this is due to the known osteoconductive properties of nHA for applications in bone tissue engineering. As it is evident in Figure 34, the fabricated structure does not represent the proposed bitmap design very well hence not accurate, which can be due to light scattering caused by micro-scale HA particles that can be improved further by using employing smaller HA particle size (nHA).

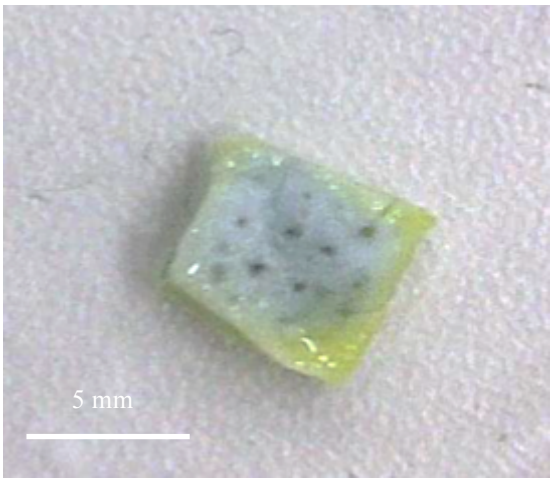

Figure 34: PLA/HA (20% w/w) structure recreated from design 3 via DMD stereolithography [Images courtesy of C.Gabbott].

5.5 Stereolithography

5.5.1 Non-biodegradable Acrylate Based PolyHIPE

A significant constraint in employing stereolithography in tissue engineering field is deficiency of suitable and biocompatible photocurable materials, however this SFF technology offers time efficiency, high accuracy and reproducibility. Therefore, it is reasonable to investigate alternative materials to be employed via this technology. One of the most attractive and promising materials is polyHIPEs. As it was mentioned previously in section 2.4.1.3, polyHIPEs are range of versatile materials in which the porosity is inherited via phase separation templating. The porous nature of these materials together with its tunability toward pore sizes and mechanical properties are highly cherished and attractive in tissue engineering applications. In this section, fabrication of customised 3D polyHIPE structure is investigated.

Conventionally polyHIPE synthesis is based on thermal polymerisation of the continuous phase which is a relatively long process and can continue up to 24 hours [112]. Hydrophobic styrene and its derivatives are known as the most conventional monomers employed in polyHIPE chemistry together with divinylbenzene crosslinker [52,108,113,114]. However, acrylate based monomers such as 2-ethylhexyl acrylate, isobornyl acrylate and butyl acrylate are known to form stable emulsions and polyHIPEs [108,113–115]. In order to investigate the possibilities of fabricating polyHIPE-based materials via photopolymerisation, initially it was attempted to assess the possibilities by employing a conventional acrylate based polyHIPE materials. In this section, acrylate based polyHIPE materials were prepared by co-polymerisation of 2-ethylhexyl acrylate and isobornyl acrylate together with crosslinker triacrylate at room temperature. This polyHIPE material is similar in employing elastomer monomer EHA and IBOA monomer, however the major difference is in the polymerisation process of this polyHIPE material, which is via photopolymerisation rather than thermal polymerisation. The water content of EHA80 polyHIPE was chosen to be relatively low, as it is known that high water level content would be disadvantageous for structuring as it destabilises the emulsion.

Table 13: Composition of photopolymerised EHA80 polyHIPE.

	EHA[a]/*g*	IBOA[b]/*g*	Triacrylate[c]/*g*	PI[d]/ *g*	Surfactant[e]/*g*	Water/*mL*	<D>[f]/*μm*
EHA80	3.66	1.56	1.4	0.34	0.199	28	33.3

[a] 2-Ethylhexyl Acrylate

[b] Isobornyl Acrylate

[c] Trimethylolpropane Triacrylate

[d] Photoinitiator (Diphenyl(2,4, 6-trimethylbenzoyl) phosphine oxide/ 2-hydroxy-2-methylpropiophenone)

[e] Hypermer B246

[f] Average void diameter measured by SEM.

The morphology of synthesised polyHIPEs was investigated via SEM showing that the polyHIPE structures were successfully fabricated using UV irradiation (see Figure 36). The structures exhibit open cellular macro-structures with microinterconnected porosity and pore sizes varying between 10 - 70 μm. The pore diameters were investigated using Image J based on cross sectional polyHIPE disks and the average pore diameter is 33.3 μm (mean standard deviation: ±10.5 μm) after applying statistical correction factor [116]. The statistical correction factor is applied to normalise any underestimations of measured pore diameters.

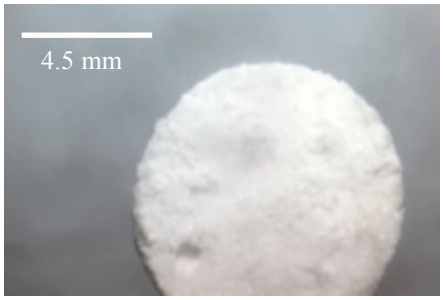

Figure 35: Light microscope image of EHA80 polyHIPE disk bulk photopolymerised with 9 mm diameter dimension.

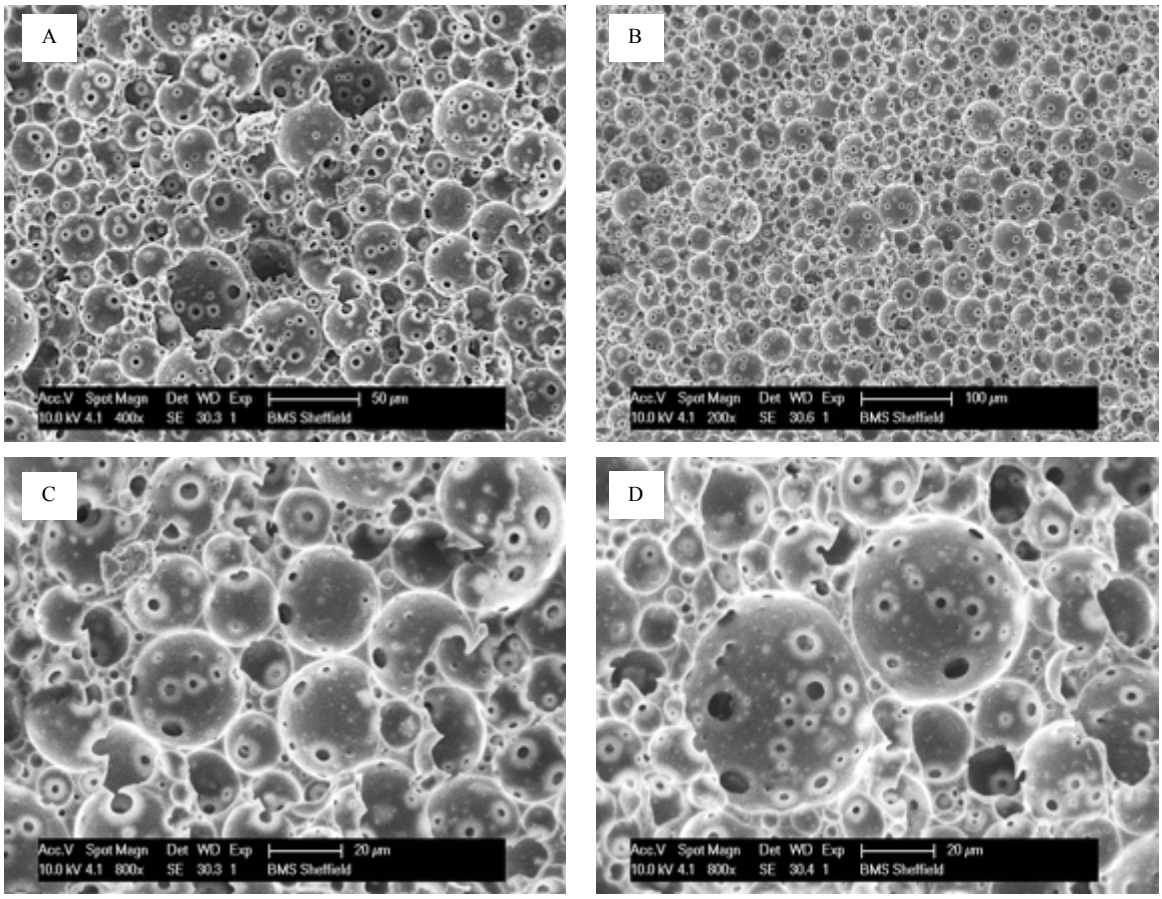

Figure 36: (A-D) SEM micrographs of EHA80 polyHIPE disks (80% nominal porosity) showing the porous interconnected morphology at different magnifications [117].

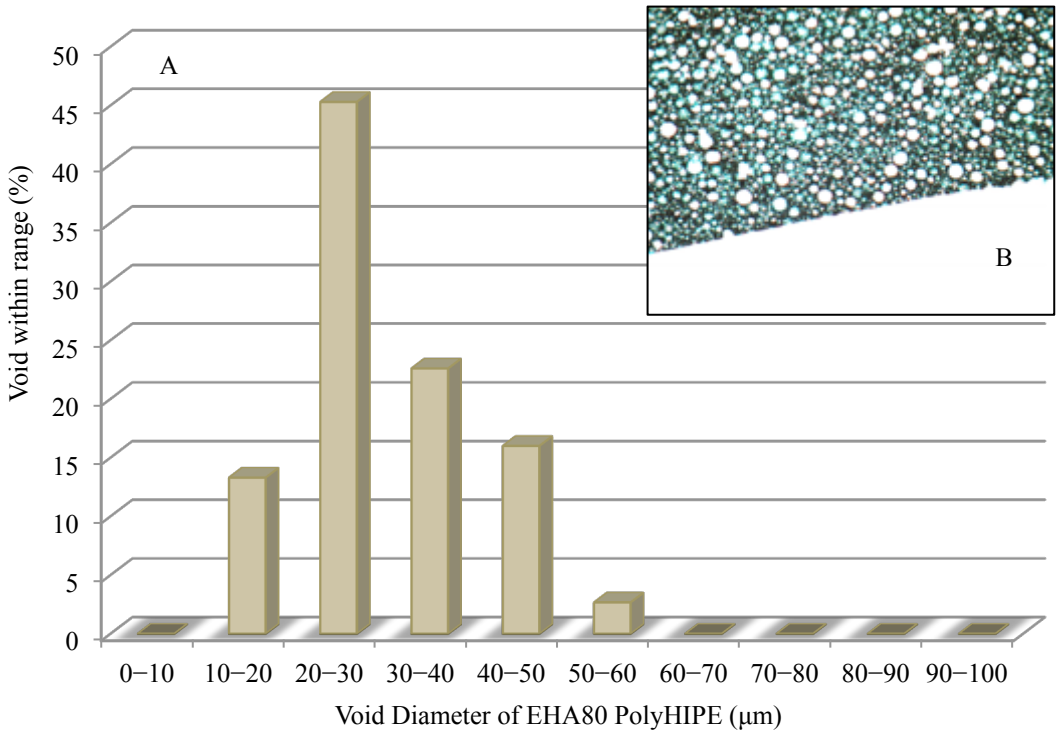

Figure 37: (A) void diameter distribution of photopolymerised EHA80 polyHIPE materials (80% nominal porosity) based on SEM micrographs. (B) porous morphology of cryosectioned EHA80 polyHIPE disk [117].

Following successful photopolymerisation of EHA80 polyHIPE, it was decided to assess biocompatibility of polyHIPE disks hence its suitability for *in vitro* bone tissue engineering models, as this acrylate-based polyHIPE is non-biodegradable. As it was mentioned previously, acrylate based monomers have hydrophobic properties which are beneficial for formation of stable emulsion and disadvantage for cell attachment and proliferation. Therefore, in prior to assess the polyHIPE samples for biocompatibility, some of samples were treated with acrylic acid plasma polymerisation for post-modify the surface and increase its hydrophilic surface properties. *In vitro* cell culture study was carried using MG63 cell line on bulk EHA80 polyHIPE disks for 7 days period together with tissue culture plastic as positive control as demonstration of cell's proliferation and attachment of polyHIPE materials. To avoid polyHIPE sample floating in cell culture medium due to its porous nature, medical graded stainless steel rings were used to secure the samples. Viability and cytotoxicity of the samples were assessed via MTT assay, which a

yellow tetrazolium salt is transformed into soluble purple formazan in presence of viable cells (Figure 38).

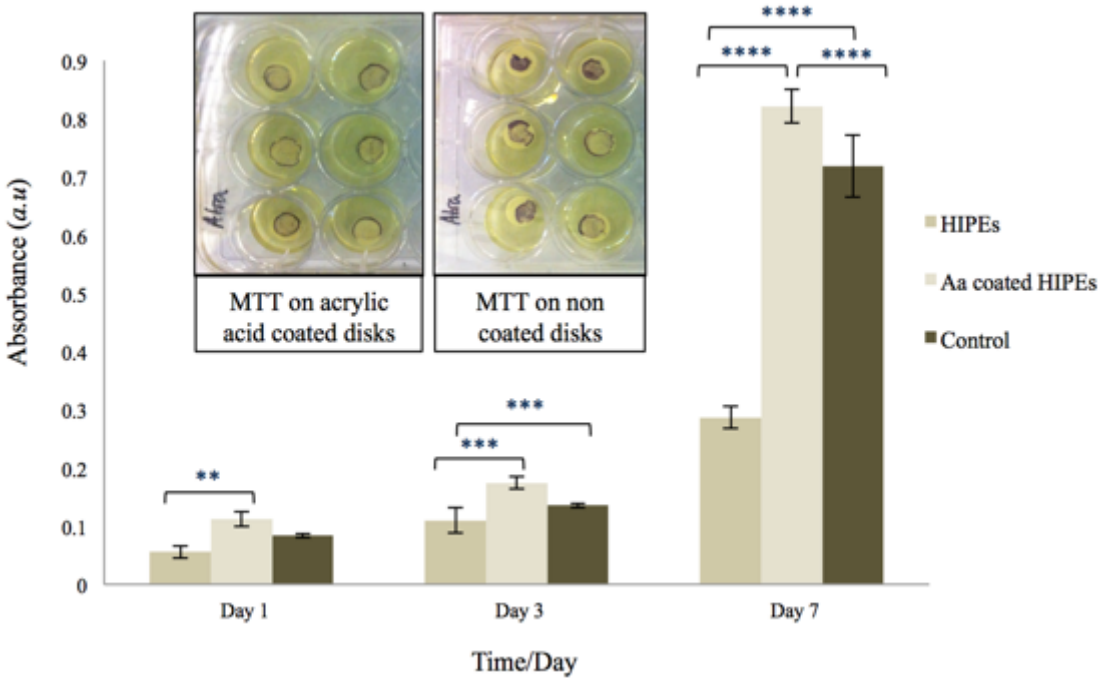

Figure 38: Viability of MG63 cultured on EHA80 polyHIPE disks treated with and without acrylic acid (Aa) plasma polymerisation as well as TCP for positive control at different time points up to 7 days. The error bars represent the standard deviation of mean [117]. Analysis of variance was carried out and tukey multiple comparison was used to show significance difference.

Figure 38 show viability of cells increased with acrylic acid post surface modification via plasma polymerisation at all time points. In other words, the cell growth rate on acrylic acid coated samples was much higher compare to the non-coated EHA80 polyHIPE disks. Therefore, the MTT test suggested that there was no toxicity in EHA80 polyHIPE materials, especially the acrylic acid coated polyHIPE that improves the hydrophilic property of the material. The results indicate significance difference between all samples at day 7 ($P \leq 0.0001$). Day 3 showed no significant difference between positive control and coated EHA80 disks, on the other hand coated and non-coated EHa80 disks were significantly different ($P \leq 0.001$). At day 1 no significant difference were observed for coated EHA80 disks and positive control

and coated EHA80 disks showed significant difference in compare to non-coated ($P \leq 0.01$). Furthermore, the morphology of adherent cells to acrylic acid coated and non-coated EHA80 polyHIPE disks were analysed via SEM (see Figure 39).

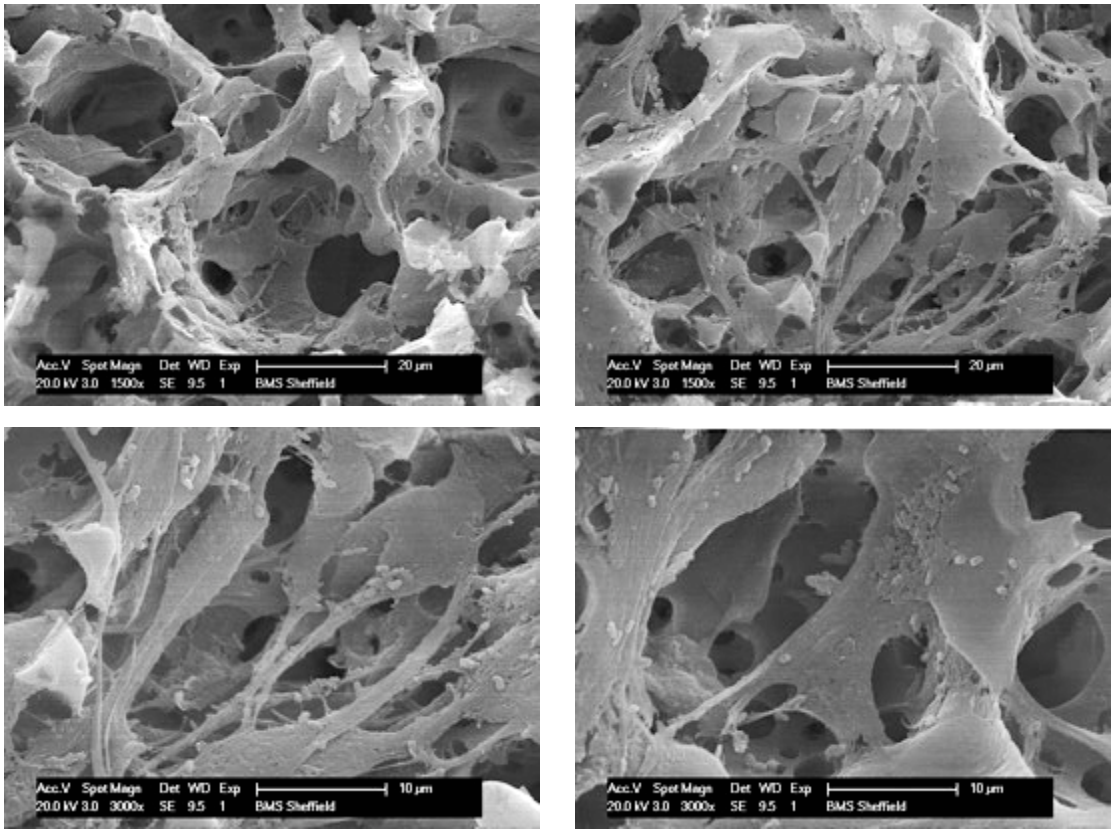

Figure 39: SEM micrographs show the attachment of the cells onto acrylic acid plasma treated EHA80 polyHIPE disks on day 7 [117].

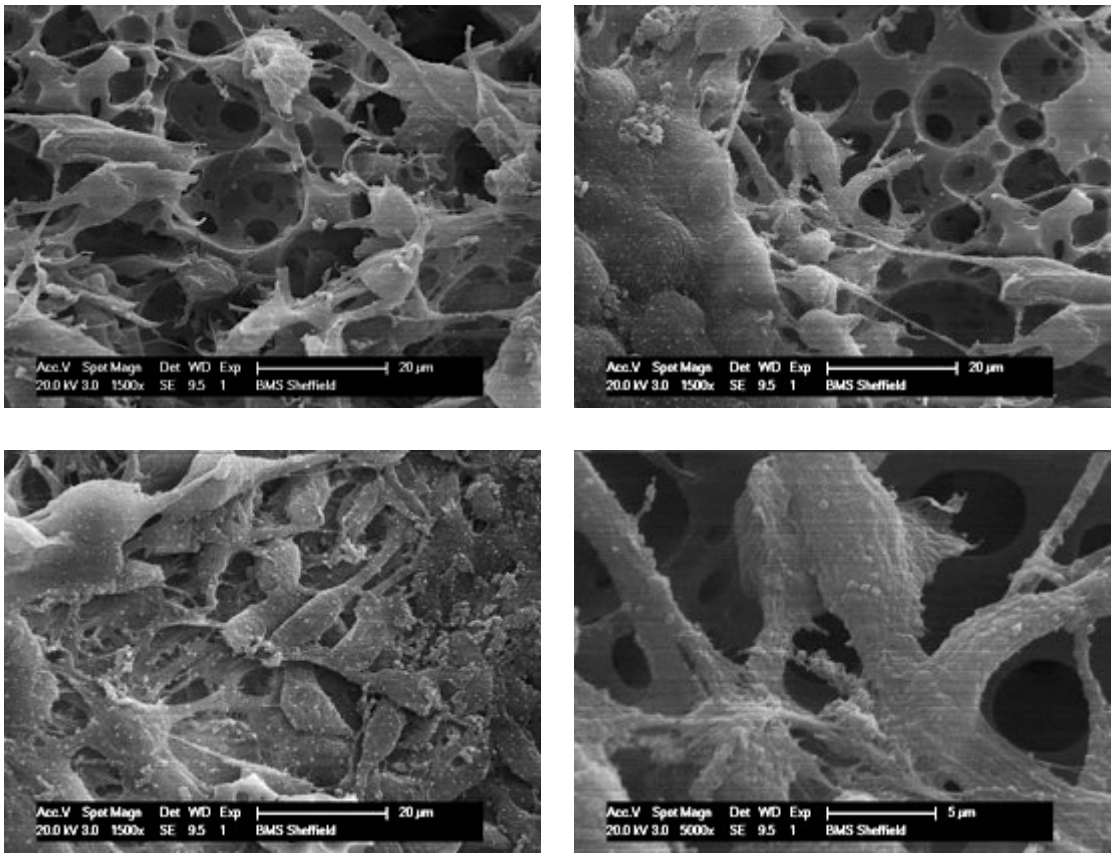

Figure 40: SEM micrographs show the attachment of the cells onto non-treated EHA80 polyHIPE disks on day 7 [117].

SEM micrographs of MG63 cell line seeded onto EHA80 polyHIPE disks show cell growth, attachment and penetration (Figure 39 and Figure 40). Morphology of the adherent cells on acrylic acid coated polyHIPE disks exhibit more flat morphology in compare to the round morphology of non-coated polyHIPE disk attached cells. In further to SEM images, the level of cell penetration within the porous structures were analysed via cryosectioned samples of EHA80 disks stained with DAPI for cell nuclei and FITC-phalloidin for actin cytoskeleton. Based on these micrographs (Figure 41) it is evident that MG63 cells penetrated and integrated successfully within the porous nature of polyHIPE within 50 µm of its depth.

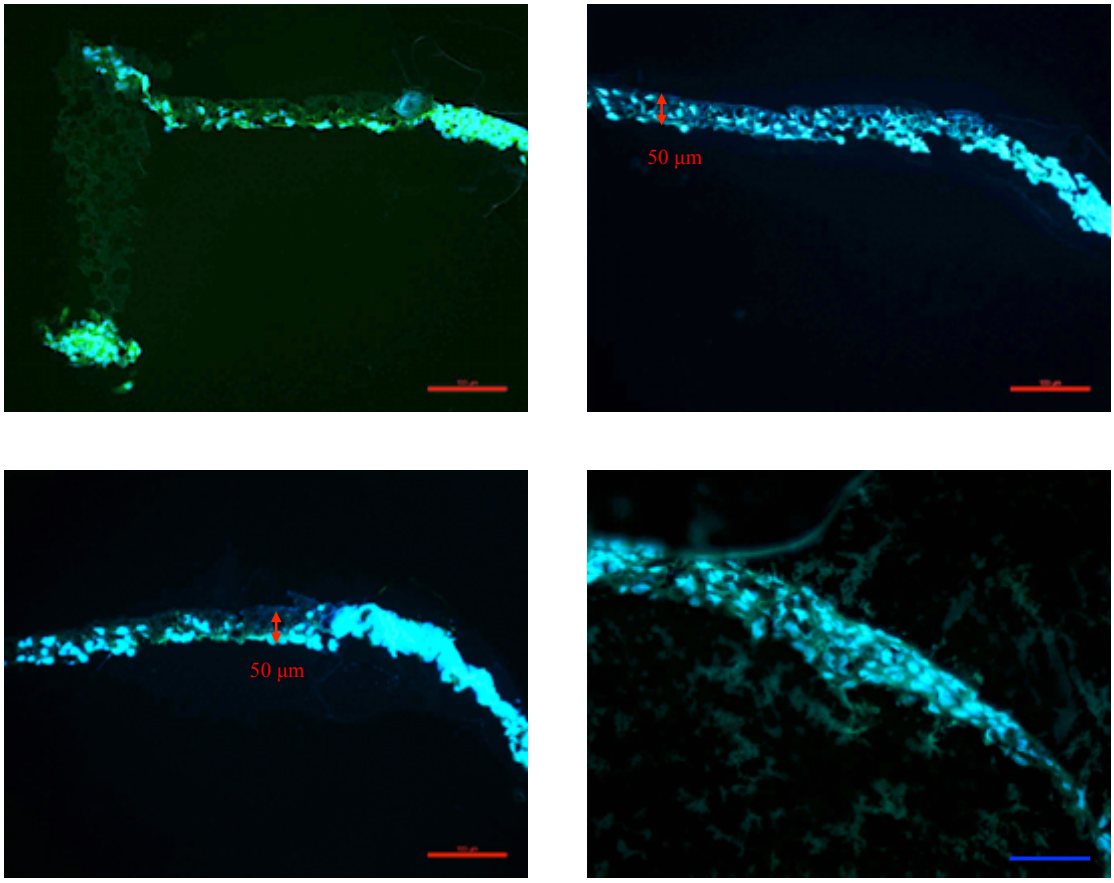

Figure 41: Fluorescence micrographs of EHA80 cryo-sectioned samples cultured with MG63 for 7 days. The samples were stained with DAPI for nuclei and FITC-phalloidin for actin cytoskeleton, some of the porous structure also appears due to its auto-fluorescence nature. (Red scale bar =100 µm) and (Blue scale bar = 200 µm) [117].

5.5.2 Woodpile Fabrication of Non-Biodegradable PolyHIPE

High internal phase emulsion of EHA80 materials was selectively photopolymerised to fabricate 3D woodpile structure via stereolithography in layer-by-layer manner. After successful fabrication of each layer, subsequently a new layer of emulsion was added to ultimately create the 3D woodpile structure, which leads the approach for more complicated structures to be fabricated. Nevertheless, increasing the dimension or quantity of layers will escalate the total fabrication time. The morphology of fabricated 3D woodpile structure was assessed using SEM micrographs (Figure 42).

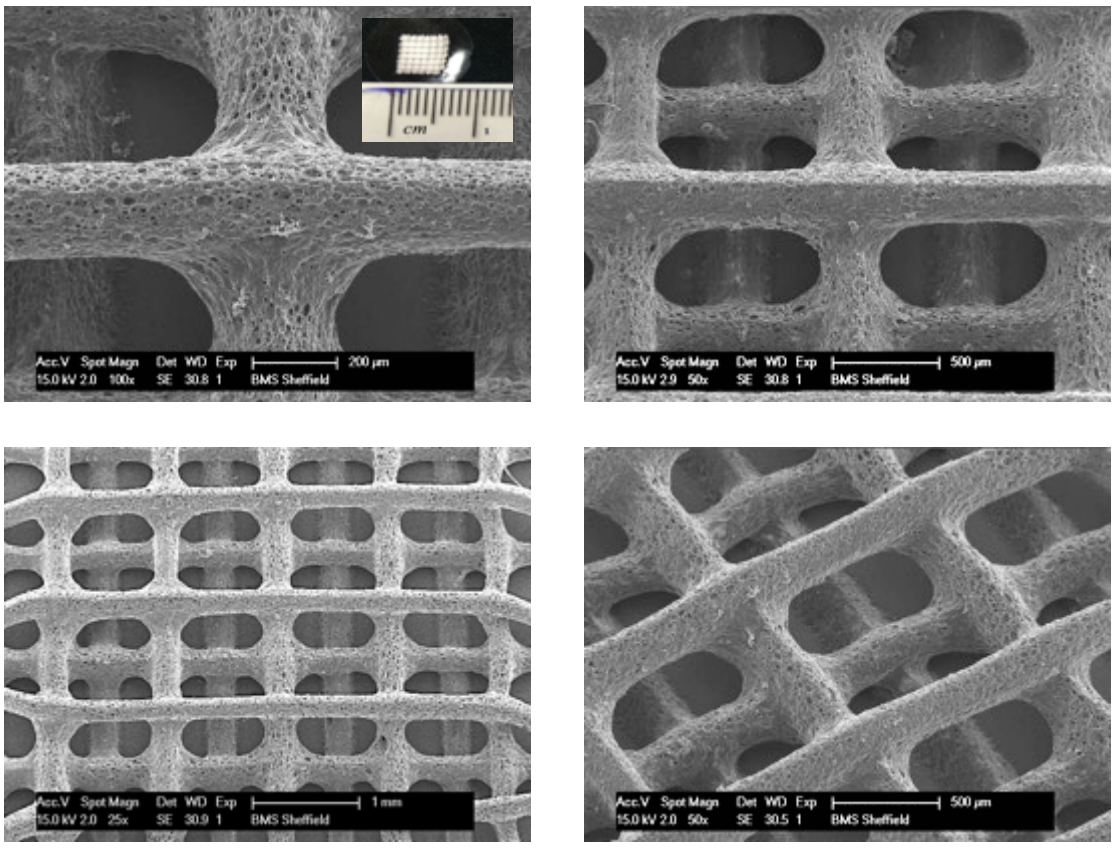

Figure 42: SEM micrographs of EHA80 3D woodpile structure fabricated via single-photon laser write stereolithography with dimension of 0.5 cm × 0.5 cm [117].

The morphology and surface assembly of fabricated structures were shown in Figure 42. PolyHIPE characteristic morphology was preserved within the structure, signifying the selective photopolymerisation of the polyHIPE and introduction of pre-designed macroporosity does not affect the inherited microporosity nature of the polyHIPE. The fabricated structure has overall dimension of 0.5 cm × 0.5 cm with four vertical layers. The structure exhibited microporosity of approximately 1 mm and inherited microporosity of 33.5 μm (standard deviation: ± 11.5), which is very close to the microporosity of EHA80 disks (33.3 μm with mean standard deviation: ±10.5 μm (n=25)) measured using Figure 36 in previous section (5.5.1). Concluding that the selective photopolymerisation of the polyHIPE material does not affect the microporosity nature of the material.

The formation of a surface skin has been stated in previous studies when the HIPE material collapses at the surface, in other words a closed non-porous surface is detected when the material is cured alongside materials such as polypropylene [52]. Similar findings were observed showing surface skin forming at the border between the cured and uncured emulsion via selective photopolymerisation which was removed with post polymerisation process including washing and drying phases. It is endorsed that this happens due to collapse of incompletely cured boundary layer on surface of the material which can be caused by the emulsion contributing as a cause of UV-light scattering and secondly loss of reactive materials from the photoinitiated section.

Following successful fabrication of 3D woodpile structures, the biocompatibility of the designed structures was assessed. As it was mentioned earlier, tissue engineering field aims to deconstruct damaged or lost tissue via help of porous scaffolds for the cells to attach and proliferate. However, due to the non-biodegradable nature of these materials, the designed scaffold would only be beneficial for *in vitro* 3D models. Overall the scaffold is designed to maximise nutrient and waste diffusion. The fabricated scaffolds were washed in acetone during post photopolymerisation stages and sterilised in 70% ethanol following PBS washes. Following that, the scaffolds were soaked in culture medium (see section 4.5.6.1) for at least 24 hours

before seeding with MG63 (100,000 cells per sample) and control (TCP) culturing for 7 days and incubated at 37° C with 5% CO_2.

During the study, tissue culture plastic (TCP) was used as a positive control, which may not signify the right foundation for comparison of cell's proliferation. Cells grown on the scaffolds had a larger surface area to the 2D counterpart. To overcome that issue, a separate study was conveyed to determine the true proportion of cells remain on (acrylic acid plasma coated and non-coated) scaffold and lost to the well plate during cell seeding procedure. The study was carried for a short period of time (day 0 of seeding), which indicated that only 36% of the seeded cell density was actually seeded effectively on the acrylic acid coated polyHIPE structure and 26% for non-coated woodpile structure and this is in compare to the tissue culture plastic control during the initial day 0 cells seeding, consequently the outcomes were normalised to account for this. MTT viability assay was carried at time point of day 1, 3 and 7 (see section 4.5.6.4.1) and the resulting blue stains imply presence of viable cells (Figure 43).

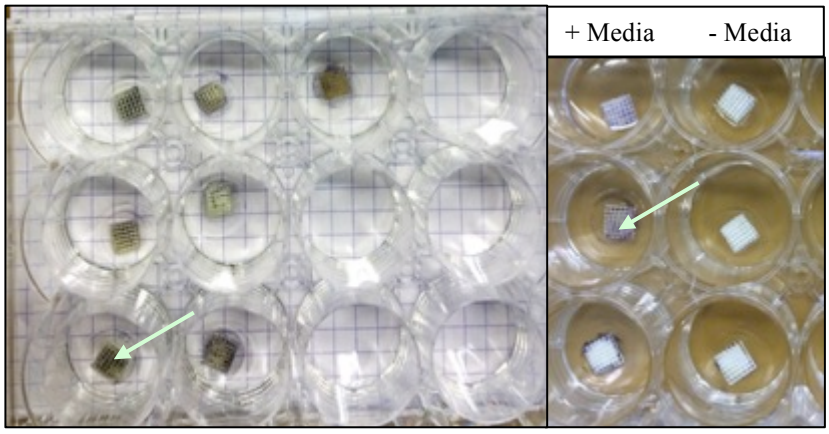

Figure 43: (A) EHA80 woodpile polyHIPE scaffold fabricated via stereolithography undergoing MTT assay showing the blue stain (presence of viable cells). (B) MTT assay carried on pre-soaked scaffold in cell culture medium versus the non-soaked scaffold. The image shows cell culture medium soaking would advance the cell attachment and viability.

The interaction of MG63 cells with EHA80 polyHIPE woodpile structure (acrylic acid plasma coated and non-coated) was investigated using MTT assay and fluorescence confocal microscopy. Human osteosarcoma cells (MG63) have been shown to proliferate successfully on woodpile structure at all investigated time points exhibiting normal cell morphology attached to the structure. However, MG63 cell spheroids have been formed within the acrylic acid coated woodpile structure as it can be seen in Figure 45-B with its cross-sectional view (Figure 45-C) with estimated size of 200 μm. Overall, it can be seen from Figure 44 that both acrylic acid plasma coated and non-coated woodpile EHA80 polyHIPE scaffolds displayed lower cell viability and proliferation activity compare to the positive control at all time points (TCP). However comparing the non-coated and acrylic acid plasma coated EHA80 polyHIPE woodpile structures, it is can be seen that the acrylic acid coated samples have significantly higher cell proliferation after day 3 and 7 ($P \leq 0.0001$). Comparing the plasma coated and non-plasma coated scaffolds with the positive control indicated significant difference at all time points ($P \leq 0.0001$). The significance levels between control and test values were compared with the two-tailed student's t-test and the significance levels are indicated in the graphs.

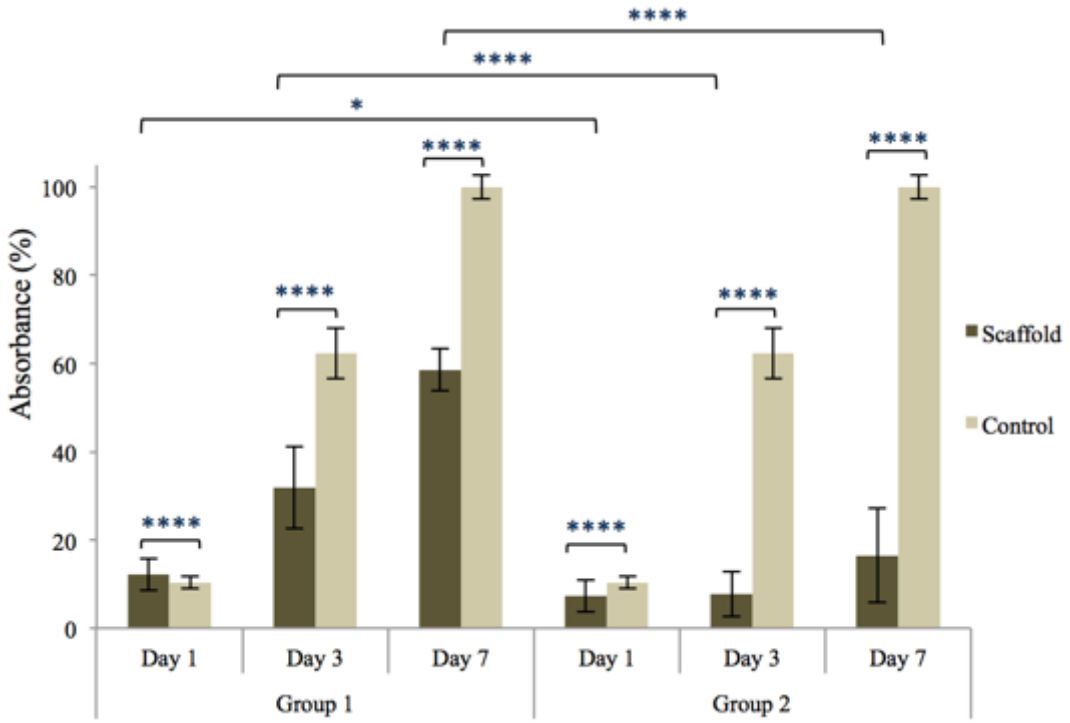

Figure 44: MTT viability assay to investigate *in vitro* biocompatibility of EHA80 polyHIPE woodpile scaffolds cultured with MG63 on acrylic-acid plasma coated woodpile scaffold (Group 1) and non-coated woodpile scaffolds/ plain EHA80 (Group 2) shown as a plot of absorbance against different time points (error bars represent 95% confidence level) [117]. Two-tailed t-test with assumption of equal variance was carried for statistical analysis.

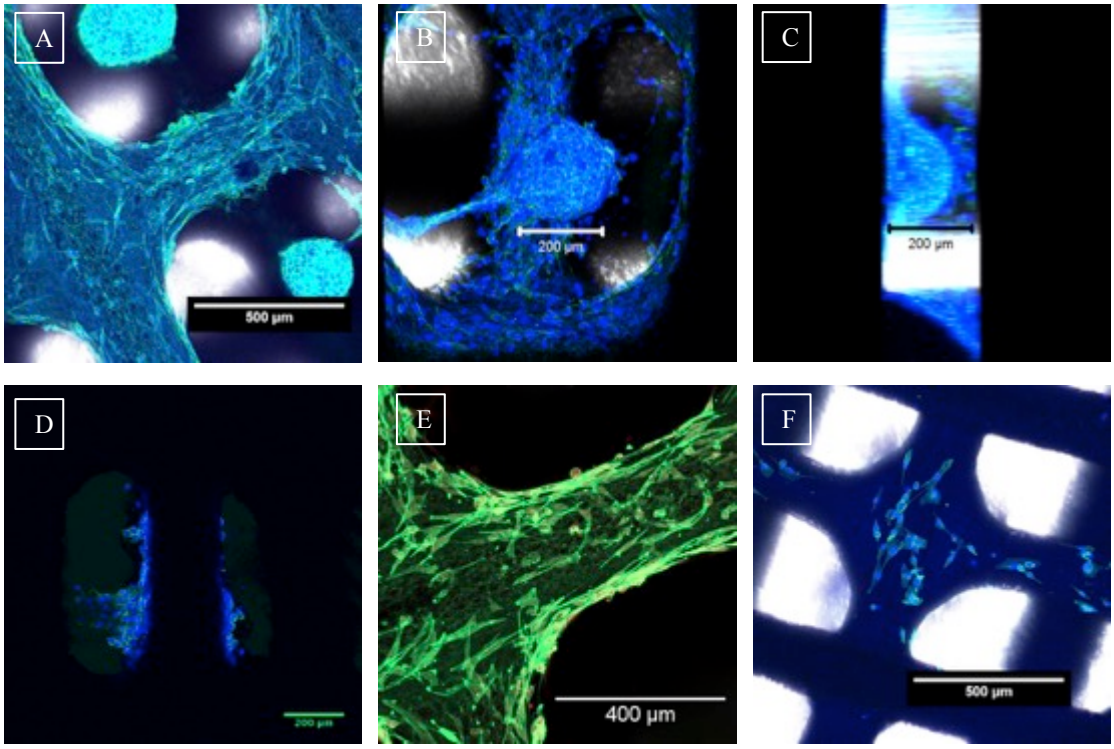

Figure 45: (A-E) Fluoresce micrographs of acrylic acid plasma coated woodpile structure cultured with MG63 for 7 days stained with (A) nuclei stain DAPI and actin cytoskeleton FITC-phalloidin, (B) MG63 cell cluster spheroid (approximate size of 200 µm) formed between macroporous of acrylic acid coated woodpile structure (C) cross sectional view of formed MG63 spheroid (D) bottom layer of the woodpile structure (E) TO-PRO-3 nuclear counter stain and FITC-phalloidin actin cytoskeleton stain. (F) Non-coated plain EHA80 polyHIPE woodpile structure seeded with MG63 for 7 days and stained with nuclei stain DAPI and actin cytoskeleton FITC-phalloidin [117].

5.5.3 Developing Degradable PolyHIPEs

5.5.3.1 Trithiol - Penta/Hexa-Acrylate PolyHIPEs

The synthesis of trimethylolpropane tris (3-mercaptopropionate) and dipentaerythritol penta-/hexa-acrylate based on thiol-ene chemistry was previously reported by Caldwell *et al*. under different mixing conditions [57]. The oil phase consists of DPEHA, trithiol, photoinitiator, surfactant and DCE, which then the water phase were added to drop wise at room temperature while mixed continuously under high shear stirrer (1000 rpm). Upon the successful formation of an emulsion at two diverse nominal porosities (80% and 85%) that is evident in form of a white paste, the emulsions were photopolymerised under UV radiation. The resulting material was washed with acetone to eliminate any aqueous phase and was left to air dry in prior to scanning electron microscopy. Furthermore it was attempted to manufacture 90% nominal porosity of trithiol-DPEHA polyHIPEs under high speed mixing (see Table 5 for formulations) which resulted in failure of emulsion formation.

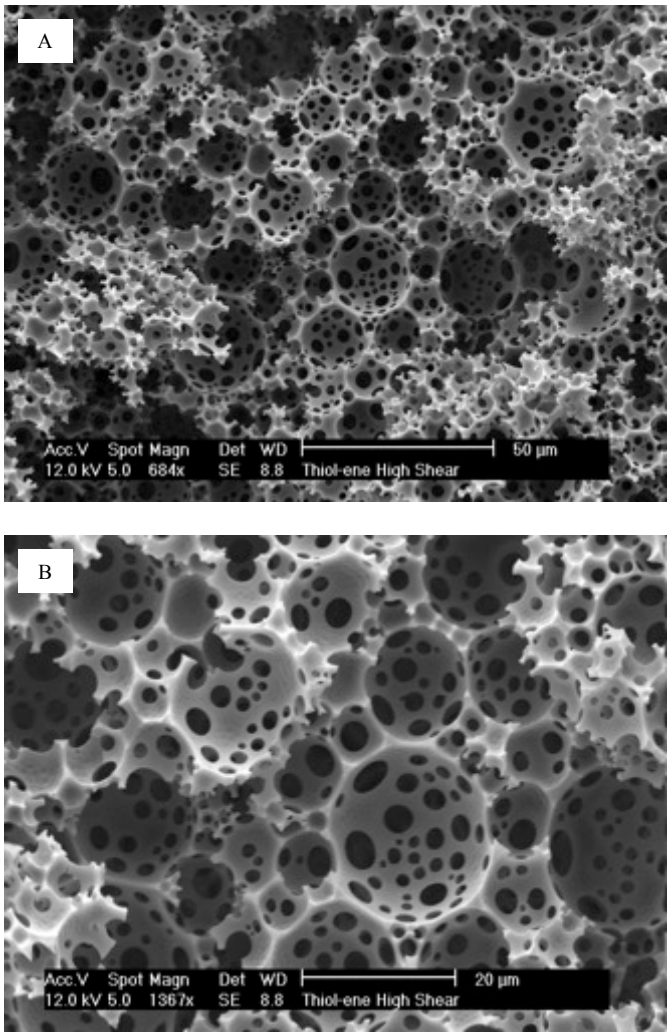

Figure 46: (A-B) SEM micrographs of 80% nominal porosity trithiol-DPEHA polyHIPE showing open cellular interconnected micro-structure.

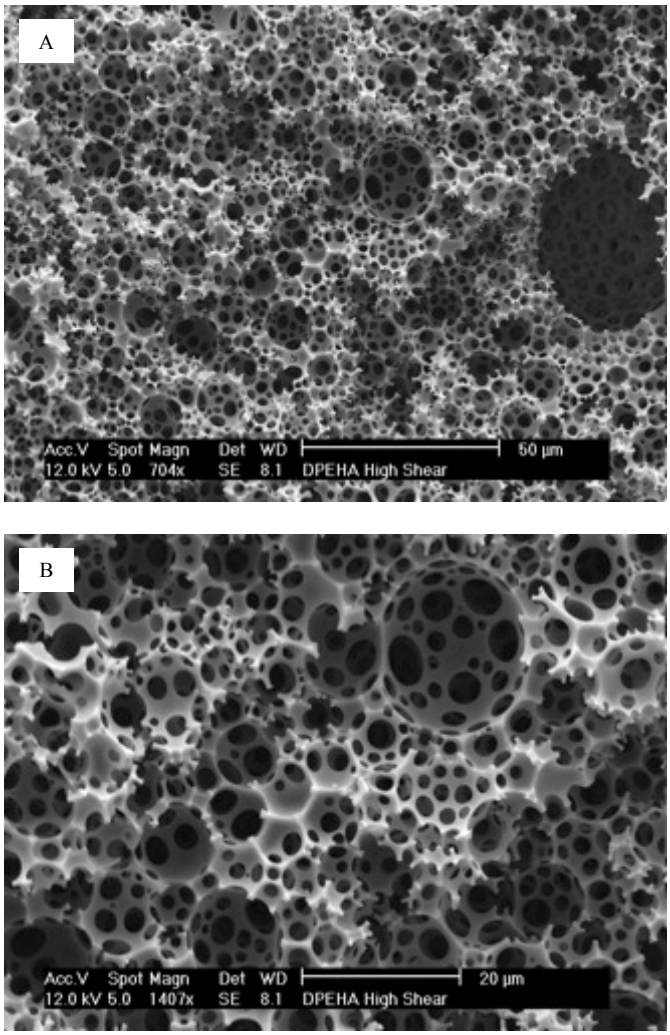

Figure 47: (A-B) SEM micrographs of 85% nominal porosity trithiol-DPEHA polyHIPE structure showing open interconnected micro-structure.

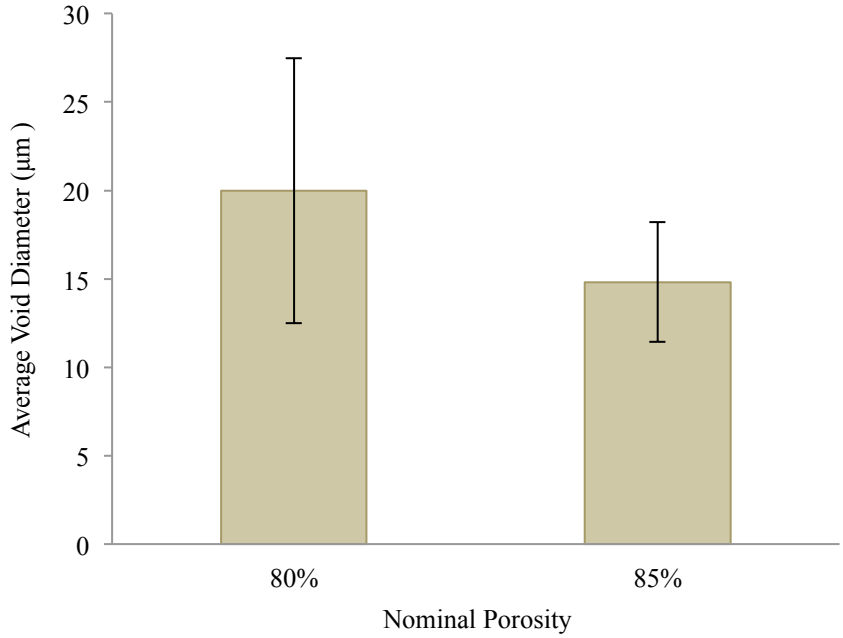

Figure 48: Average void diameter of trithiol-DPEHA polyHIPE measured via SEM micrographs using image J.

The average void diameter was investigated by SEM image analysis after statistical correction factor applied (see Figure 48). The measured void diameter of successful trithiol-DPEHA polyHIPE materials (85% nominal porosity) was found to range between 10-22 µm and 11-42 µm for 80% nominal porosity (see Figure 48 and Figure 49). The influence of higher emulsion mixing speed was investigated by comparing the finding with the work reported by Caldwell *et al.* which showed the 80% nominal porosity trithiol-DPEHA polyHIPE synthesised by via an overhead stirrer (380 rpm) to the investigated sample manufactured with high shear stirrer at noticeably high stirring speed (1000 rpm) shows that higher mixing speed will result in smaller void diameter [57]. It was found that the average void diameter of 80% nominal porosity was estimated as 20 µm in compare to 34.2 µm founded by Caldwell *et al.* [57].

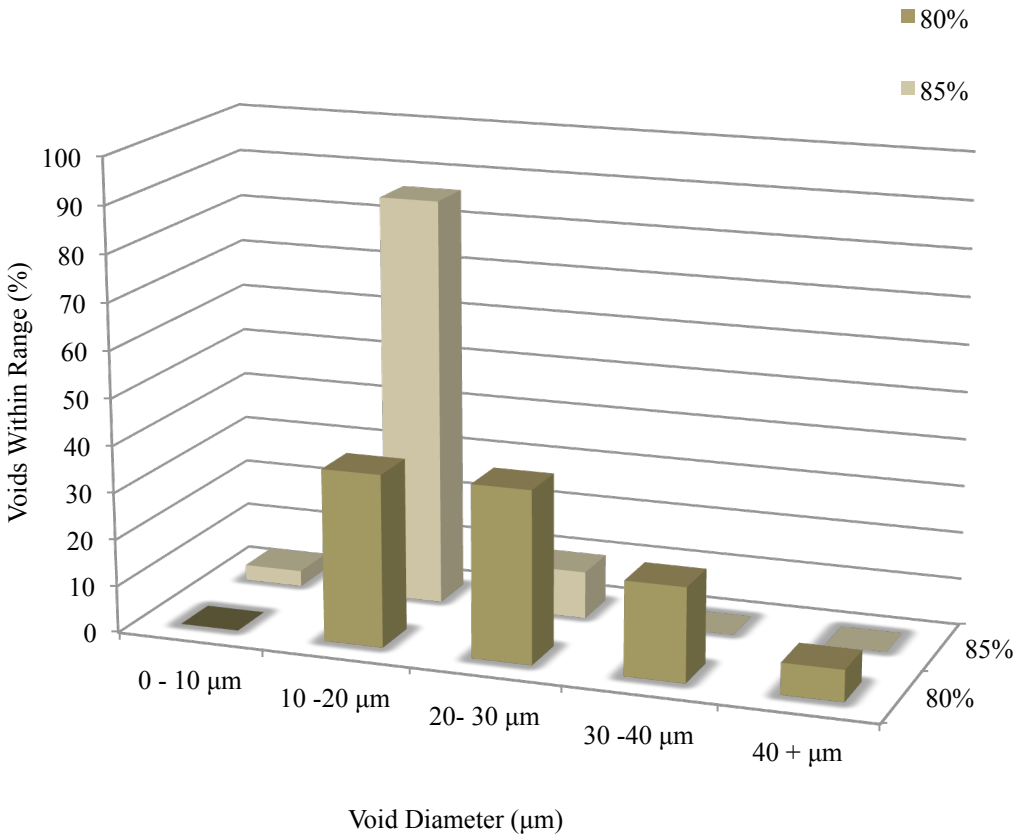

Figure 49: Void diameter distribution of 80 and 85% nominal porosity of trithiol-DPEHA polyHIPEs based on SEM micrographs after applying statistical correction factor.

5.5.3.2 Trithiol-Trimethylolpropane Triacrylate PolyHIPE

Trimethylolpropane triacrylate is another acrylate based monomers which can be used to manufacture acrylate based degradable polyHIPEs. As it was mentioned previously, Caldwell *et al.*[57] reported on manufacturing degradable acrylate based polyHIPEs using TMPTA and DEPHA monomers. However upon the report of successful formation of acrylate based polyHIPEs, in this study it was attempted to reproduce the acrylate based polyHIPEs in order to substitute acrylate or methacrylate based monomers such as methacrylated or acrylated PCL at later stages to achieve a more biocompatible polyHIPE materials. Primarily two different nominal porosities were investigated (85% and 90%) synthesised at room temperature under mixing speed of 330 rpm using an overhead stirrer (see Figure 20). A successful emulsion was formed for 85% nominal porosity formulation and unsuccessful emulsion for 90% nominal porosity trithiol-TMPTA.

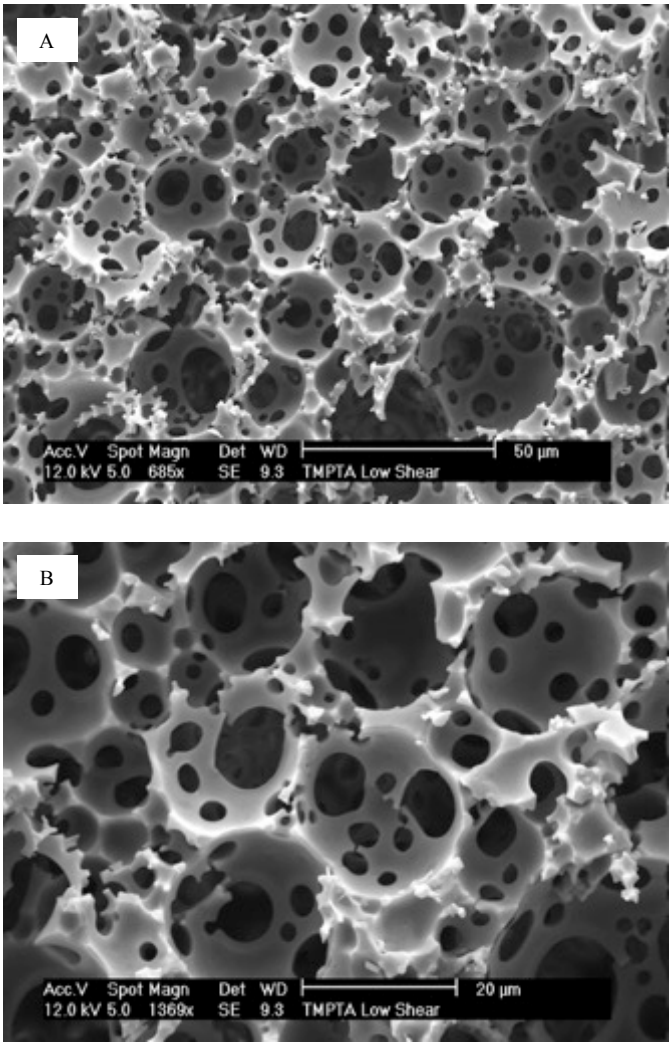

Figure 50: (A-B) SEM micrographs of trithiol-TMPTA polyHIPE (85% nominal porosity) materials via photopolymerisation showing open interconnected macro-structure.

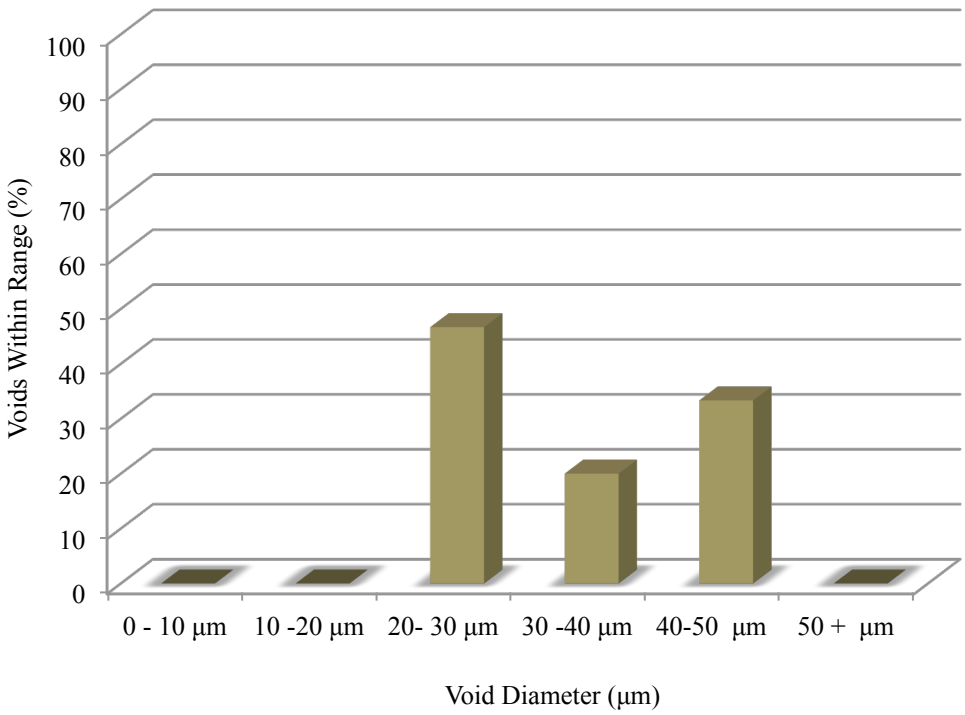

Figure 51: Void diameter distribution detected for 85% nominal porosity of trithiol-TMPTA polyHIPEs based on SEM micrographs after applying statistical correction factor.

The void diameter distribution based on SEM micrographs was measured and the findings are presented in Figure 51. The calculated average void diameter after applying statistical correction factor is approximately 34 µm (standard deviation: ±8.9 µm).

5.5.3.3 Trithiol – Triacrylated Poly (ε -Caprolactone) PolyHIPEs

In order to develop biodegradable and biocompatible based polyHIPEs, an attempt was made to substitute acrylate function groups originated from TMPTA or DPEHA in previous attempts with biodegradable acrylated PCL function groups. The procedure of preparing the polyHIPE was as it was described in section 4.6.1.3. However the volume of the solvent (DCE) was adjusted to ensure an appropriate viscosity suitable for emulsion formation as it was found that the higher viscosity mixture would result in further difficulties to incorporate the aqueous phase hence the failure of the emulsion. Four different formulations were prepared with different nominal porosities, the details of formulations are explained in Table 7. The formulations are based on different thiol:acrylate molar ratio and the maximum aqueous phase volume (nominal porosity) before the failure of the emulsion.

The highest molar ratio attempted was 70:30 (thiol:acrylate) polyHIPE with maximum nominal porosity of 80%, the development of successful emulsion was observed via formation of white thick uniform paste which was photopolymerised successfully under the UV light. However, the cured polyHIPE structure was very soft and fragile which disintegrated during the washing stages in acetone. This may be due to the incomplete crosslinking of thiol:acrylates function groups.

The 60:40 thiol:acrylate molar ratio polyHIPE formulation with achieved nominal porosity of 85% was synthesised successfully and SEM was carried for confirmation of porous morphology. However, it is known that polyHIPE's porous structures may fail during the drying stages as the aqueous phase gets eliminated hence the structural support for the pores. Therefore, the samples were dried using the freeze-drying procedure, which preserve the structure by removing the aqueous phase by sublimation. Even with the considered cautious steps taken toward the drying procedures of the samples, it is evident in Figure 52 that the macro-structure does not exhibit the conventional polyHIPE morphology and this is due to the structural collapse of the material during the drying phase. However, the structure shows evidence of porous macro-structure as the remains of pores can be observed (Figure 52).

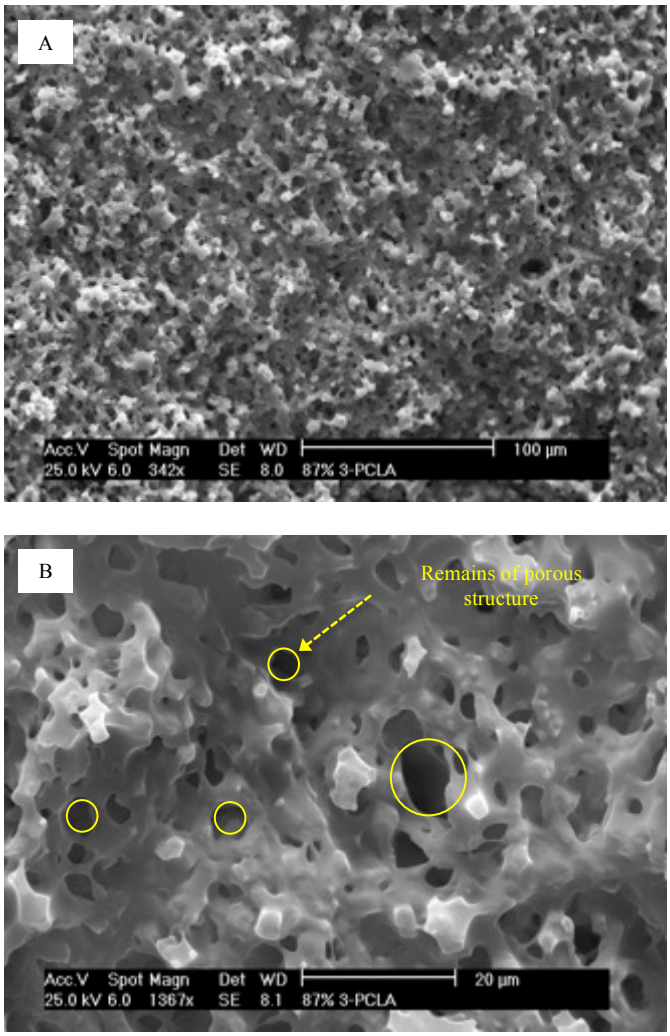

Figure 52: (A-B) SEM micrographs of 60:40 thiol:PCLA (85% nominal porosity) polyHIPE material.

The lowest molar ratio of thiol:acrylate (50:50) with nominal porosity of 80% was synthesised via photopolymerisation and SEM characterisation was conveyed for validation of porous macro-structure. As it was mentioned previously due to the high risk of structural failure during the drying stages, the samples were therefore freeze-dried in prior to SEM. As it is shown in Figure 53, the porous structure of the polyHIPE has collapsed which does not represent the characteristic polyHIPE morphology. However, the remaining of the porous structure is evident via the existence of many hemispheres in Figure 53.

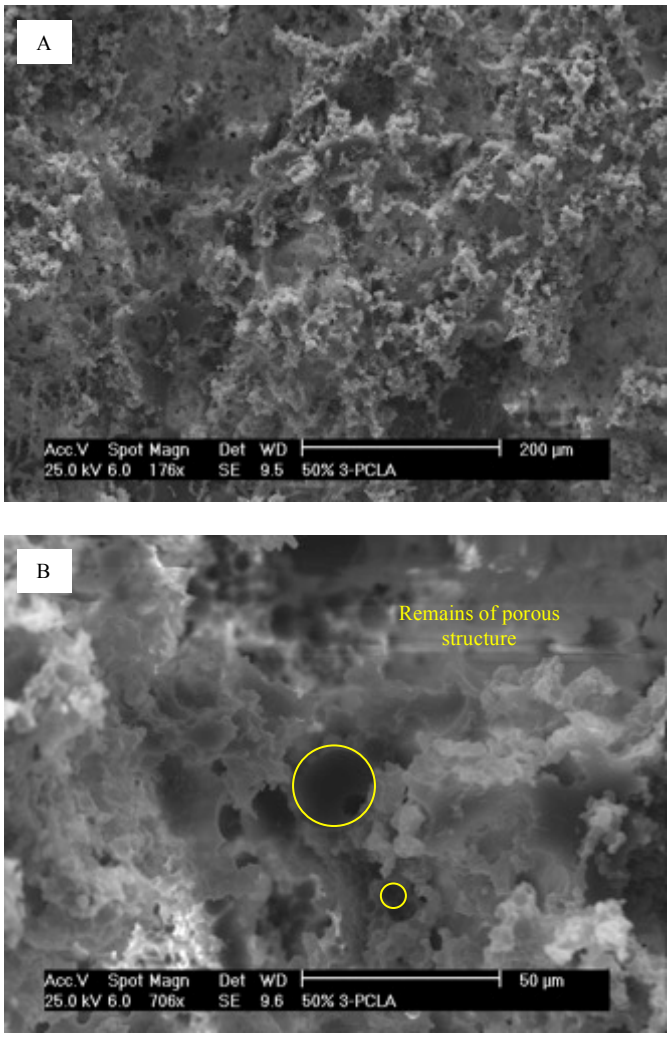

Figure 53: (A-B) SEM micrographs of 50:50 thiol:PCLA (80% nominal porosity) polyHIPE material.

5.5.3.4 Thiol-ene Methacrylated Poly (ε-caprolactone) PolyHIPE

5.5.3.4.1 Trithiol : Tetramethacrylated PCL (1200 g/mol) PolyHIPE

Methacrylates have many advantages such as reasonably low cost, ready availability, rapid polymerisation, toughness, its degradable properties and tunable mechanical properties. Methacrylated-PCL (PCLMA) has higher hydrophobic properties compare to non-methacrylated PCL. Therefore, methacrylated-PCLs are more likely to form stable emulsion compare to the non-methacrylated PCLs in w/o emulsions. Tetramethacrylated-PCL and trithiol can react via thiol-ene reaction in a 1:1 molar ratio of –SH (trithiol) to C=C (methacrylates) groups. The attempts were mainly concentrated on 50:50 ratio of PCLMA (1200 g/mol) to trithiol but at different percentage of surfactant and temperature. It is known that increasing the surfactant will increase the window interconnectivity and increasing the temperature will increase the average void diameter. Successful emulsions were formed in case of the PT2-PT2b and PT2d-PT2f polyHIPE formulations without any noticeable signs of a broken/ unsuccessful emulsion. However, PT2c polyHIPE formulation did not form an emulsion.

The samples were freeze-dried prior to SEM. Samples PT2-PT2b were imaged successfully via SEM. PT2 samples (80% nominal porosity) which were synthesised at room temperature with 3% (w/w) surfactant exhibited interconnected porous morphology confirming successful polyHIPE formation. The synthesised polyHIPE exhibited open interconnected morphology similar to polyHIPE nature with average void diameter of 19.6 μm (mean standard deviation: ± 5.7 μm).

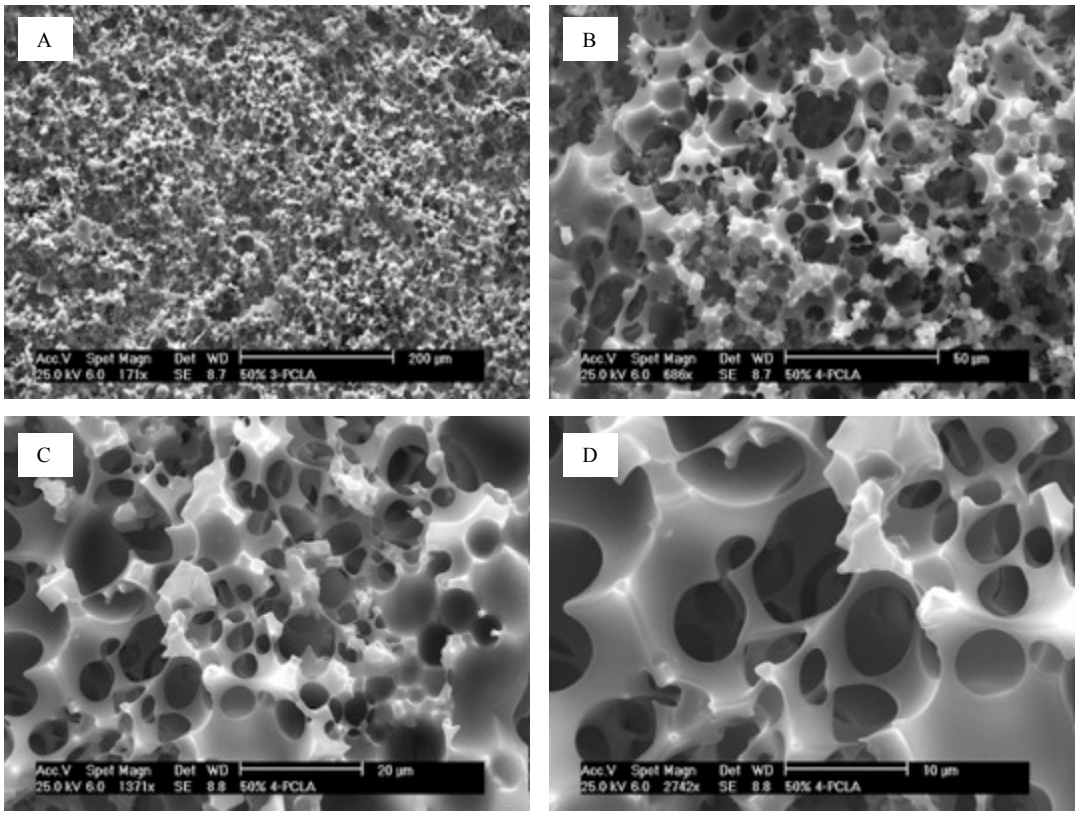

Figure 54: (A-D) SEM micrographs of 50:50 thiol:PCLMA (80% nominal porosity) (PT2) polyHIPE materials.

On the other hand even with the successful emulsion formation of PT2a (Figure 55) and PT2b (Figure 56) the SEM images did not show the genuine morphology of the HIPE structure.

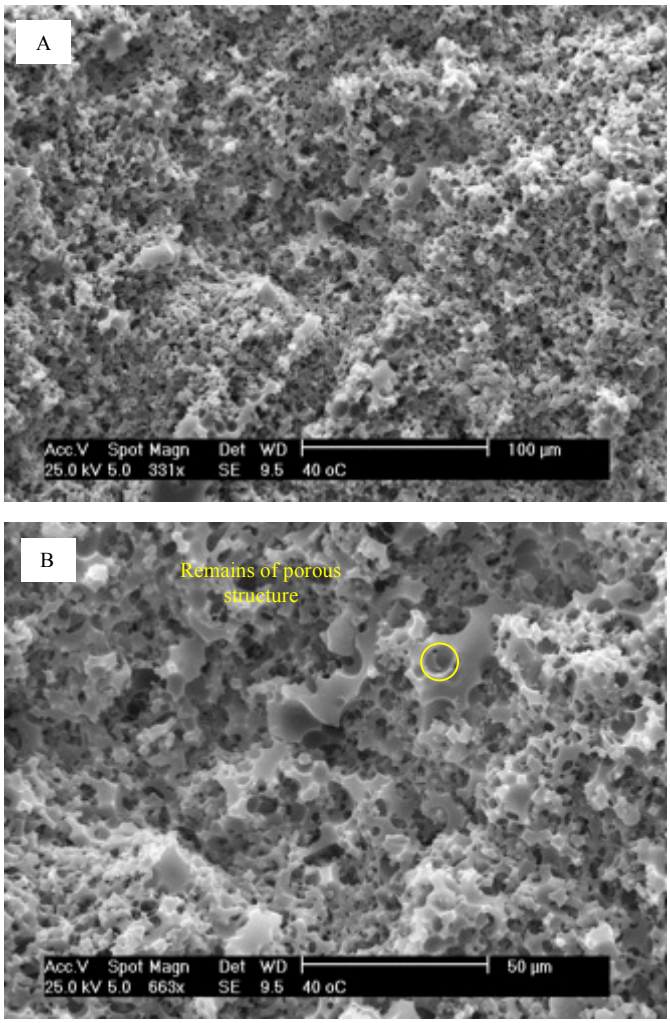

Figure 55: (A-B) SEM micrographs of 50:50 thiol:PCLMA (80% nominal porosity) (PT2a) synthesised at 40°C polyHIPE materials.

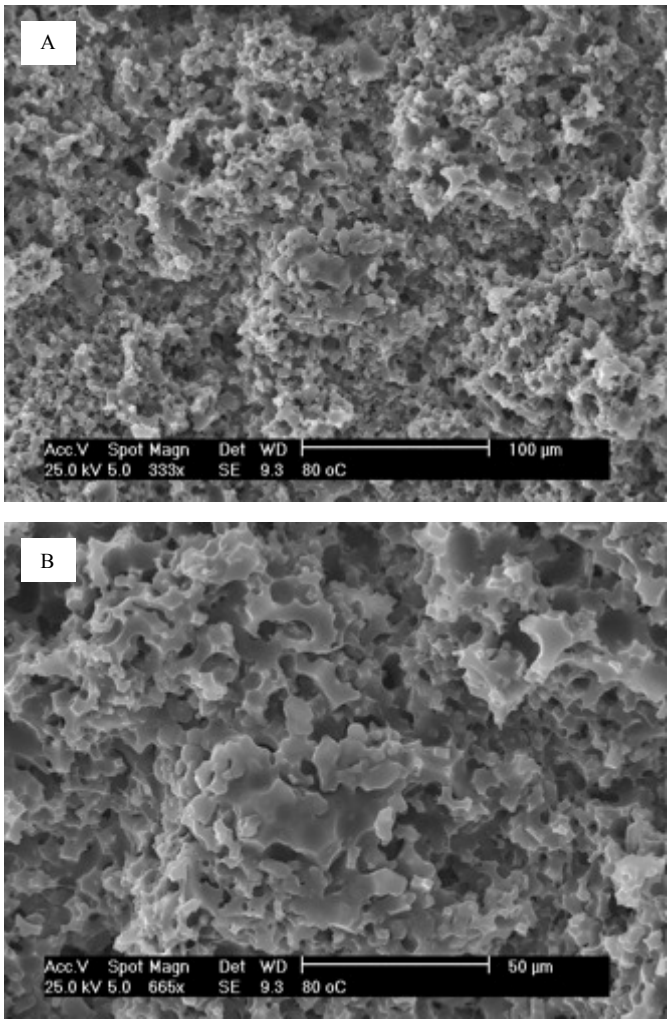

Figure 56: (A-B) SEM micrographs of 50:50 thiol : PCLMA (80% nominal porosity) (PT2b) synthesised at 80°C polyHIPE material.

The PT2d-PT2f emulsions were formed successfully however during post photopolymerisation stage (acetone washes), the material disintegrated which may be due to the incomplete crosslinking of trithiol and methacrylate group functions.

Following the successful tetramethacrylated PCL:trithiol (PT2) polyHIPE formation with preserved typical morphology, same formulation with different molecular weight tetramethacrylated PCL was attempted which is explained further in next section.

5.5.3.4.2 Trithiol:tetramethacrylated PCL (20000 g/mol) PolyHIPE

Photocurable poly (ϵ-caprolactone) with a higher molecular weight (20000 g/mol) was synthesised based on the methods described in 4.6.1.4.1, which was further functionalised with methacrylate oligomers. The molecular weight of the synthesised polymer was confirmed via GPC.

Upon the successful formation of trithiol:tetramethacrylated functionalised PCL (1200 g/mol) (PT2), an attempt was made to synthesise the PT2 formulation with higher molecular weight methacrylated PCL. The formulation used is shown in Table 9. The PT1 emulsion was formed successfully and photopolymerised as it was previously described in section 4.6.1.4.3. The morphology of the sample was explored via SEM (Figure 57 and Figure 58), after post-photopolymerisation steps including acetone washes and drying stages (freeze-drying). As it can be seen from Figure 57, the morphology of PT1 polyHIPE sample does not exhibit typical polyHIPE morphology, which is due to the open curing of the top surface, to avoid this the top surface of the emulsion must be cured over a flat surface hence between two glass sheets. However, the cross-sectional morphology of the polyHIPE sample shows the typical polyHIPE morphology hence the successful formation of the polyHIPE.

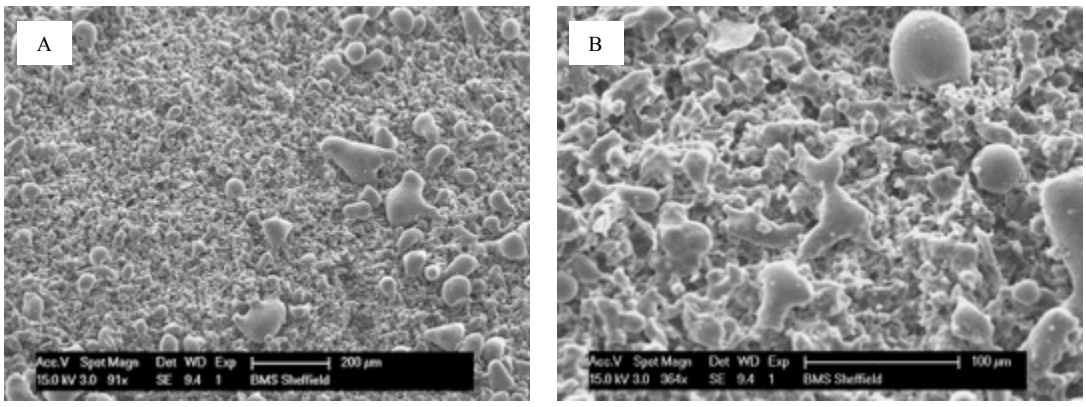

Figure 57: (A-B) SEM micrographs of the top surface 50:50 trithiol:PCLMA (80% nominal porosity) (PT1) synthesised at room temperature polyHIPE material.

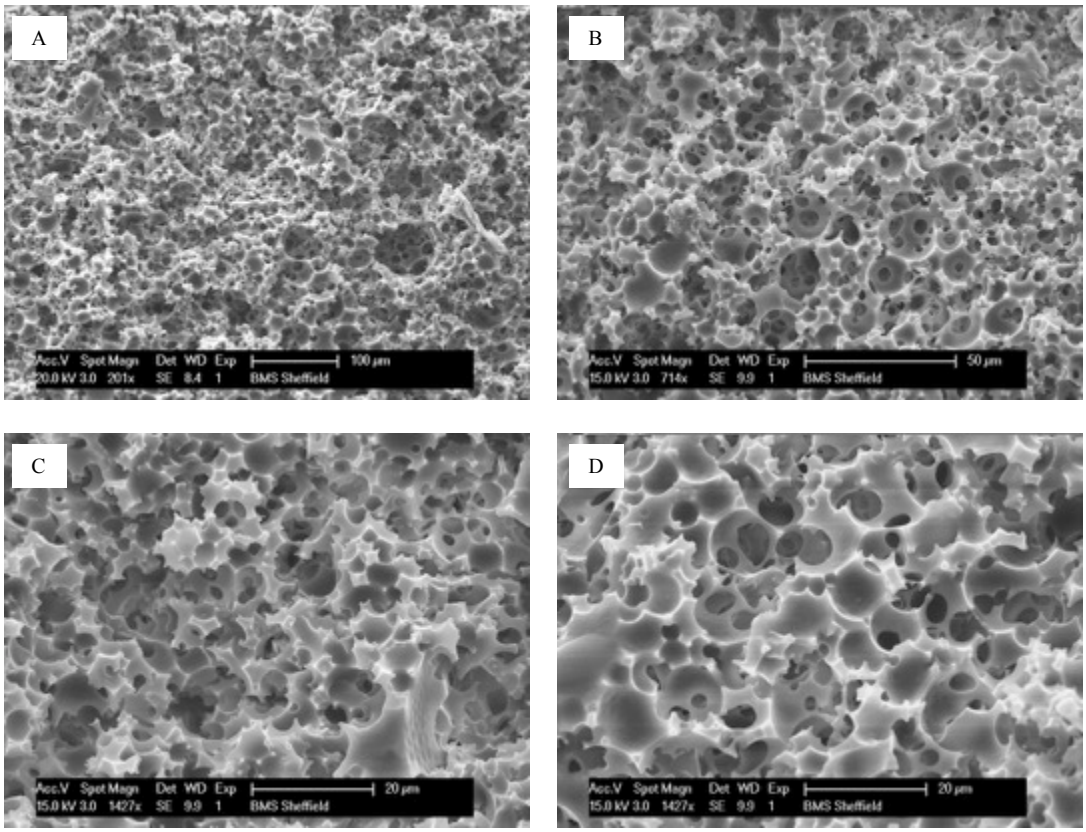

Figure 58: (A-D) SEM micrographs of cross-sectioned 50:50 trithiol:PCLMA (80% nominal porosity) (PT1) synthesised at room temperature polyHIPE material.

The polyHIPE (PT1) demonstrates open interconnected porous morphology with average cell diameter of 15.4 μm (mean standard deviation: ± 4.8 μm) after applying statistical correction factor [108]. The average void diameter of similar polyHIPE formulations with different molecular weight tetramethacrylated PCL (PT1 and PT2) is displayed in Figure 59 and the void diameter distribution of both samples are demonstrated in Figure 60. The difference between the average void diameter of PT1 and PT2 polyHIPE samples with two different molecular weights (1200 and 20000 g/mol) has shown to not being significant.

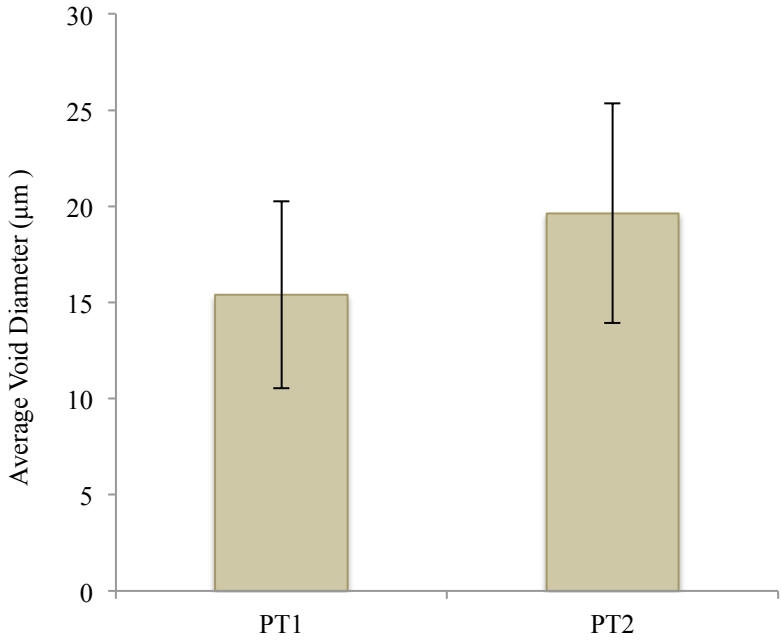

Figure 59: Average void diameter of trithiol-tetramethacrylated PCL polyHIPEs (PT1 and PT2) measured via SEM micrographs using Image J after applying statistical correction factor [108].

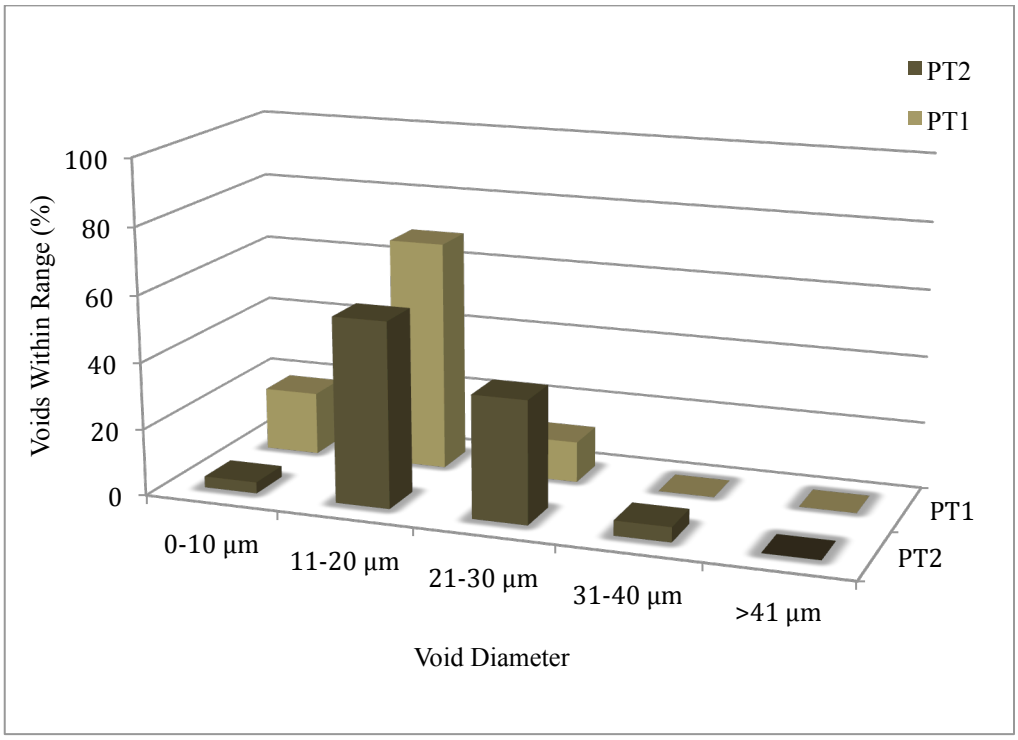

Figure 60: Void diameter distribution estimated for trithiol-tetramethacrylated PCL polyHIPEs (PT1 and PT2) based on SEM micrographs after applying statistical correction factor [108].

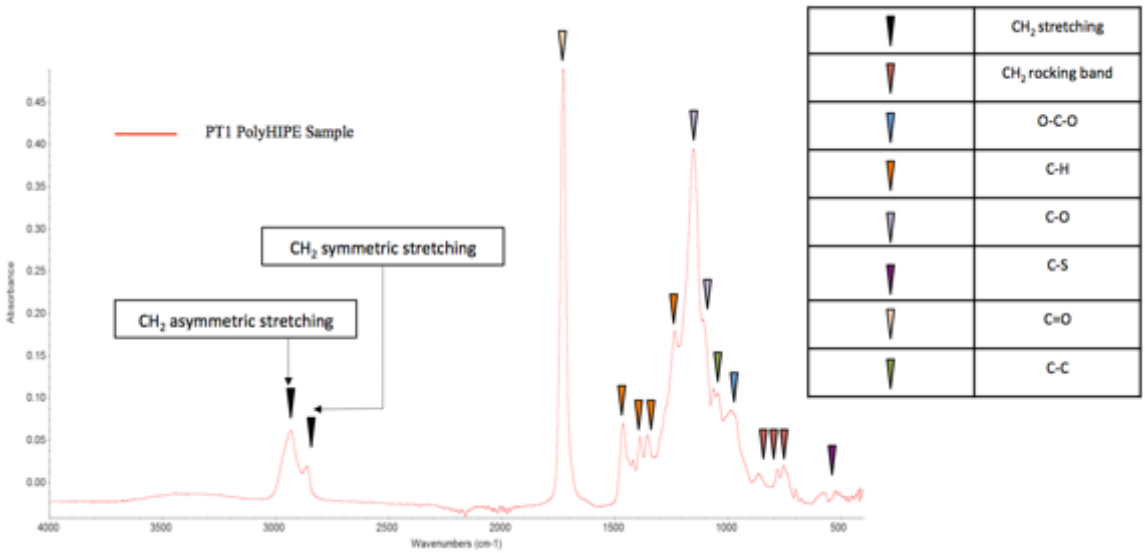

Figure 61: FTIR spectrum of PT1 polyHIPE disks.

The FTIR data on PT1 samples show –CH_2 rocking bands between 500-900 cm^{-1} at 753, 780 and 863 cm^{-1}, O-C-O symmetric stretching between 900-1000 cm^{-1} at 985 cm^{-1}. C-C stretching band between 1000-1100 cm^{-1} at 1024 and 1063 cm^{-1}. O-C-O stretching band between 1150-1200 cm^{-1} at 1151 cm^{-1}. C-H symmetric band between 1350-1480 at 1354, 1387, 1418 and 1461 cm^{-1}. C=O stretching between 1700-1760 cm^{-1} at 1726 cm^{-1}. CH_2 symmetric stretching between 2800-2900 cm^{-1} at 2859 cm^{-1} and asymmetric stretching between 2900-3000 cm^{-1} at 2931 cm^{-1}. C-O stretch bands between 1000-1300 cm^{-1} at 1108 cm^{-1} and 1234 cm^{-1}. Small band between 570-710 cm^{-1} representing C-S band.

5.5.3.5 Biocompatibility Analysis of Trithiol-Tetramethacrylated PCL PolyHIPEs

Further to the trithiol:tetramethacrylated PCL polyHIPE materials (samples PT1 and PT2) development, the biocompatibility of the developed materials were verified using human osteosarcoma cell line (MG63) via PicoGreen® DNA quantitation assay which was verified further by LIVE/ DEAD® staining and immunofluorescence confocal microscopy. PT1 and PT2 polyHIPE disks with ϕ of 9 mm were manufactured as it was explained in section 4.5.3 and the biocompatibility study was carried as it was described in 4.6.2. Initially MTT assay, which is a colorimetric cell proliferation assay was used to assess the biocompatibility of PT1 and PT2 samples. However, the initial attempt of biocompatibility analysis via MTT proved less reliable as MTT reacted with the thiol groups of polyHIPE material and produced blue solution, which was not sourced from the presence of cells (see Figure 62).

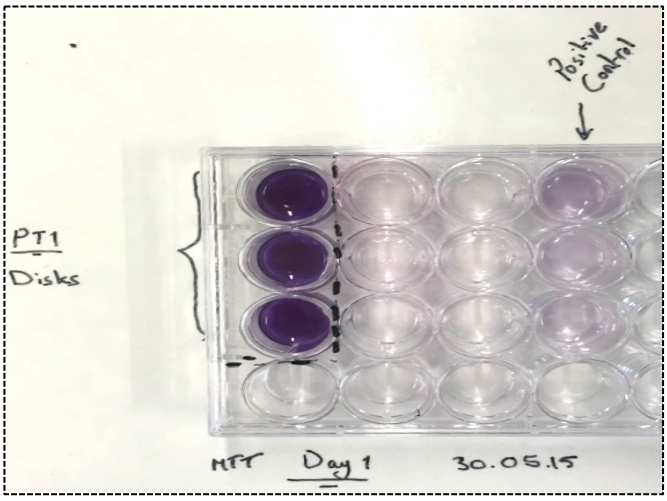

Figure 62: MTT assay carried on PT1 and PT2 samples which stained blue as result of MTT reacting with thiol groups demonstrated the irrelevance of this biocompatibility analysis.

In order to overcome the problem associated with MTT assay, PicoGreen® DNA quantitation assay was used to assess the DNA content of the samples hence its biocompatibility. The samples were cultured for 7 days (n=3) and the assay was carried at day 3 and 7 as it was explained in 4.6.2.2 (the experiment was repeated twice). Figure 63 indicates that the DNA content of both materials increased gradually until day 7. However, PT1 polyHIPE material has relatively higher DNA content at all time point in compare to PT2 polyHIPE sample. In order to confirm the findings from DNA quantitation assay, LIVE/ DEAD® staining was carried at day 7 to confirm the viability of the attached MG63 cells to PT1 and PT2 samples.

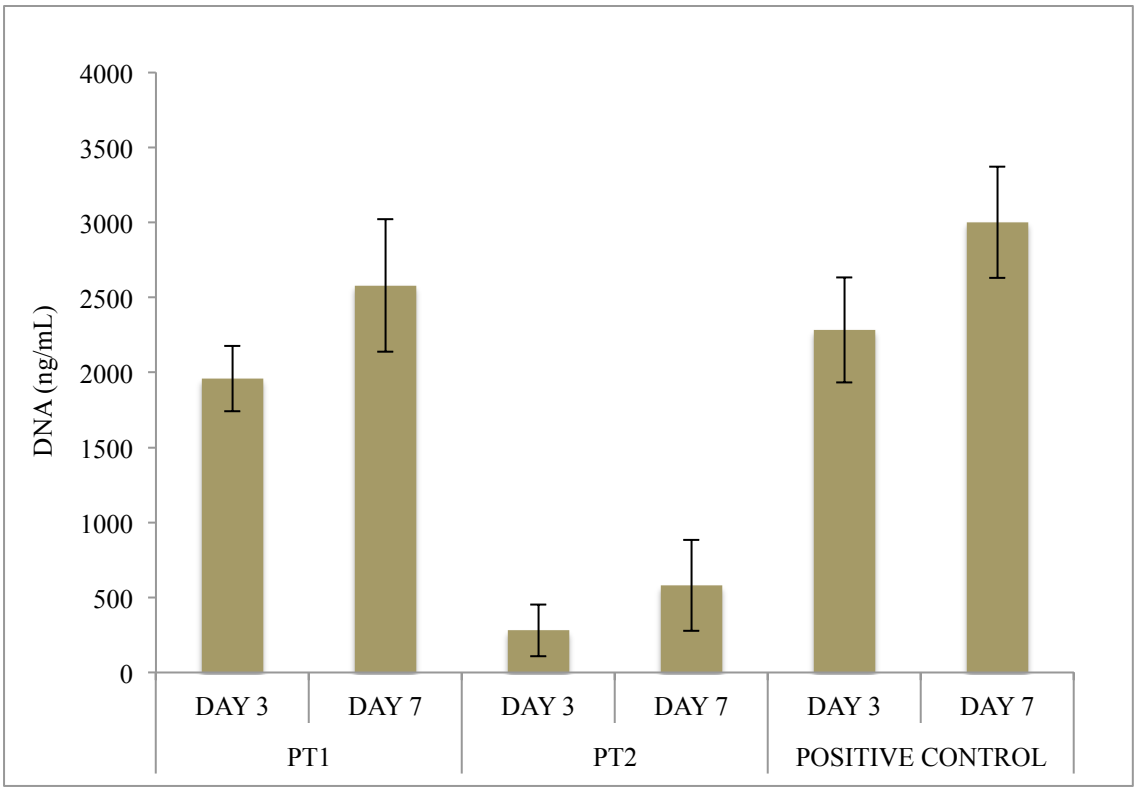

Figure 63: PicoGreen® assay of MG63 cultured cells on PT1 and PT2 disks vs. tissue culture plastics (error bars represent ± mean standard deviation).

LIVE/ DEAD® viability kit is a fluorescence-based cell viability assay kit, which determines live cells from dead via two different stains. The viable cells are stained in green and the dead cells are stained in red. As it is evident from fluorescence images shown in Figure 64, there is a high percentage of viable cells compared to dead cells for PT1 polyHIPE samples. On the other hand, no viable cells were observed for PT2 polyHIPE sample confirming its relative lower biocompatibility. Due to auto-fluorescence properties of polyHIPEs it is very difficult to distinguish dead cells from the material. However with further inspection of images, no viable cells could be observed for PT2 samples. The findings are presented in form of percentage of viable cells in Figure 65, which indicates higher number of viable cells (approximately 90%) for PT1 sample.

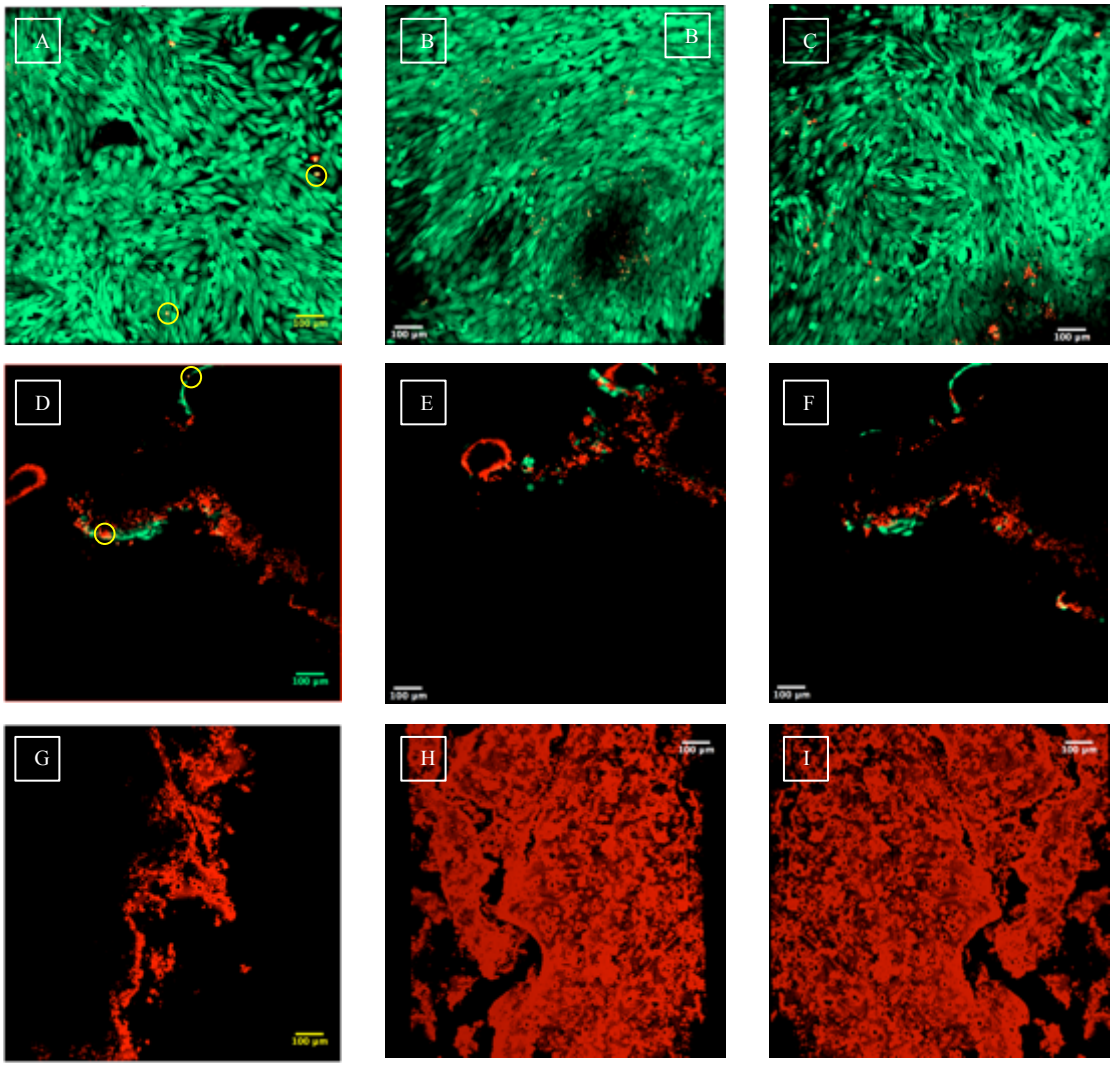

Figure 64: Immunofluorescence images of LIVE/ DEAD® staining of positive control, PT1 and PT2 polyHIPE samples at day 7 where green indicates live cells and red indicates dead cells. However it is evident that both PT1 and PT2 PolyHIPE samples are auto-fluorescence, hence the red in these images indicates the porous polyHIPE structure. A-C) tissue culture plastic (positive control). D-E) PT1 polyHIPE samples, where the green dye indicate the live cells and examples of red cells are circled in yellow. G-I) PT2 polyHIPE sample where absence of green dye is indication of no live cells (H-I images are 3D-stack of PT2 polyHIPE samples). The scale bars =100 μm.

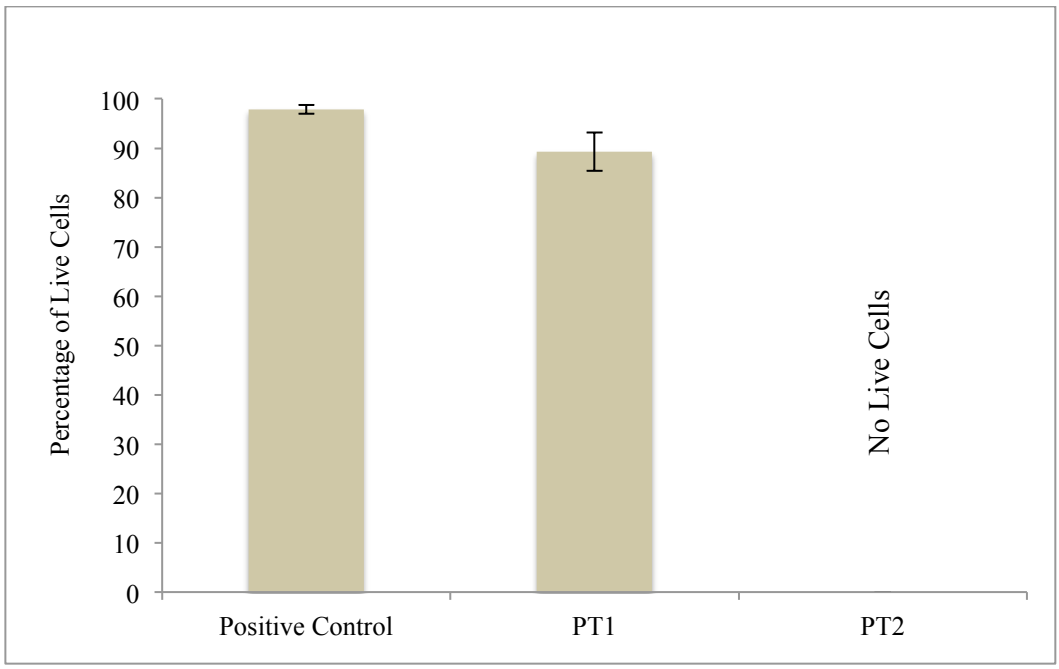

Figure 65: Viability of human osteosarcoma cell line (MG63) cultured on tissue culture plastic (positive control), PT1 and PT2 polyHIPE samples at day 7, the error bars represent mean standard deviation.

Further to PicoGreen® DNA quantitation and LIVE/ DEAD® staining, the immunofluorescence confocal microscopy was carried to observe the morphology and ingrowth of cells. The samples were stained with DAPI, TRITC-phalloidin and FITC-phalloidin at day 7 following the fixation and washing procedures to assess nuclei and f-actin of attached cells (see section 4.6.2.5.2). From the images (see Figure 66), it can be observed that MG63 cells attached and proliferated well on PT1 polyHIPE material. However, in some images it can be seen that the polyHIPE material is auto-fluorescence and some of its porous morphology can be seen as blue porous structure (see Figure 66D-E). Figure 66B showed that the cells were capable of penetrating within the pores, which is confirmed by presence of their nuclei and actin.

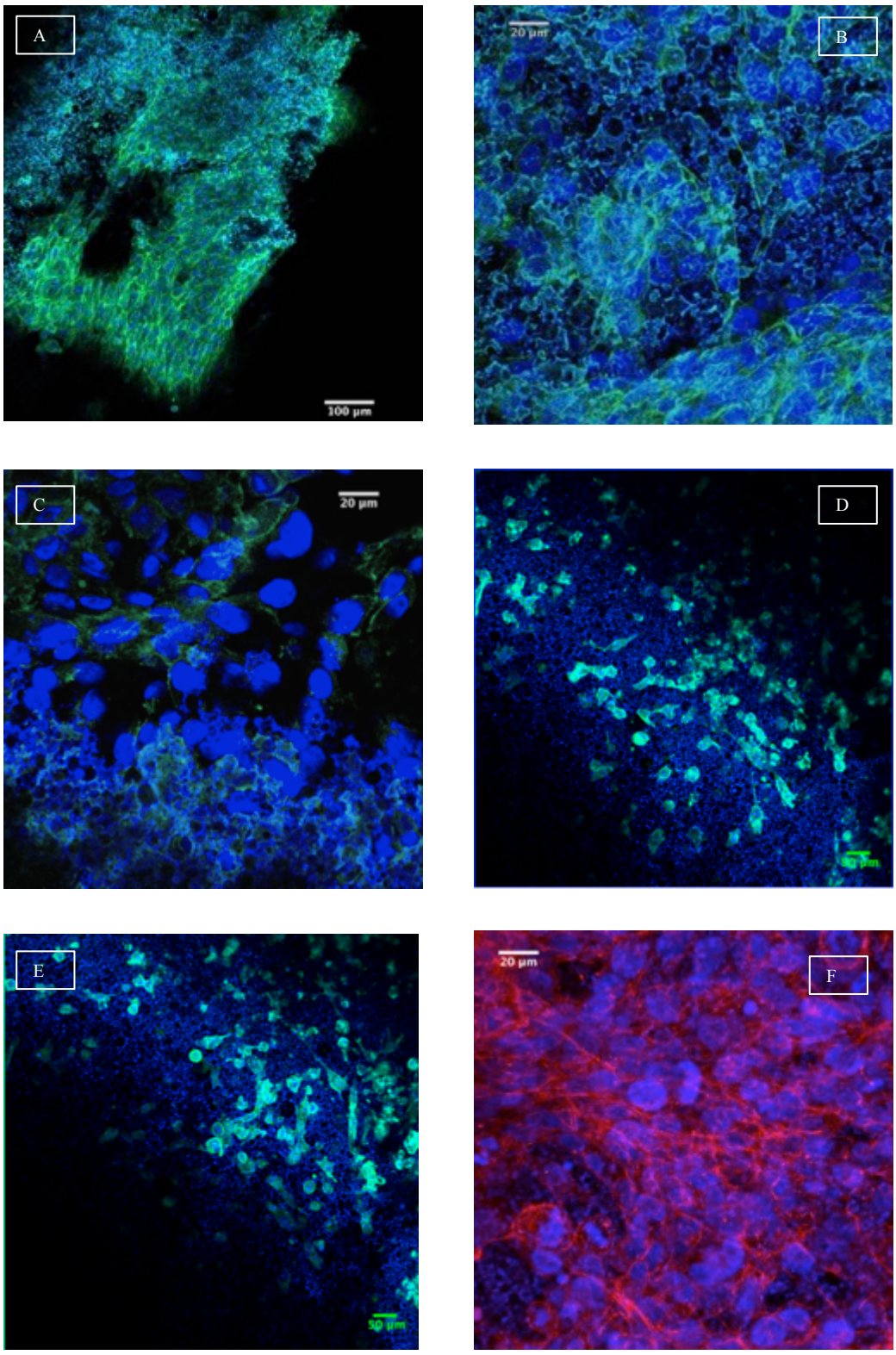

Figure 66: Immunofluorescence micrographs of PT1 polyHIPE sample cultured with MG63 for 7 days and stained with (A-E) DAPI and FITC-phalloidin and (F) DAPI and TRITC-phalloidin.

Confocal images of PT2 polyHIPE samples are shown in Figure 67. Figure 67A-C were stained with DAPI and FITC-phalloidin and Figure 67D was stained with DAPI and TRITC-phalloidin. From the images it can be observed that lower number of cells were adhered and proliferated on PT2 polyHIPE samples in compare to PT1 Samples. The presence of cells is more notable via FITC-phalloidin staining rather than nuclei DAPI staining due to auto-fluorescence nature of the polyHIPE material.

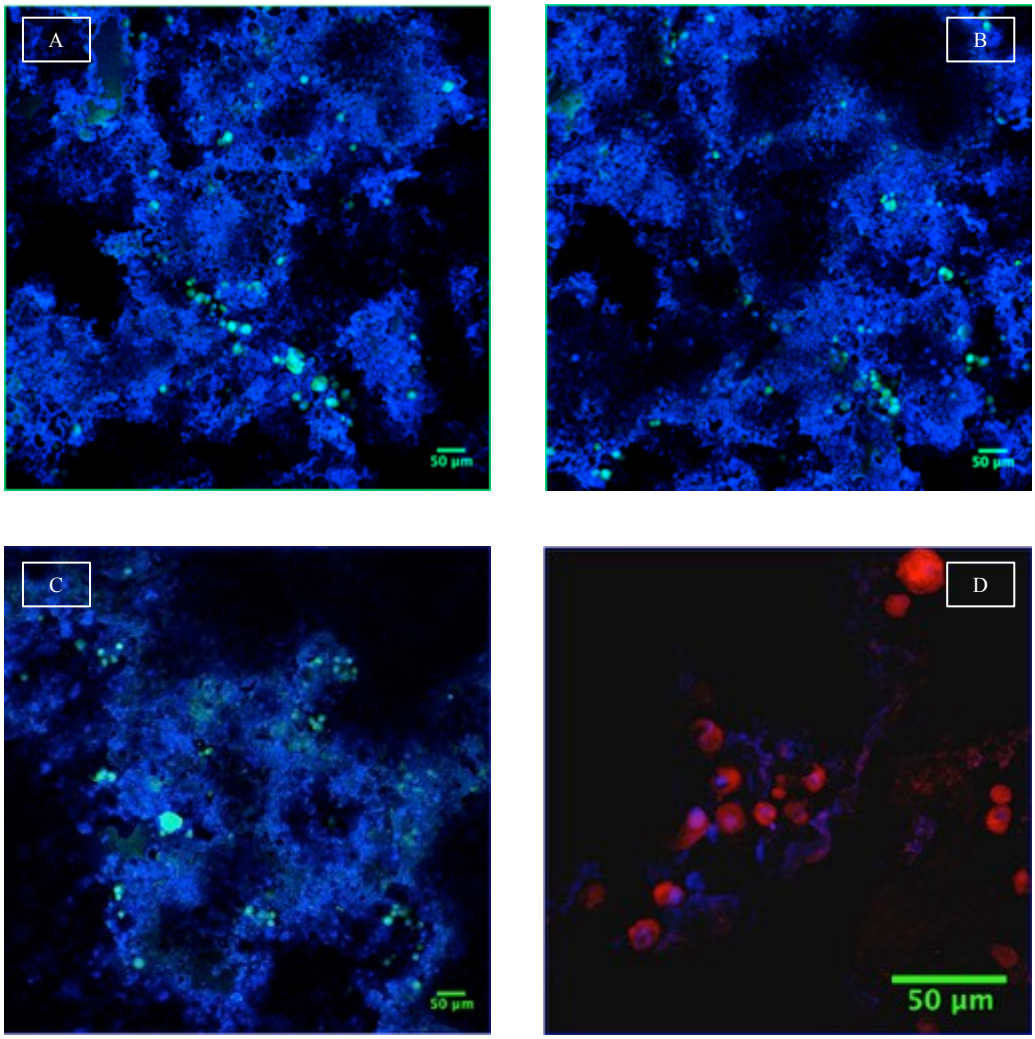

Figure 67: Immunofluorescence micrographs of PT2 polyHIPE sample cultured with MG63 for 7 days and stained with (A-C) DAPI and FITC-phalloidin and (D) DAPI and TRITC-phalloidin.

Non-accelerated degradation study was carried for 4 days period to observe the degradation rate of PT1 and PT2 samples via using Lipase as degradation catalyst. As it can be seen from Figure 68, PT2 polyHIPE samples have higher degradation in compare to PT1 polyHIPE samples. In other words the trithiol-tetramethacrylated PCL polyHIPE with higher molecular weight PCL have lower degradation rate. In order to ensure complete biodegradation of trithiol-tetramethacrylated PCL, an accelerated degradation study was carried using NaOH (0.1M) at 37°C. The total time taken to achieve full degradation of PT1 and PT2 samples were approximately 57 days (see which shows disintegration of polyHIPE samples in form of floating particles).

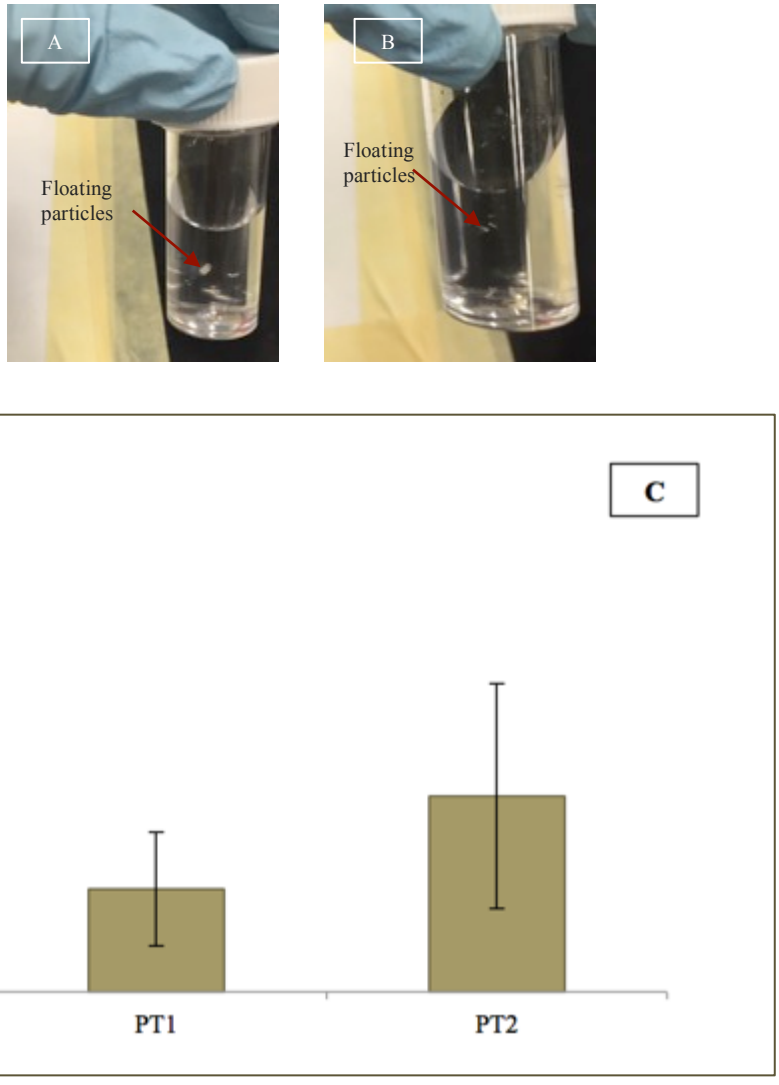

Figure 68: A-B) The images show complete degradation of PT1 and PT2 samples after accelerated degradation study after 57 days C) Rate of non-accelerated degradation of PT1 and PT2 polyHIPE samples after 4 days (the error bars represent the mean standard deviation).

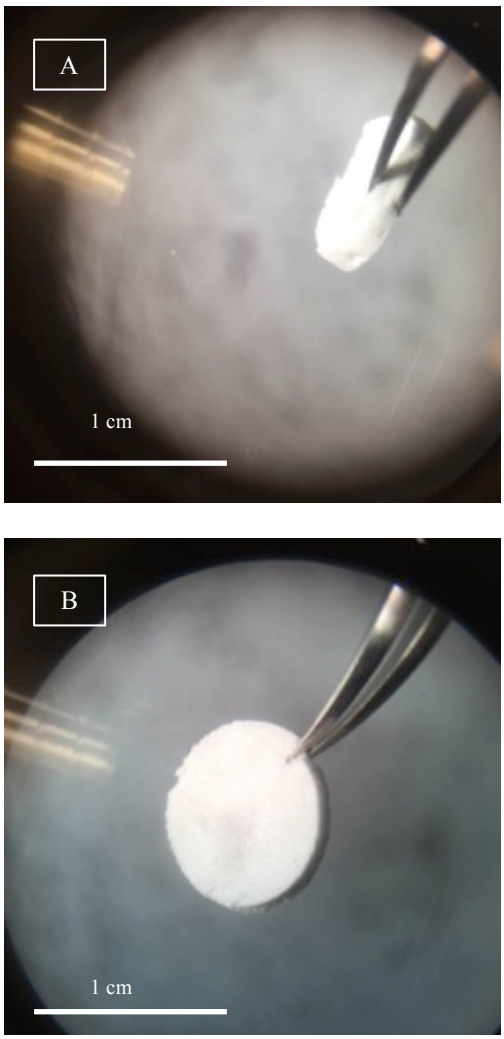

Figure 69: A) Images of PT1 and B) PT2 samples with diameter of 9 mm.

The mechanical properties of PT1 and PT2 were not studied thoroughly in this study, however as it can be seen from Figure 69, PT2 samples have more rigid mechanical properties compared to PT1 samples that are more soft and flexible.

5.5.3.6 Incorporation of nHA particles with Trithiol-Tetramethacrylated PCL PolyHIPEs

As it was aforementioned in section 2.4.1.1, presence of hydroxyapatite in composite materials enhance the osteogenic differentiation of cultured cells, in other words hydroxyapatite is known as a osteoconductive material [33]. Therefore, the incorporation of nHA to PT1 (Trithiol-tetramethacrylated PCL) polyHIPE sample was investigated to enhance its suitability for bone tissue engineering biomaterials. As it was discussed earlier incorporation of micro-HA particles may scatter the laser and reduce the accuracy of fabrication (see section 5.4.1). Therefore, nHA was prepared via Prakash method to optimise the accuracy of stereolithography fabrication (as it was explained in section 4.7) and it was characterised via XRD, FTIR-ATR spectroscopy and TEM. Attenuated total reflectance-Fourier transform infrared spectroscopy (ATR-FTIR) was used to analyse nHA samples to confirm the presence of nano-scale HA.

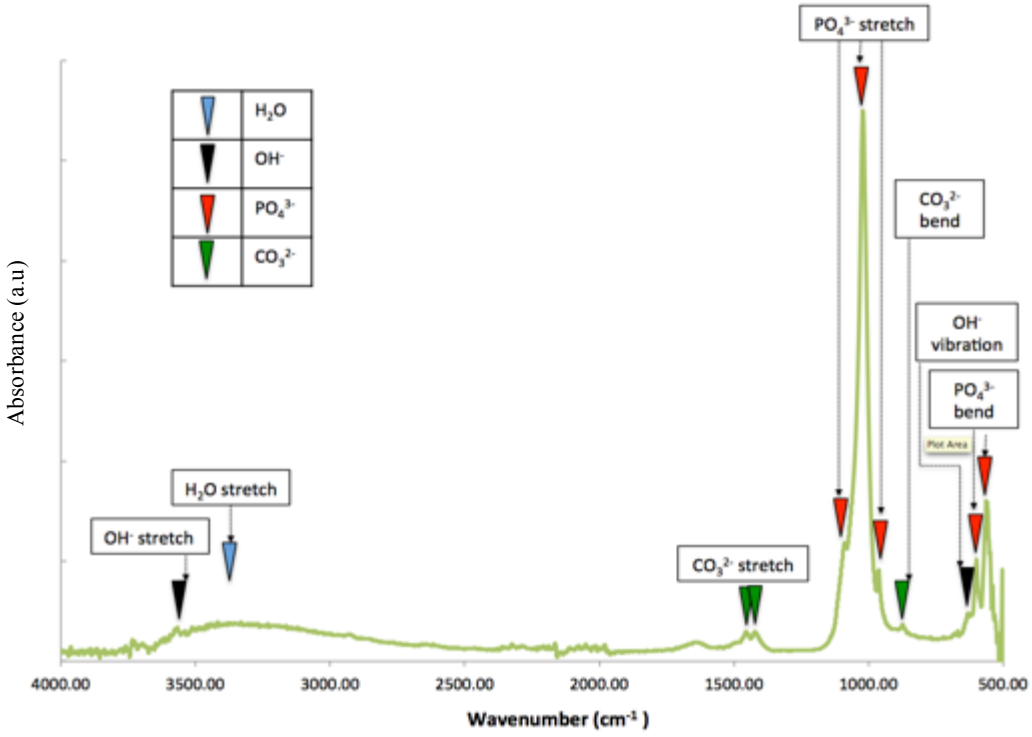

Figure 70: FTIR spectra of HA prepared by Prakash method.

Figure 70 shows FTIR spectra of hydroxyapatite prepared by Prakash method. The infrared band positions at 861, 1409 and 1464 cm^{-1} is due to carbonate ions. The bands observed at 562, 599, 982, 1019, 1074 cm^{-1} confirm the presence of PO^{3-}_4 ions. The band at 3545 cm^{-1} is associated with –OH stretch and 610 cm^{-1} is due to –OH vibration. The broad band observed at 3419 cm^{-1} is due to H_2O stretch.

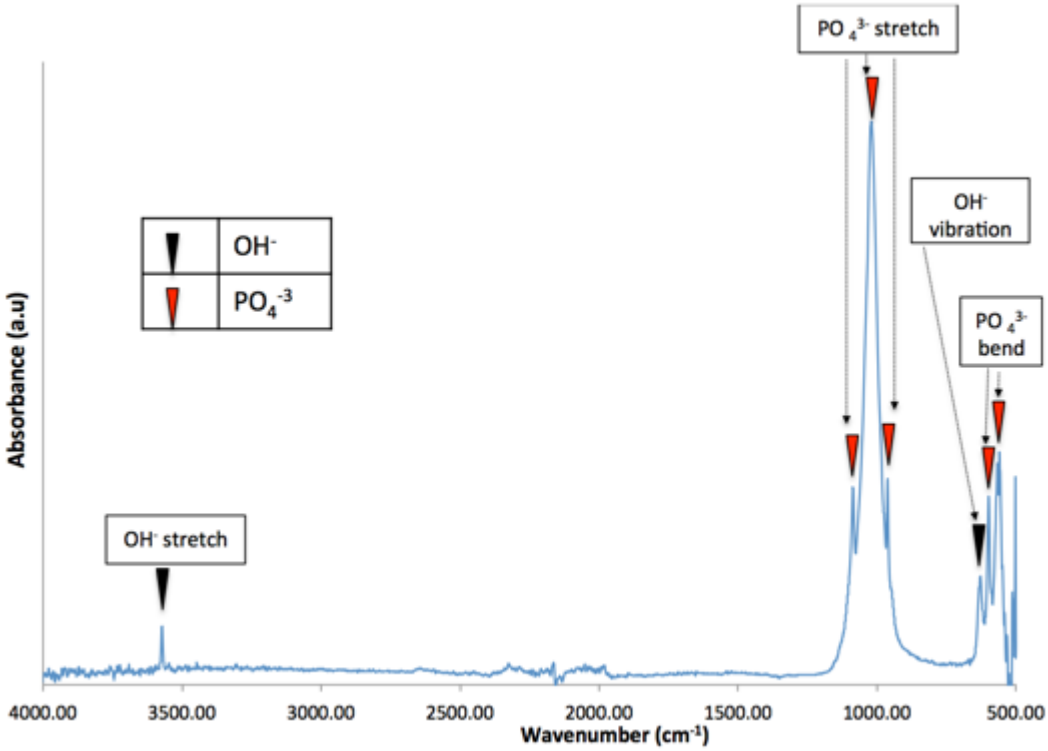

Figure 71: FTIR spectra of HA prepared by Prakash method sintered at 1000°C.

The FTIR-ATR Ū/cm^{-1} for sintered nHA shows characteristic band due to PO_4^{3-} ions at 1061 cm^{-1}, 1016 cm^{-1}, 961 cm^{-1}, 558 cm^{-1} and 554 cm^{-1}. OH^- groups stretching at 3572 cm^{-1} and 604 cm^{-1}.

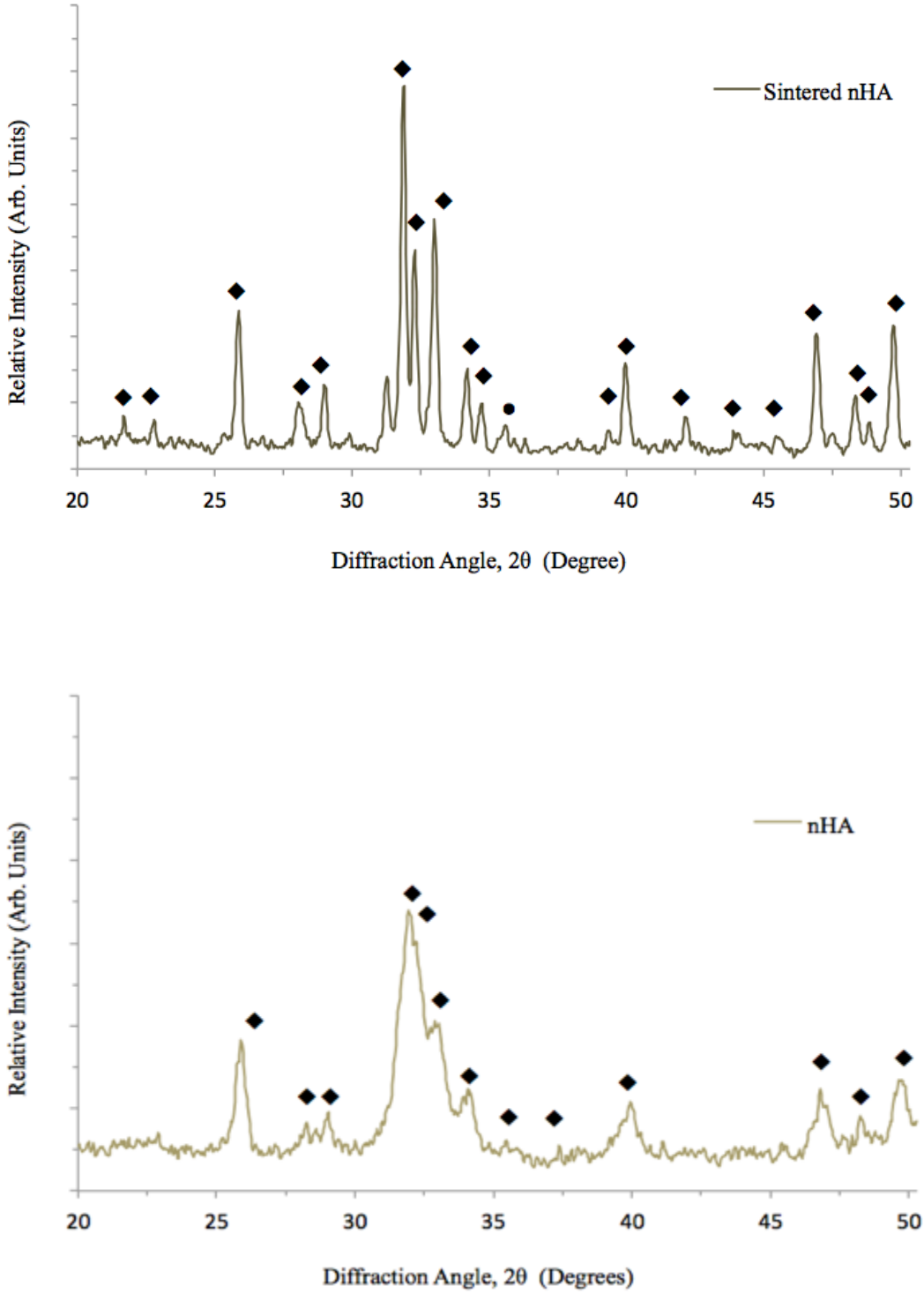

Figure 72: X-ray diffraction patterns for hydroxyapatite synthesised by Prakash method for sintered nHA (at 1000°C) and non-sintered nHA particles, ◆ hydroxyapatite and ● calcium oxide.

The XRD profile of hydroxyapatite ceramic synthesised by Prakash method has been shown in Figure 72. The XRD phase analysis and peak locations (see Figure 72) are identified as (ICDD: 01-073-0293) hydroxyapatite standard card confirming the presence of hydroxyapatite crystals. However, the XRD-pattern of sintered samples at 1000°C for 2 hours also showed low intensity calcium oxide peak (see Figure 72).

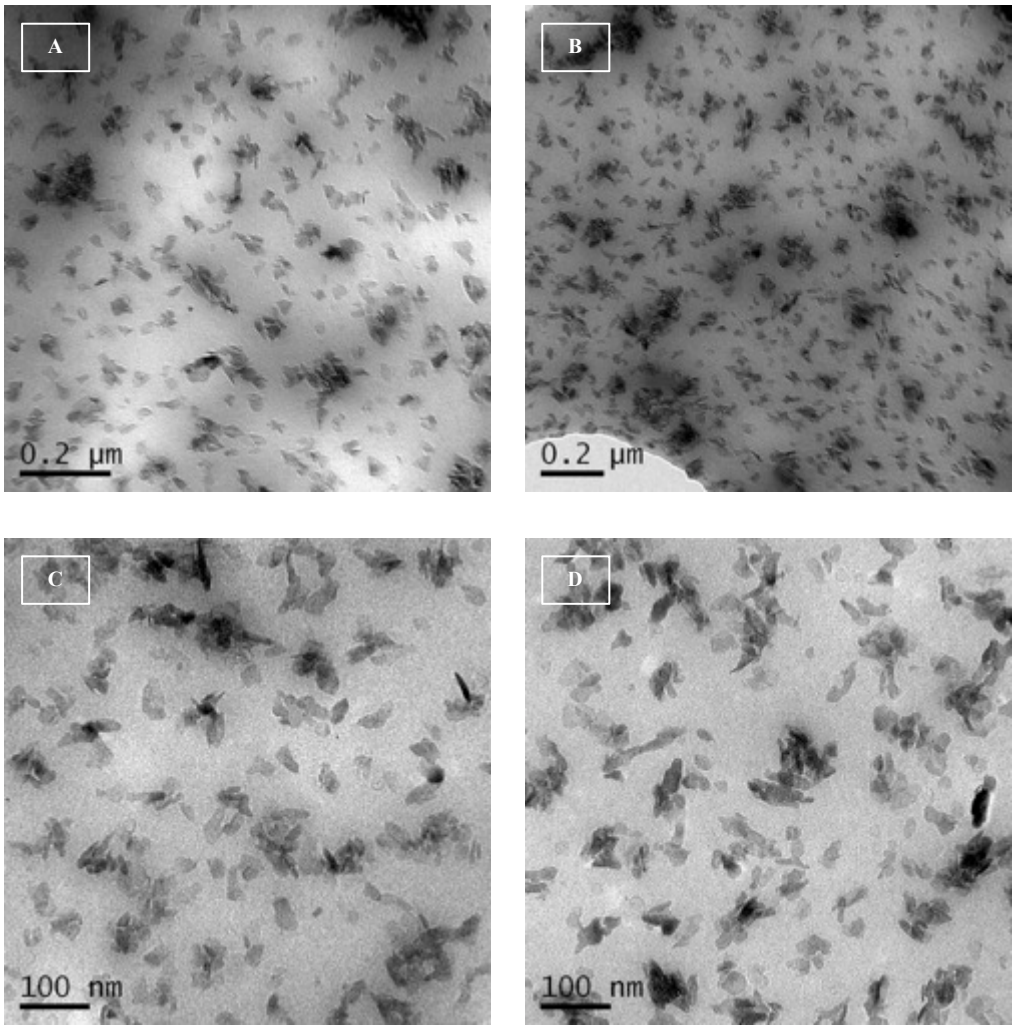

Figure 73: (A-D) Morphology of nHA particles fabricated via Prakash method, which was determined via transmission electron microscopy.

The size distribution of nHa particles were analysed via TEM. The TEM observation indicates nano-crystalline nature of the materials with dimensions of 42.4 nm long (standard deviation: ±13.3 nm) with 16.4 nm width (standard deviation: ±3.6 nm) that was determined by Image J analysis. The aspect ratio detected (length/ width of particles) was approximately 2.5.

Upon the successful preparation of nHA particles, the incorporation of HA particles with PT1 (trithiol-tetramethacrylated PCL) polyHIPE sample is investigated. Previously, attempts were made to incorporate nano-scale hydroxyapatite with polyHIPE samples by combining the hydroxyapatite particles into aqueous phase [118]. The synthesised hydroxyapatites were stored in deionised water that was added to the aqueous phase in prior to adding it to the oil phase. The addition of hydroxyapatite particles to polyHIPE samples were started with very low concentration as it may disturb the emulsification process. Unfortunately, no successful emulsion was formed. However, initially 2PT110 polyHIPE (see Table 10 for formulations) showed formation of successful emulsion in form of a white paste, but it was disintegrated during the acetone washing steps which questions the successful emulsion.

6 DISCUSSION

Despite many advances in craniofacial bone tissue engineering, the successful reconstruction of bone craniofacial defects rests a major challenge, as there is a substantial need due to critical sized defects caused by congenital disorders and injuries. With prosperous progression in medical imaging, bioresorbable materials and scaffold fabrication technology, it is now possible to design customised biodegradable craniofacial scaffold to enhance bone tissue regeneration. Currently surgical strategies involves harvesting bone tissue from a distant area to the site of surgery such as iliac crest, and fibula to deform and implant to the site of the defect which is used as a standard approach against new coming strategies. Overall, the ideal biomaterial used for craniofacial tissue engineering should be readily available, flexible with using different fabrication technologies as customised fabrication is essential, nonimmunogenic as well as preserving its macro- and micro- structure while implanting *in vivo*. Majority of current research investigate new approach involving employing conventional biomaterials with use of free form fabrication technology to develop customised bone tissue engineering scaffolds. However, little progress has been made in achieving a combined desirable approach. Therefore the main aim of this research was therefore to investigate novel biomaterials with free form fabrication technology to fabricate customised craniofacial scaffolds. The evaluated results of fabrication technologies and the polyHIPE materials were described in Chapter 5.

6.1 Evaluation of a Feasible SFF Technology

6.1.1 Scaffold Micro-Design and FDM Technology

In order to evaluate feasibility of different SFF fabrication technologies, initially the study evaluated a desirable open-cellular scaffold design. The process of designing Design 1 was explained and discussed in Chapter 5.1 in which the requirements for a bone tissue engineered scaffold was taken into account such as the minimal pore size and its porosity. As it was mentioned earlier the craniofacial ossification takes place via intramembranous ossification succeeding in capillary ingrowth which requires a minimum 300 μm pore size to encourage capillary penetration within the open-porous macro-structure.

Two different models of fused deposition modelling technology were investigated for their feasibilities to fabricate customised scaffolds (RepRap pro Mendel® and RapMan® 3.1). Overall, the choice of a feasible SFF technology depends highly on material availability, cost, fabrication time and accuracy.

The first issue that was encountered was the limited availability of the feeding materials in form of biocompatible medical-grade polymers with specific thickness required for each type of FDM models. Currently, these models of FDM technology are not being used widely in medical field. Therefore, the manufacturing of the feeding materials in form of filaments with consistent thickness was explored in prior to the fabrication of the prototype. The fabrication of filaments was explored via using Rondol® twin screw extruder which melt the feeding biocompatible granules and extrudes in form of filaments, the thickness of filament depends on the thickness of collection point (10 mm for Rondol®) and the speed of filament collection at the extrusion point. In other words the higher the collection speed is, the lower the filament thickness is as it is pulled faster and stretches out. Due to the extruder's limitations, fabrication of filaments were limited to 3 mm thickness which limits its application to RapMan 3.1® model.

Additional concerned issue is the cost effectiveness of this approach as there is a lot of material wastage involved in filament fabrication which it negate the low material wastage benefit of the SFF technology. As it was mentioned earlier in section 5.2 (Figure 26), 12.5% proportion of total fabricated filament had the appropriate filament thickness to be used for RapMan® FDM model. Also the study carried by Zein *et al.* showed slight change of molecular weight distribution of PCL polymer after filament fabrication, however the semi-crystalline property of the PCL polymer did not change significantly [89]. Another issue that was encountered while fabricating PCL filaments was the contamination of the medical grade PCL materials with foreign materials that may encourage foreign body reaction when implanted *in vivo* even with conventional pre-surgical sterilisation processes as this contamination had penetrated within the filaments and would only release while degrading which would be a major issue in tissue engineering applications. Later in the study, the proposed prototype with 400 μm pore size and 74% porosity was created on AutoCAD programme to evaluate reproducibility capability of tissue engineering scaffolds via RapMan® FDM model. The proposed design was exported in STL file format to the slicing programme Axon 2, which is only compatible with this FDM model and contains the model's limitations within its parameters. Parameters such as minimum height of each layer which is limited to >200 μm and in case of macro-structures with higher precision the slicing program distorts the design as the FDM model. In this proposed design hence application of bone tissue engineering higher accuracy is required and proposed and as we experienced this FDM model was not capable of printing at this accuracy as the beam thickness was designed as 200 μm.

In this chapter feasibility of FDM technology for fabrication of customised scaffolds were investigated, however the initial challenges that was confronted due to the preparation of the materials in prior to the fabrication process shaped this technology to become less appealing. Other concerns involved risks of contamination and software compatibilities. Overall, due to the lack of availability of biocompatible biomaterials, cost effective, reliability and the problems associated with the slicing software, this technique has proved to be a less feasible choice of fabrication technique.

6.1.2 Robocasting SFF Technology

Another fabrication technology which was investigated was robocasting that was explained in details in section 5.3. Robocasting SFF technology is based on direct writing of polymer ink layer-by-layer through an appropriate nozzle, which results in the formation of structure via consolidation transition of liquid to gel as the solvent evaporates following extrusion of ink via nozzle. A micro-structure with 80% porosity, pore size of 400 μm spacing and rod thickness of 150 μm (11 × 11 mm total dimension) was generated as a G-code format and imported into the transitional stage. This technology involves preparation of the ink/ material in form of dissolution in a solvent (dichloromethane and ethanol) and printing in the direction managed by the transitional stage. The amount and type of the solvent plays a crucial role in obtaining a consistent printing pattern as it modifies the ink viscosity and its drying rate. In order to avoid structural failure, it is crucial to allow complete drying of each layer so as to tolerate the weight of the subsequent layers. Therefore, this technology bears long build time and has restricted tolerance toward geometry as its limited due to the translational stage movements. During fabrication of the ink the solvent evaporates and solidifies the skin of printing ink, which provides a subtle three-dimensional construct for underlying structures. Another crucial factor that was found was the printing speed of the ink, as the higher the printing speed is the thinner the printed filament would be and might result in discontinuous printed line. On the other hand if the printing speed is too low, the solvent appeared to evaporate in the printing nozzle and result in congestion.

Apart from the parameters that were mentioned earlier, other crucial factors are such as dispensing pressure, dispensing nozzle size, transitional movement's speed and liquid flow. Even with consideration of using an appropriate nozzle size (0.1 mm), the thickness of the printed lines are not definite as they also depend highly on the dispensing speed and flow. For instance, Russias *et al.* also reported similar challenges in regards to the effect of printing speed on the printed filament thickness [65].

In general, robocasting SFF technology is a relatively complex technique that depends highly on many different parameters such as ink flow, printing speed and pressure, transitional stage speed and drying rate of ink. Some of these parameters such as ink flow and drying rate of the ink also depends highly on secondary parameters such as room temperature and amount/ type of solvents which make this technology relatively complex and less feasible as fabricating medical devices or scaffolds require high accuracy, time efficiency, inexpensive procedure and high reproducibility. In addition to that, it is favourable to avoid using solvents in fabrication process of medical scaffolds, as it may introduce toxic and encourage foreign body reaction.

6.1.3 Digital Micromirror Device Stereolithography

The digital micromirror device stereolithography (DMD stereolithography) was used to reconstruct pattered design from photocurable materials in order to examine its capability to reinvent the input bitmap. In order to achieve high fabrication accuracy within DMD projection stereolithography limitations, it is crucial to harmonise the intensity, the range of curing and length of curing exposure.

The photocurable PEG material was used to investigate pattern recreation of DMD projection stereolithography. As shown in Figure 31, the bitmap input was recreated successfully via DMD stereolithography fabrication technology showing precise structure. Further attempts were made to fabricate photocurable PLA based designs 3 (see Figure 13) and in order to create the 3D structure, a layer-by-layer approach was used by adding 150 μL of the photocurable material before curing the subsequent layers. During this step, calibrations between intensity, curing time and its extent were made to ensure prevention of over curing and hence increase in penetration depth. Similar finding were observed by Gill, where decrease in curing time and exposure resulted in a fragile structure due to curing failure [119]. On the other hand excessive curing were experienced due to over exposure and curing duration, which can result in deterioration of resolution [119]. However, the depth of curing can be improved by using a light absorbing dye (Eosin-Y) as it absorbs the curing radiation which was also demonstrated by Gill and Choi *et al.* [119,120].

Further to the successful fabrication of PEG materials, later fabrication of PLA based structures was demonstrated. Overall, the fabrication of the conventional photocurable material (PEG) was more successful in compare to the photocurable 100% PLA, however the structure of PLA can be further improved by harmonising curing exposure time and intensity of curing.

Later the feasibility of the fabrication technology was investigated for structuring the composite materials as its osteoconductive properties is beneficial to bone regeneration [33,121]. Hydroxyapatite particles (20% w/w) were incorporated with photocurable PLA with addition of Camphorquinone and DCM (to control the viscosity). Each layer was fabricated by pipetting 150 µL of PLA/HA solution on to a piece of Teflon (to avoid attachment), and was cured for 7 minutes before addition of further 150 µL of solution for subsequent layers. As it was shown in Chapter 5.4.1 (Figure 34), the fabricated structure does not exhibit the proposed design hence demonstrated lower feasibility for fabrication of composite materials. This is due to the fact that hydroxyapatite particles scatter the laser, which prevents accurate structuring. The accuracy of the structure can be improved by using a light absorber such as Eosin Y. In addition to that, smaller HA particle size (nano-scale) can result in less light scattering hence improve the structuring.

In this chapter the application of projection stereolithography was demonstrated and its potential as a fabrication technology for tissue engineering was investigated. Overall, this technology shows great promise from fabrication points of view, however there are various factors that still remains a challenge such as the lack of biocompatible material and the risks associated with reactive photoinitiator residues [122]. With this conclusion, the research was therefore concentrated on developing alternative biocompatible materials to be employed with laser-based SFF technology as it demonstrated great advantages.

6.1.4 Stereolithography

6.1.4.1 Non-Biodegradable Acrylate based PolyHIPE

As it was discussed in Chapter 2 (section 2.4.2.1.1) and 5.4.1, laser-based SFF technology is most accurate and advanced fabrication technology as it was also confirmed by Melchels *et al.* [123]. However, the main drawback associated with this technology is the lack of biocompatible and biodegradable polymers. Since stereolithography shows great promise in fabrication of pre-customised design, it was decided to develop alternative biocompatible and biodegradable polymer based materials to use with this technology for fabrication of scaffolds. Some studies argue that introduction of heterogeneous pore sizes induce bone regeneration as it exhibit similar morphological environment to the natural bone. Due to these evidences, polyHIPE materials seemed like a promising route to be investigated as they exhibit inherited porous morphology, which was discussed in details in Chapter 2 (section 2.4.1.3).

It has been reported that polyHIPEs can also be cured via photopolymerisation approach rather than the conventional techniques such as thermal curing [57,112,124,125]. This approach is beneficial due to the flexibility of employing less stable emulsions as well as better time efficiency. Currently, PolyHIPEs (Alvetex, Reinnervate Ltd, UK) have been commercialised for being used as 3D cell culture controls as the 3D environment encourages the development of a more physiologically suitable tissue configuration.

The use of polyHIPE materials in tissue engineering field is still juvenile, however recently studies have been carried to assess fabrication technology to be employed with this material [53,64,126]. Combining polyHIPE materials with laser-based SFF technology offers a range of advantages for the tissue engineering field. In this study the employment of stereolithography permits to readily modify the macro-structure morphology of the scaffold in terms of overall shape, size and pore size independently from the micro-structure of the scaffold. Only lately, studies have shown successful

manufacture of user-defined 3D polyHIPE scaffolds via layer-by-layer stereolithography technique [53,64,126].

The polymer chosen to demonstrate the feasibility of introducing the inherited microporosity inherited by chemical/ physical templating of polyHIPEs and then introducing macroporosity via selective photopolymerisation (stereolithography) was two acrylate monomers EHA/IBOA (at 66-33% ratio) with 80% nominal porosity since previous studies in our group informed successful emulsion formation [53]. However this material is non-biodegradable hence not suitable for tissue engineering applications and its applications are limited to *in vitro* tissue models specially bone tissue.

Prior to the selective photocuring of the polyHIPE materials, the emulsion with continuous phase/ oil phase consists of IBOA, EHA, TMPTA, surfactant and photoinitiator was formed successfully. The bulk photopolymerisation of EHA80 (see Table 13 for formulation) with 80% nominal porosity polyHIPE was tested which exhibited typical PolyHIPE morphology hence proved the successful curing of the emulsion via UV curing (see Figure 36). It is known that the microporosity can be controlled via the speed of stirring during emulsion formation, in this study with speed of 350 rpm the average pore size of 33.3 μm (mean standard deviation: ±10.6 μm) determined via SEM analysis was achieved after applying the statistical correction factor found by Barbetta *et al*. [127]. The diversity of pore diameters were present in Figure 37 (section 5.5.1), and pore size are ranged from 10-70 μm which was in similar range to pore size of EHA80 (5 to 35 μm) and average of 23 μm found by Johnson *et al.* with the same mixing speed (350 rpm) [53]. Overall, polyHIPE pore sizes is dictated by the temperature of the aqueous phase (water) as well as the mixing speed of the emulsion, which can be controlled during emulsion formation stages. The higher the water temperature is, the more destabilise the emulsion is hence larger void diameter [57].

The range of pore sizes for EHA80 in this study and other studies indicates adequate pore size for cell ingrowth and nutrient/ wastage transfer [53]. Therefore, the biocompatibility of this polyHIPE was investigated in prior to introducing readily designed macroporosity. Due to the hydrophobic nature of the monomers

(IBOA and EHA) that is unavoidable for formation of the successful emulsion (discussed in detail in section 2.4.1.3), the surface chemistry of EHA80 must be improved in prior to tissue engineering applications. Consequently, plasma polymerisation surface chemistry modification was performed similar to the approach made by Owen *et al.* to increase the hydrophilicity [64]. Initially MG63 were seeded onto EHA80 disks and allowed to adhere and proliferate for up to 7 days. After this time, the results indicate higher cell viability activity on acrylic acid coated polyHIPE disks in compare to the control at all time points and both SEM and fluorescence microscopy images confirmed the successful cell attachment and penetration up to 50 μm depth (see Figure 41). The observation of cell morphology on plasma-polymerised surface confirmed the hydrophilic improvement of the material with a flattened morphology.

Furthermore, the 3D woodpile scaffold from EHA80 polyHIPE material was fabricated consecutively via single-photon direct laser write. The resultant structure had a total dimension of 0.5 x 0.5 cm with fibre spacing of 1.1 mm and thickness of 425 μm (82% macroporosity), which was accurately reproduced from the proposed design. In this study the fabricated woodpile structure had higher macroporosity and pore size (82% porosity and 425 μm) in compare to the 58% macroporosity with 150 μm pore size reported within the group [64]. Another study within the group also indicated accurate reproducibility of EHA/IBOA (at different nominal porosities and monomer ratios) woodpile structure based polyHIPE material via single-photon laser direct-write [64]. During fabrication of the scaffolds, the viscosity of the emulsion played an important role as the higher the viscosity is, the more non-uniform the laying emulsion is in prior to curing and hence harder to accurately pipette the consequent 50 μL. Furthermore, upon the selective fabrication of EHA80, skin closed surface was formed against cured and non-cured region which was also reported and explained in literature due to the failure of the emulsion at the surface [124]. This may be due the following issues i) scattering of UV light due to the underlying HIPE materials ii) lack of reactive materials in photoinitiated area. The ratio of each monomer in EHA/IBOA based polyHIPE plays a crucial role in its mechanical properties as increase in IBOA content would improve the stiffness and the EHA content would improve the elastic properties [53,128]. Different study within

our group concentrated on exploring the mechanical properties of different ratios of IBOA and EHA woodpile scaffolds fabricated via microstereolithography as well as its feasibility to support osteogenic differentiation of mesenchymal stem cells on plasma and non-treated surfaces [64]. Owen *et al*. discovered that the plasma coated polyHIPE scaffold with the highest IBOA content supported osteogenic differentiation of mesenchymal stem cells stronger in compare to other ratios of the monomers [64].

Further to the 3D woodpile fabrication of EHA80, its potential for the use of 3D bone tissue engineering construct was assessed during 7 days culture period with human osteosarcoma cell line (MG63). The results highlighted that the cells attached and proliferated well on the plasma polymerised woodpile structure on compare to the non-coated, however both types of the scaffold showed lower cell viability in compare to the TCP control. Further confirmation was made by nuclei and actin filament staining using DAPI and FITC-phalloidin. Immunofluorescence micrographs showed cell attachment and ingrowth to macroporous structure as well as the porous polyHIPE fibre. Remarkably, MG63 tumour like spheroids was observed in macro-pores of plasma coated EHA80 woodpile structure (Figure 45A-B), which can be indication of cancerous cell behaviour in accordance to its natural environment hence *in vitro*. Similar MG63 cells behaviour was also reported by a number of studies where the tumour spheroids were formed in *ex vivo* bone models or 3D culture systems [129–131]. In this study, a 2D surface (TCP) was used as a control instead of 3D constructs (Alvetex, Reinnervate Ltd, UK) previously used by other studies [57]. However to take into account the differences between 2D and 3D controls, a separate study was carried to investigate the percentage of cells successfully seeded to the plasma and non-plasma polymerised scaffolds as well as the control (TCP). The study showed that only 36% of total number of attempted seeded cells were successfully seeded on plasma-polymerised scaffolds versus 26% of cells seeded successfully on non-plasma coated scaffolds in compare to the control (TCP) on day 0 as the result, the value for the control (TCP) have been normalised.

The application of conventional fabrication technologies to manufacture porous scaffolds with sufficient level of interconnectivity, regularity and reproducible morphology that is also solvent free is not achievable [132]. This emphasise the novelty of fabricating polyHIPE materials via SFF technology as random interconnected porous micro-structure (10 -70 μm) together with ability to introduce customised macroscopic porous structures with controlled level of porosity and morphology. The accuracy and size of macro-pores are destined by the type of stereolithography used as the projection or scanning stereolithography that is capable of producing structures with up to 1 μm resolution while higher resolutions can be achieved by employing two photon polymerisation (up to 150 nm) [133,134]. Although this technique combines the fabrication of macro and random porosity successfully, the use of EHA80 polyHIPE materials is limited to the 3D *in vitro* applications. Therefore, after successful fabrication of polyHIPE scaffolds, the following studies concentrated on developing biocompatible and biodegradable polyHIPE materials to widen its application to bone tissue engineering.

6.1.5 Developing Degradable PolyHIPEs

Recent studies have reported successful preparation of porous materials via thiol-ene reaction facilitated high internal phase emulsions. Advances in the field of thiol-ene chemistry polyHIPEs have opened opportunities to develop biodegradable thiol-acrylated PCL or methacrylated polyHIPEs. However to begin with, network of thiol-acrylate was investigated to develop understanding for developing thiol-methacrylate based polyHIPEs. As acrylates are more hydrophobic and hence more stable emulsions.

The first polyHIPE network studied was thiol-DPEHA polyHIPE at two different nominal porosity (80% and 85%) mixed via high shear mixing as it has been reported that increasing the mixing speed would reduce the void diameter. Synthesis of thiol-DPEHA has been reported previously by Caldwell *et al.* [57]. The morphology of the photopolymerised polyHIPE showed typical open interconnected macroporous with average pore size of 20 μm for 80% porosity and 15 μm for 85% porosity. Comparing the average pore size (80% porosity at 380 rpm) found by Caldwell *et al.* to the measured pore diameter (80% porosity at 1000 rpm) shows reduced pore diameter from 34.2 μm to 20 μm [57]. However the average MG63 cell diameter is 25 μm which concludes that the lower mixing speed must be used to ensure penetration and attachment of cells within the polyHIPE voids [135]. Further to this study, another successful acrylate based crosslinker (TMPTA) was used to develop thiol-acrylate polyHIPE network with 85% nominal porosity and 34 μm void diameters.

Upon the successful development of thiol-acrylate based polyHIPE (thiol-DPEHA and thiol- TMPTA), the following studies concentrated on substituting the acrylate function groups sourced from TMPTA or DPEHA with more biodegradable triacrylated PCL. Acrylated PCL in compare to non-acrylated PCL is more beneficial due to its hydrophobic properties hence more stable emulsion formation. Successful thiol-triacrylated PCL high internal phase emulsions with three different thiol:acrylate molar ratios (50:50, 60:40, 75:25) and nominal porosities were developed. However, the SEM images of these polyHIPEs did not exhibit the typical

polyHIPE morphology (see Figure 52 and Figure 53) despite the successful emulsion formations, which is observed via thick white paste formation in prior to photocuring. This is due to polyHIPE collision during the drying phases. However due to this the drying phase (air drying) was improved to more rapid drying process such as freeze-drying to minimise the risk of structural collapse. Despite freeze-drying the SEM micrographs showed structural collision and some evidence of the remains' of porous structure (Figure 52 and Figure 53).

It is known that methacrylated functioned monomers are more hydrophobic in compare to the non-methacrylated functions group hence more stable emulsion in w/o emulsions. Tetramethacrylated PCL was synthesised with two different molecular weight (1200 and 20000 g/mol) to be used with thiol in thiol-ene chemistry polyHIPE formation. To the best of our knowledge, this is the first ever attempt on developing methacrylated PCL-thiol polyHIPEs via thiol-ene chemistry. The emulsion formulations were reported in Table 8, to determine the effect of increase in surfactant and temperature (aqueous phase) on tetramethacrylated PCL:thiol emulsions. However despite the vigilant steps regarding the drying stages of the successful emulsions, samples (PT2a-b) did not exhibit typical polyHIPE morphology in SEM micrographs due the aforementioned reasons. A significant characteristic of polyHIPE materials is its level of interconnectivity, it has been reported in literature that increase in surfactant would increase the level of interconnectivity. However large amount of surfactant can cause mechanical destabilisation and may leach hence effecting the biocompatibility of the polyHIPE [136]. In other words, the amount and type of surfactant used affects both rates of coalescence and Ostwald ripening. Overall, it is more desirable to use minimum required amount of surfactant to obtain a stable emulsion but yet achieve desirable amount of interconnectivity to allow efficient waste and nutrient transport. The effect of increasing temperature (aqueous phase) on increasing void diameter has also been reported in literature [57]. Despite other samples, polyHIPE PT2 displayed typical morphology with average void diameter of 19.6 (standard deviation: ± 5.7) (see Figure 54).

To investigate whether or not the molecular weight of PCL affects the biocompatibility of the polyHIPE material, different molecular weight PCL was synthesised (20000 g/mol) and later was functionalised with tetramethacrylated function groups. Similar molar ratios and formulations were used to develop PT1 sample to compare with PT2 polyHIPE samples, however the nominal porosity is different as during emulsion formation we aimed to achieve the highest nominal porosity. Initial biocompatibility studies using MTT cell viability assay showed very high cell viability for all samples (PT1 and PT2) as well as control, hence we questioned the reliability of this assay to be used with thiol-ene chemistry polyHIPE materials. Previous studies by Johnson *et al.* investigated cell viability of PCL triacrylated-thiol polyHIPE via MTT assay, despite that we encountered problems using MTT as a separate study showed that MTT reduced the thiol groups and produces the purple colour hence it is not reliable as this is a colorimetric assay [63]. Finally the PicoGreen® DNA assay was used to evaluate DNA content of the sample. The quantitation assay showed significant difference between PT1 and PT2 samples, PT1 sample showed higher DNA content hence better biocompatibility. Furthermore, on the day 7 the LIVE/ DEAD® staining showed high proportion of live cells on PT1 and the control. Unfortunately due to the auto fluorescence characteristics of the polyHIPE, it was challenging to distinguish live or dead cell from the material (see Figure 64B). Immunostaining on PT1 and PT2 also confirmed higher cell viability on PT1 in compare to PT2 sample. LIVE/ DEAD® analysis and Immunostaining of PT2 samples showed low number of live cells suggesting its lower biocompatibility in compare to PT1 sample.

Although the thiol-tetramethacrylated polyHIPEs showed relatively encouraging biocompatibility, its biodegradation plays a crucial role in its competence for a suitable biomaterial to be used in bone tissue engineering applications. Both materials (PT1 and PT2) showed complete degradation within 57 days of accelerated degradation study proving the complete degradation of both materials and the non-accelerated degradation study exhibited higher degradation rate for PT2 in compare to PT1 sample. It is known that higher molecular weight polymers have lower degradation rate due to the long chain of macromolecules.

6.1.5.1 Incorporation of nHA particles with Trithiol-Tetramethacrylated PCL PolyHIPEs

Bioceramics such as hydroxyapatite have same chemical composition to the natural bone. Therefore, the use of hydroxyapatite in bone tissue engineering scaffolds is ideal. However, hydroxyapatite does not have suitable mechanical properties for bone tissue engineering applications despite its great potential for osteoconductive and osteoinductive properties [72,137,138]. Therefore, the incorporation of hydroxyapatite particles into polymers is considered as a promising route for fabrication of bone tissue engineering scaffolds, as the mechanical properties are tuneable with advantage of osteogenic potentials.

PT1 polyHIPE samples showed the most promising biocompatible properties in compare to the other polyHIPE sample. The use of nano-particles as a pickering polyHIPE was previously reported by Hua *et al.* where inorganic nano-particles were used as stabiliser in oil/water emulsions where the particles were added to the oil phase hence causing the coating of porous structure with nano-particles after removing the emulsion droplets [139]. Later our group reported successful coating of EHA/IBOA based polyHIPEs with HA particles and fabrication of 3D woodpile composite structures [68]. Therefore an attempt was made to incorporate nHA particles into PT1 polyHIPE formulation to potentially enhance cell adhesion, the osteoconductive and osteoinductive potentials together with versatility of polyHIPEs. However, unfortunately the attempt was unsuccessful despite observing emulsion formation for sample 3PT110, which disintegrated during post-curing acetone washing steps. Overall, it is known that there is high success rate of fabricating woodpile structures made from polyHIPEs composite materials (nHA) as it was previously reported within our groups. However, due to the time constraints it was decided to carry this study during future works.

7 CONCLUSION

The literature review demonstrated that additive manufacturing has considerable potential for use in the preparation of custom scaffolds and devices, but relatively little work had been published and the few examples of clinical use typically describe metallic implants. The aim of this research was therefore to investigate a range of advanced manufacturing technologies to determine if they were suitable for these applications (see Chapter 3). During the course of this PhD, it also became apparent that the range of biomaterials available for additive manufacturing of scaffolds for tissue engineering-type approaches was very limited, stimulating additional research into polyHIPEs. The main conclusions of this PhD were:

1. In total, four different SFF fabrication technologies were investigated for manufacturing of user-defined structures. The most promising fabrication approach identified here was stereolithography from the SFF technologies family. This technology offered greater accuracy, and it was therefore selected for further investigation. Limitations were however noted, firstly there are only a limited range of biomaterials that can be fabricated via stereolithography, and this method may not be ideal for fabrication of nHA composite materials due to light scattering.

2. Given the limitations noted above, PolyHIPEs were investigated as a promising material for fabrication of user-defined scaffolds for bone tissue engineering applications. They offer a further potential advantage of inherited hierarchical porosity, which can be further customised via selective photopolymerisation. These materials are emulsion-templated porous polymers and hence fabrication of composite polyHIPE and nHA materials may be possible due to potentially reduced light scattering. In order to investigate feasibility of stereolithography for polyHIPE fabrication, an EHA80 non-degradable polyHIPE was chosen initially. The EHA80 polyHIPE was fabricated successfully by bulk photopolymerisation as well as selective photopolymerisation via stereolithography. The *in vitro* biocompatibility analysis demonstrated promising MG63 cell viability on both disk and woodpile polyHIPE. It was noted that the 3D woodpile structure supported development of

3D spheroids, which was not observed on control or 2D disk surface. Overall, EHA80 polyHIPE materials demonstrated promising foundation for development of 3D *in vitro* models as they replicate the hierarchical structure of the native tissue. Because this material's application to bone tissue engineering is limited to *in vitro* models due to its non-biodegradability, the development of a biodegradable polyHIPE was desirable and therefore investigated.

3. Thiol-ene chemistry was chosen to synthesize the polyHIPE material, as this route offers biodegradability versus the acrylate based polyHIPEs. Methacrylated PCL:thiol based polyHIPE materials with two different molecular weights were developed successfully via photopolymerisation, and the resulting material showed typical macroporous structure. When cultured *in vitro* with MG63, the material with higher molecular weight was biocompatible (PT1) and the polyHIPE scaffolds showed complete degradation following hydrolysis in NaOH. This study demonstrated a new class of highly promising biodegradable materials for fabrication of customised tissue engineering scaffolds, as they are successfully processed via photopolymerisation, using stereolithography (as demonstrated previously for EHA80 polyHIPE).

4. Further modification of the selected polyHIPE material (PT1) with nHA was not achieved, despite successful manufacture of an nHA and initial success with the 2PT110 polyHIPE. This, however, disintegrated during washing steps and it was thought that the structure had poor crosslinking and had formed an unstable emulsion. However, recent work by our group demonstrated successful nHA incorporation to the conventional acrylate based polyHIPEs [68]. We believe that incorporation of nHA in polyHIPE materials with result in nHA particles to cover the surface of pores, hence improving the osteogenic differentiation. Therefore, with further modifications and trials we believe this can be achieved (see Chapter 8 Future Work).

To summarise, the investigation reported in this thesis demonstrated the successful development of biodegradable and biocompatible methacrylated PCL: thiol polyHIPEs that have the potential for use in bone tissue engineering. These materials are particularly useful for fabrication of customised tissue engineering scaffolds as they may be selectively fabricated via stereolithography as demonstrated here using acrylate-based polyHIPEs. It was concluded that this research has great potential to advance the bone tissue engineering field, particularly for applications in craniofacial bone tissue engineering where custom devices or scaffolds offer significant advantages. However, additional studies are required for the development of the clinical product, which is detailed in the following chapter.

8 FUTURE WORK

In order to develop a medical device product based on this work, the following works must be carried:

1. As it was mentioned previously incorporation of nHA particles with polyHIPE materials can benefit the osteogenic differentiation hence its osteoconductivity. Due to time constraints, this work was not investigated thoroughly, therefore further attempts with different synthesising parameters such as the amount of surfactant and nHA concentration must be carried as the other works within group have reported promising results in regards to this [68].

2. Secondly, the chosen material must be fabricated via stereolithography providing a real patient data to investigating the reliability of the process considering real situations hence optimising the process as the time efficiency and accuracy plays a crucial role in achieving a desirable surgical outcome.

3. Further to this, an extensive *in vitro* testing for differentiation of cells must be carried in prior to any animal testing to optimise its biocompatibility. Analysing its biological behaviour with different cell lines as well as exploring surface chemistry modification if needed can initialise this.

4. Furthermore *in vivo* behaviour of these scaffolds must be explored and investigated via animal testing to investigate the behaviour of bone regeneration interacting with the chosen materials.

5. Finally like any other medical device products, the product must be investigated for its safety in clinical use as well as optimising the procedure from pre-clinical planning to the operating room to limit risks associated with employing tissue engineering medical devices.

9 REFERENCES

1. Hutmacher, D. W., Schantz, J. T., Lam, C. X. F., Tan, K. C. & Lim, T. C. State of The Art and Future Directions of Scaffold-Based Bone Engineering from a Biomaterials Perspective. *J. Tissue Eng. Regen. Med.* **1,** 245–60 (2007).

2. Rho, J. Y., Kuhn-Spearing, L. & Zioupos, P. Mechanical Properties and The Hierarchical Structure of Bone. *Med. Eng. Phys.* **20,** 92–102 (1998).

3. McMahon, R. E., Wang, L., Skoracki, R. & Mathur, A. B. Development of Nanomaterials for Bone Repair and Regeneration. *J. Biomed. Mater. Res. B. Appl. Biomater.* **101,** 387–97 (2013).

4. Marieb, E. N. & Hoehn, K. N. *Human Anatomy & Physiology*. (Pearson Education, 2015).

5. Schantz, Jan Thorsten. Machenz, Hans-Gunther. Schilling, Arndt F. Teoh, S. Regenerative Medicine: Implication for Craniofacial Surgery. *J. Craniofac. Surg.* **23,** 530–535 (2012).

6. Norton, M. R. & Gamble, C. Bone Classification: An Objective Scale of Bone Density Using The Computerised Tomography Scan. *Clin. Oral Implants Res.* **12,** 79–84 (2001).

7. Brånemark, P.-I., Zarb, G. A. & Albrektsson, T. *Tissue-Integrated Crostheses: Osseointegration in Clinical Dentistry*. (Quintessence, 1985).

8. Chia, H. N. *et al.* Recent Advances in 3D Printing of Biomaterials. *J. Biol. Eng.* **9,** (2015).

9. Kinoshita, Y. & Hatsuhiko, M. Recent Developments of Functional Scaffolds for Craniomaxillofacial Bone Tissue Engineering Applications. *Sci. World J.* 1–21 (2013).

10. Bell, R. B. & Gregoire, C. Reconstruction of Mandibular Continuity Defects Using Recombinant Human Bone Morphogenetic Protein 2: A Note of Caution in an Atmosphere of Exuberance. *J. Oral Maxillofac. Surg.* **67,** 2673–2678 (2009).

11. Karabouta-Voulgaropoulou, I., Tsodoulos, S. & Pantelas, G. The Use of Autogenous Rib Bone Grafts in Maxillofacial Surgery. *Hell Period Stomat Gnathopathoprosopike Cheir* **4,** 107–13 (1989).

12. Betz, R. R. Limitations of Autograft and Allograft: New Synthetic Solutions. *Orthopedics* **25,** 561–70 (2002).

13. Brierly, G. I., Tredinnick, S., Lynham, A. & Woodruff, M. A. Critical Sized Mandibular Defect Regeneration in Preclinical In Vivo Models. *Curr. Mol. Biol. Reports* **2,** 83–89 (2016).

14. Horch, H.-H. & Pautke, C. Regeneration Instead of Reparation: a Critical Review of The Autogenous Bone Transplant as 'Golden Standard' of Reconstructive Oral Surgery. *Mund Kiefer Gesichtschir* **10,** 213–20 (2006).

15. Kolk, A. *et al.* Current Trends and Future Perspectives of Bone Substitute Materials - from Space Holders to Innovative Biomaterials. *J. cranio-maxillofacial Surg. Off. Publ. Eur. Assoc. Cranio-Maxillofacial Surg.* **40,** 706–18 (2012).

16. Giesenhagen, B. & Schlee, M. Maxgraft Brochure. *Straumann* (2014).

17. Tutogen Brochure. *TUTOGEN Medical GmbH* (2014).

18. Aghaloo, T. L. & Moy, P. K. Which hard tissue augmentation techniques are the most successful in furnishing bony support for implant placement? *The International Journal of Oral & Maxillofacial Implants* 49–73 (2007).

19. Plooij, J. M. *et al.* Digital Three-Dimensional Image Fusion Processes for Planning and Evaluating Orthodontics and Orthognathic Surgery. A Systematic Review. *Int. J. Oral Maxillofac. Surg.* **40,** 341–52 (2011).

20. Angle, E. H. Double Resection of the Lower Maxilla. *Dent. Cosmos; A Mon. Rec. Dent. Sci.* **40,** 635–638 (1898).

21. Babcock, W. The Surgical Treatment of Certain Deformities of Jaw-Associated with Malocclusion of Teeth. *J. Am. Med. Assoc.* **53,** 833–839 (1909).

22. Schwarz, R. New Cephalometric Method and Apparatus and Its Application to Orthodontia. *Int. J. Orthod. Oral Surg. Radiogr.* **11,** 989–1017 (1925).

23. Broadbent, B. H. A New X-ray Technique and Its Application To Orthodontia. *Angle Orthod.* **1,** 45–66 (1931).

24. Matsuo, A., Chiba, H., Takahashi, H., Toyoda, J. & Abukawa, H. Clinical Application of a Custom-Made Bioresorbable Raw Particulate Hydroxyapatite/poly-L-lactide Mesh Tray for Mandibular Reconstruction. *Odontology* **98,** 85–8 (2010).

25. Landes, C. a & Ballon, A. Skeletal Stability in Bimaxillary Orthognathic Surgery: P(L/DL)LA-Resorbable Versus Titanium Osteofixation. *Plast.*

Reconstr. Surg. **118,** 703–22 (2006).

26. Giannoudis, P. V, Dinopoulos, H. & Tsiridis, E. Bone Substitutes: an update. *Injury* **36,** 20–7 (2005).

27. Scheller, E. L. & Krebsbach, P. H. Gene Therapy: Design and Prospects for Craniofacial Regeneration. *J. Dent. Res.* **88,** 585–96 (2009).

28. Liu, Y., Zhu, F., Dong, X. & Peng, W. Digital Design of Scaffold for Mandibular Defect Repair Based on Tissue Engineering. *J. Zhejiang Univ. Sci. B* **12,** 769–79 (2011).

29. Skalak, R. & Fox, C. F. *Tissue Engineering*. (Liss, 1988).

30. Langer, R. Vacanti, J. P. Tissue Engineering. *Science (80-.).* **260,** 920–926 (1993).

31. Yang, S., Leong, K. F., Du, Z. & Chua, C. K. The Design of Scaffolds for Use in Tissue Engineering. Part I. Traditional Factors. *Tissue Eng.* **7,** 679–89 (2001).

32. Hutmacher, D. H. in *Advanced Manufacturing Technology for Medical Applications* (ed. Gibson, I.) 163–189 (Wiley, 2005).

33. Kuznetsov, S. A., Cherman, N. & Robey, P. G. In Vivo Bone Formation by Progeny of Human Embryonic Stem Cells. *Stem Cells Dev.* **20,** 269–87 (2011).

34. Kahle, M. *et al.* Embryonic Stem Cells Induce Ectopic Bone Formation in Rats. *Biomed. Mater. Eng.* **20,** 371–80 (2010).

35. Xu, M. *et al.* Enhanced Critical Size Defect Repair in Rabbit Mandible by Electrospun Gelatin/ β -TCP Composite Nanofibrous Membranes. *J. Nanomater.* 1–9 (2015).

36. Guo, J. *et al.* Restoration of Critical-Size Defects in the Rabbit Mandible Using Porous Nanohydroxyapatite-Polyamide Scaffolds. *Tissue Eng. Part A* **18,** 1239–1252 (2012).

37. Petrovic, V., Zivkovic, P., Petrovic, D. & Stefanovic, V. Craniofacial Bone Tissue Engineering. *Oral Surg. Oral Med. Oral Pathol. Oral Radiol.* **114,** 1–9 (2012).

38. Abukawa, H. *et al.* Reconstruction of Mandibular Defects with Autologous Tissue-Engineered Bone. *J. Oral Maxillofac. Surg.* **62,** 601–6 (2004).

39. Loh, Q. L. & Choong, C. Three-Dimensional Scaffolds for Tissue Engineering: Role of Porosity and Pore Size. *Tissue Eng. Part B. Rev.* **19,** 485–502 (2013).

40. Peltola, S. M., Melchels, F. P. W., Grijpma, D. W. & Kellomäki, M. A Review of Rapid Prototyping Techniques for Tissue Engineering Purposes. *Ann. Med.* **40,** 268–80 (2008).

41. Woodruff, M. A. & Hutmacher, D. W. *The Return of a Forgotten Polymer—Polycaprolactone in the 21st Century. Progress in Polymer Science* **35,** (2010).

42. Supp, D. M. & Boyce, S. T. Engineered Skin Substitutes: Practices and Potentials. *Clin. Dermatol.* **23,** 403–412 (2005).

43. Grayson, W. L. *et al.* Engineering Anatomically Shaped Human Bone Grafts. *Proc. Natl. Acad. Sci. United States Am.* **107,** 3299–3304 (2010).

44. Anderson, J. M. *et al.* Recent Advances in Biomedical Polyurethane Biostability and Biodegradation. *Polym. Int.* **46,** 163–171 (1998).

45. Liu, X. & Ma, P. X. Polymeric scaffolds for bone tissue engineering. *Ann. Biomed. Eng.* **32,** 477–86 (2004).

46. Heljak, M. K., Święszkowski, W., Lam, C. X. F., Hutmacher, D. W. & Kurzydłowski, K. J. Evolutionary Design of Bone Scaffolds with Reference to Material Selection. *Int. j. numer. method. biomed. eng.* **28,** 789–800 (2012).

47. Rubin, J. P. & Yaremchuk, M. J. Complications and Toxicities of Implantable Biomaterials Used in Facial Reconstructive and Aesthetic Surgery: A Comprehensive Review of the Literature. *Plast. Reconstr. Surg.* **100,** 1336–53 (1997).

48. Wu, L. & Ding, J. In Vitro Degradation of Three-Dimensional Porous Poly(D,L-lactide-co-glycolide) Scaffolds for Tissue Engineering. *Biomaterials* **25,** 5821–30 (2004).

49. Schuckert, K.-H., Jopp, S. & Teoh, S.-H. Mandibular Defect Reconstruction Using Three-Dimensional Polycaprolactone Scaffold in Combination with Platelet-Rich Plasma and Recombinant Human Bone Morphogenetic Protein-2: De Novo Synthesis of Bone in a Single Case. *Tissue Eng. Part A* **15,** 493–499 (2009).

50. Price, J. C., Roach, P. & El Haj, A. J. Liquid Crystalline Ordered Collagen Substrates for Applications in Tissue Engineering. *ACS Biomater. Sci. Eng.* **2,** 625–633 (2016).

51. Inzana, J. A. *et al.* 3D printing of composite calcium phosphate and collagen scaffolds for bone regeneration. *Biomaterials* **35,** 4026–4034 (2014).

52. Cameron, N. R. High Internal Phase Emulsion Templating as a Route to Well-Defined Porous Polymers. *Polymer (Guildf).* **46,** 1439–1449 (2005).

53. Johnson, D. W. *et al.* Macrostructuring of Emulsion-Templated Porous Polymers by 3D Laser Patterning. *Adv. Mater.* **25,** 3178–3181 (2013).

54. Barby, D. & Haq, Z. Low Density Porous Cross-Linked Polymeric Materials and Their Preparation and Use as Carriers for Included Liquids. (1985).

55. Busby, W., Cameron, N. R. & Jahoda, C. A. Tissue Engineering Matrixes by Emulsion Templating. *Polym. Int.* **51,** 871–881 (2002).

56. Busby, W., Cameron, N. R. & Jahoda, C. A. B. Emulsion-Derived Foams (PolyHIPEs) Containing Poly(ε-caprolactone) as Matrixes for Tissue Engineering. *Biomacromolecules* **2,** 154–164 (2001).

57. Caldwell, S. *et al.* Degradable Emulsion-Templated Scaffolds for Tissue Engineering from Thiol–ene Photopolymerisation. *Soft Matter* **8,** 10344–10351 (2012).

58. Lovelady, E. *et al.* Preparation of Emulsion-Templated Porous Polymers Using Thiol–ene and Thiol–yne Chemistry. *Polym. Chem.* **2,** 559–562 (2011).

59. Prasath, R. A., Gokmen, M. T., Espeel, P. & Du Prez, F. E. Thiol-ene and Thiol-yne Chemistry in Microfluidics: a Straightforward Method Towards Macroporous and Nonporous Functional Polymer Beads. *Polym. Chem.* **1,** 685–692 (2010).

60. Gong, X., Wen, W. & Sheng, P. Microfluidic Fabrication of Porous Polymer Microspheres: Dual Reactions in Single Droplets. *Langmuir* **25,** 7072–7 (2009).

61. Roach P., A. M. in *Methods in Bioengineering: 3D Tissue Engineering* (ed. Berthiaume F., M. J.) 1–20 (Artech House Publishers, 2010).

62. Sušec, M., Liska, R., Russmüller, G., Kotek, J. & Krajnc, P. Microcellular Open Porous Monoliths for Cell Growth by Thiol-ene Polymerisation of Low-Toxicity Monomers in High Internal Phase Emulsions. *Macromol. Biosci.* **15,** 253–61 (2015).

63. Johnson, D. W. *et al.* Fully Biodegradable and Biocompatible Emulsion Templated Polymer Scaffolds by Thiol-Acrylate Polymerisation of Polycaprolactone Macromonomers. *Polym. Chem.* **6,** 7256–7263 (2015).

64. Owen, R. *et al.* Emulsion Templated Scaffolds with Tunable Mechanical Properties for Bone Tissue Engineering. *J. Mech. Behav. Biomed. Mater.* **54,** 159–172 (2015).

65. Russias, J. *et al.* Fabrication and In Vitro Characterisation of Three-Dimensional Organic/Inorganic Scaffolds by Robocasting. *J. Biomed. Mater.*

Res. A **83,** 434–45 (2007).

66. Russias, J. *et al.* Fabrication and Mechanical Properties of PLA/HA Composites: A Study of In Vitro Degradation. *Mater. Sci. Eng. C, Biomim. Supramol. Syst.* **26,** 1289–1295 (2006).

67. Sukegawa, S. *et al.* Clinical Evaluation of an Unsintered Hydroxyapatite/Poly-L-Lactide Osteoconductive Composite Device for the Internal Fixation of Maxillofacial Fractures. *J. Craniofac. Surg.* **27,** 1391–1397 (2016).

68. Wang, A. *et al.* Photocurable high internal phase emulsions (HIPEs) containing hydroxyapatite for additive manufacture of tissue engineering scaffolds with multi-scale porosity. *Mater. Sci. Eng. C* **67,** 51–58 (2016).

69. Nyberg, E. L. *et al.* 3D-Printing Technologies for Craniofacial Rehabilitation, Reconstruction, and Regeneration. *Ann. Biomed. Eng.* 1–13 (2016). doi:10.1007/s10439-016-1668-5

70. Fernandes, J. S. *et al.* Reinforcement of Poly-l-Lactic Acid Electrospun Membranes with Srontium Borosilicate Bioactive Glasses for Bone Tissue Engineering. *Acta Biomater.* (2016).

71. Santocildes-Romero, M. E. *et al.* Preparation of Composite Electrospun Membranes Containing Strontium-Substituted Bioactive Glasses for Bone Tissue Regeneration. *Macromol. Mater. Eng.* **301,** 972–981 (2016).

72. Kim, S.-S., Sun Park, M., Jeon, O., Yong Choi, C. & Kim, B.-S. Poly(Lactide-co-Glycolide)/Hydroxyapatite Composite Scaffolds for Bone tissue Engineering. *Biomaterials* **27,** 1399–1409 (2006).

73. Wu, F., Wei, J., Liu, C., O'Neill, B. & Ngothai, Y. Fabrication and Properties of Porous Scaffold of Zein/PCL Biocomposite for Bone Tissue Engineering. *Compos. Part B Eng.* **43,** 2192–2197 (2012).

74. Smith, M. H. *et al.* Computed Tomography-Based Tissue-Engineered Scaffolds in Craniomaxillofacial Surgery. *Int. J. Med. Robot.* **3,** 207–216 (2007).

75. Hollister, S. J. Porous Scaffold Design for Tissue Engineering. *Nat. Mater.* **4,** 518–524 (2005).

76. Gibson, I. in *Advanced manufacturing technology for medical applications* (ed. Gibson, I.) 1–14 (Wiley, 2005).

77. Seol, Y.-J., Kang, T.-Y. & Cho, D.-W. Solid Freeform Fabrication Technology Applied to Tissue Engineering with Various Biomaterials. *Soft Matter* **8,** 1730–1735 (2012).

78. Fu, Q., Saiz, E. & Tomsia, A. P. Direct Ink Writing of Highly Porous and Strong Glass Scaffolds for Load-Bearing Bone Defects Repair and Regeneration. *Acta Biomater.* **7,** 3547–3554 (2011).

79. Lee, S.-J. *et al.* Application of Microstereolithography in The Development of Three-Dimensional Cartilage Regeneration Scaffolds. *Biomed. Microdevices* **10,** 233–241 (2008).

80. Nair, L. S. & Laurencin, C. T. Biodegradable Polymers as Biomaterials. *Prog. Polym. Sci.* **32,** 762–798 (2007).

81. Elomaa, L. *et al.* Preparation of poly(ε-caprolactone)-based tissue engineering scaffolds by stereolithography. *Acta Biomater.* **7,** 3850–3856 (2011).

82. Mäkitie, A. A. *et al.* Novel Additive Manufactured Scaffolds for Tissue Engineered Trachea Research. *Acta Otolaryngol.* **133,** 412–417 (2013).

83. Melissinaki, V. *et al.* Direct Laser Writing of 3D Scaffolds for Neural Tissue Engineering Applications. *Biofabrication* **3,** (2011).

84. Popov, V. K. *et al.* Laser Stereolithography and Supercritical Fluid Processing for Custom-Designed Implant Fabrication. *J. Mater. Sci. Mater. Med.* **15,** 123–128 (2004).

85. Leong, K. F., Cheah, C. M. & Chua, C. K. Solid Freeform Fabrication of Three-Dimensional Scaffolds for Engineering Replacement Tissues and Organs. *Biomaterials* **24,** 2363–2378 (2003).

86. Williams, J. M. *et al.* Bone Tissue Engineering Using Polycaprolactone Scaffolds Fabricated via Selective Laser Sintering. *Biomaterials* **26,** 4817–4827 (2005).

87. Scott, S. Apparatus and Method for Creating Three-Dimensional Objects. (1992).

88. Fedorovich, N. E., Alblas, J., Hennink, W. E., Oner, F. C. & Dhert, W. J. a. Organ Printing: The Future of Bone Regeneration? *Trends Biotechnol.* **29,** 601–606 (2011).

89. Zein, I., Hutmacher, D. W., Tan, K. C. & Teoh, S. H. Fused Deposition Modeling of Novel Scaffold Architectures for Tissue Engineering Applications. *Biomaterials* **23,** 1169–1185 (2002).

90. Berner, A. *et al.* Effects of Scaffold architecture on cranial bone healing. *Int. J. Oral Maxillofac. Surg.* **43,** 506–513 (2014).

91. Arafat, M. T. *et al.* Biomimetic Composite Coating on Rapid Prototyped

Scaffolds for Bone Tissue Engineering. *Acta Biomater.* **7,** 809–820 (2011).

92. Sachlos, E. & Czernuszka, J. T. Making Tissue Engineering Scaffolds Work. Review: The Application of Solid Freeform Fabrication Technology to The Production of Tissue Engineering Scaffolds. *Eur. Cell. Mater.* **5,** 29–40 (2003).

93. Michna, S., Wu, W. & Lewis, J. A. Concentrated Hydroxyapatite Inks for Direct-Write Assembly of 3-D Periodic Scaffolds. *Biomaterials* **26,** 5632–5639 (2005).

94. Zhang, R. & Ma, P. X. Synthetic Nano-Fibrillar Extracellular Matrices with Predesigned Macroporous Architectures. *J. Biomed. Mater. Res.* **52,** 430–8 (2000).

95. Chumnanklang, R., Panyathanmaporn, T., Sitthiseripratip, K. & Suwanprateeb, J. 3D Printing of Hydroxyapatite: Effect of Binder Concentration in Pre-Coated Particle on Part Strength. *Mater. Sci. Eng. C* **27,** 914–921 (2007).

96. Warnke, P. H. *et al.* Ceramic Scaffolds Produced by Computer-Assisted 3D Printing and Sintering: Characterisation and Biocompatibility Investigations. *J. Biomed. Mater. Res. B. Appl. Biomater.* **93,** 212–7 (2010).

97. Sherwood, J. K. *et al.* A Three-Dimensional Osteochondral Composite Scaffold for Articular Cartilage Repair. *Biomaterials* **23,** 4739–4751 (2002).

98. Roy, T. D. *et al.* Performance of Degradable Composite Bone Repair Products Made via Three-Dimensional Fabrication Techniques. *J. Biomed. Mater. Res.* **66A,** 283–291 (2003).

99. Leukers, B. *et al.* Hydroxyapatite Scaffolds for Bone Tissue Engineering Made by 3D Printing. *J. Mater. Sci. Mater. Med.* **16,** 1121–1124 (2005).

100. Lee, J.-Y., Choi, B., Wu, B. & Lee, M. Customised Biomimetic Scaffolds Created by Indirect Three-Dimensional Printing for Tissue Engineering. *Biofabrication* **5,** (2013).

101. Butscher, a, Bohner, M., Hofmann, S., Gauckler, L. & Müller, R. Structural and Material Approaches to Bone Tissue Engineering in Powder-Based Three-Dimensional Printing. *Acta Biomater.* **7,** 907–20 (2011).

102. Christensen, A. M. & Humphries, S. M. in *Advanced Manufacturing Technology for Medical Applications* (ed. Gibson, I.) 15 (John Wiley and sons Ltd, 2005).

103. Petrie Aronin, C. E. *et al.* Comparative Effects of Scaffold Pore Size, Pore Volume, and Total Void Volume on Cranial Bone Healing Patterns Using Microsphere-Based Scaffolds. *J. Biomed. Mater. Res. A* **89,** 632–641 (2009).

104. Hollister, S. J. *et al.* Engineering Craniofacial Scaffolds. *Orthod. Craniofac. Res.* **8,** 162–173 (2005).

105. Roosa, S. M. M., Kemppainen, J. M., Moffitt, E. N., Krebsbach, P. H. & Hollister, S. J. The Pore Size of Polycaprolactone Scaffolds has Limited Influence on Bone Regeneration in an In Vivo Model. *J. Biomed. Mater. Res. A* **92,** 359–368 (2010).

106. Bullock, P., Dunaway, D., McGurk, L. & Richards, R. *Integration of image guidance and rapid prototyping technology in craniofacial surgery. International Journal of Oral and Maxillofacial Surgery* **42,** (2013).

107. Zhao, L., Patel, P. K. & Cohen, M. Application of Virtual Surgical Planning with Computer Assisted Design and Manufacturing Technology to Cranio-Maxillofacial Surgery. *Arch. Plast. Surg.* **39,** 309–316 (2012).

108. Carnachan, R. J., Bokhari, M., Przyborski, S. A. & Cameron, N. R. Tailoring the Morphology of Emulsion-Templated Porous Polymers. *Soft Matter* **2,** 608 (2006).

109. Prakash, K. H., Kumar, R., Ooi, C. P., Cheang, P. & Khor, K. A. Apparent Solubility of Hydroxyapatite in Aqueous Medium and its Influence on the Morphology of Nanocrystallites with Precipitation Temperature. *Langmuir* **22,** 11002–11008 (2006).

110. Chantarapanich, N. *et al.* Scaffold Library for Tissue Engineering: a Geometric Evaluation. *Comput. Math. Methods Med.* **2012,** 407805 (2012).

111. Karageorgiou, V. & Kaplan, D. Porosity of 3D Biomaterial Scaffolds and Osteogenesis. *Biomaterials* **26,** 5474–5491 (2005).

112. Kimmins, S. D., Wyman, P. & Cameron, N. R. Photopolymerised Methacrylate-Based Emulsion-Templated Porous Polymers. *React. Funct. Polym.* **72,** 947–954 (2012).

113. Foudazi, R., Gokun, P., Feke, D. L., Rowan, S. J. & Manas-Zloczower, I. Chemorheology of Poly(High Internal Phase Emulsions). *Macromolecules* **46,** 5393–5396 (2013).

114. Gitli, T. & Silverstein, M. S. Bicontinuous Hydrogel–Hydrophobic Polymer Systems Through Emulsion Templated Simultaneous Polymerisations. *Soft Matter* **4,** 2475 (2008).

115. Bokhari, M., Carnachan, R. J., Przyborski, S. A. & Cameron, N. R. Emulsion-Templated Porous Polymers as Scaffolds for Three Dimension1. Bokhari, M., Carnachan, R. J., Przyborski, S. A. & Cameron, N. R. Emulsion-Templated Porous Polymers as Scaffolds for Three Dimensional Cell Culture: Effect of

Synthesis Parameters on S. *J. Mater. Chem.* **17,** 4088–4094 (2007).

116. Barbetta, A. & Cameron, N. R. Morphology and Surface Area of Emulsion-Derived (PolyHIPE) Solid Foams Prepared with Oil-Phase Soluble Porogenic Solvents: Span 80 as Surfactant. *Macromolecules* **37,** 3188–3201 (2004).

117. Malayeri, A. *et al.* Osteosarcoma Growth on Trabecular Bone Mimicking Structures Manufactured via Laser Direct Write. *Int. J. Bioprinting* **2,** (2016).

118. Akay, G., Birch, M. A. & Bokhari, M. A. Microcellular PolyHIPE Polymer Supports Osteoblast Growth and Bone Formation In Vitro. *Biomaterials* **25,** 3991–4000 (2004).

119. Gill, A. A. Applications of Microstereolithography in Tissue Engineering. (University of Sheffield, 2012).

120. Choi, J.-W., Wicker, R. B., Cho, S.-H., Ha, C.-S. & Lee, S.-H. Cure depth control for complex 3D microstructure fabrication in dynamic mask projection microstereolithography. *Rapid Prototyp. J.* **15,** 59–70 (2009).

121. Puwanun, S. Developing a Tissue Engineering Strategy for Cleft Palate Repair. (The University of Sheffield, 2014).

122. Atala, A. & Yoo, J. J. *Essentials of 3D Biofabrication and Translation*. (Elsevier Inc., 2015).

123. Melchels, F. P. W., Feijen, J. & Grijpma, D. W. A Review on Stereolithography and its Applications in Biomedical Engineering. *Biomaterials* **31,** 6121–6130 (2010).

124. Kimmins, S. D. & Cameron, N. R. Functional Porous Polymers by Emulsion Templating: Recent Advances. *Adv. Funct. Mater.* **21,** 211–225 (2011).

125. Pierre, S. J. *et al.* Covalent Enzyme Immobilisation onto Photopolymerised Highly Porous Monoliths. *Adv. Mater.* **18,** 1822–1826 (2006).

126. Sušec, M., Ligon, S. C., Stampfl, J., Liska, R. & Krajnc, P. Hierarchically Porous Materials from Layer-by-Layer Photopolymerisation of High Internal Phase Emulsions. *Macromol. Rapid Commun.* **34,** 938–43 (2013).

127. Barbetta, A. & Cameron, N. R. Morphology and Surface Area of Emulsion-Derived (PolyHIPE) Solid Foams Prepared with Oil-Phase Soluble Porogenic Solvents: Span 80 as Surfactant. *Macromolecules* **37,** 3188–3201 (2004).

128. Jerenec, S. *et al.* Glycidyl Methacrylate and Ethylhexyl Acrylate Based PolyHIPE Monoliths: Morphological, Mechanical and Chromatographic Properties. *React. Funct. Polym.* **78,** 32–37 (2014).

129. Santini, M. T. *et al.* MG-63 Human Osteosarcoma Cells Grown in Monolayer and as Three-Dimensional Tumor Spheroids Present a Different Metabolic Profile: a 1H NMR Study. *FEBS Lett.* **557,** 148–154 (2004).

130. Trojani, C. *et al.* Three-Dimensional Culture and Differentiation of Human Osteogenic Cells in an Injectable Hydroxypropylmethylcellulose Hydrogel. *Biomaterials* **26,** 5509–5517 (2005).

131. Kale, S. *et al.* Three-Dimensional Cellular Development is Essential for Ex Vivo Formation of Human Bone. *Nat. Biotechnol.* **18,** 954–958 (2000).

132. Hutmacher, D. W. Scaffold Design and Fabrication Technologies for Engineering Tissues-State of the Art and Future Perspectives. *J. Biomater. Sci. Polym. Ed.* **12,** 107–124 (2001).

133. Zhang, A. P. *et al.* Rapid Fabrication of Complex 3D Extracellular Microenvironments by Dynamic Optical Projection Stereolithography. *Adv. Mater.* **24,** 4266–4270 (2012).

134. Kawata, S., Sun, H.-B., Tanaka, T. & Takada, K. Finer Features for Functional Microdevices. *Nature* **412,** 697–698 (2001).

135. Docheva, D. *et al.* Researching into the Cellular Shape, Volume and Elasticity of Mesenchymal Stem Cells, Osteoblasts and Osteosarcoma Cells by Atomic Force Microscopy. *J. Cell. Mol. Med.* **12,** 537–552 (2008).

136. Huš, S. & Krajnc, P. PolyHIPEs from Methyl Methacrylate: Hierarchically Structured Microcellular Polymers with Exceptional Mechanical Properties. *Polymer (Guildf).* **55,** 4420–4424 (2014).

137. Kim, H.-W., Kim, H.-E. & Salih, V. Stimulation of Osteoblast Responses to Biomimetic Nanocomposites of Gelatin-Hydroxyapatite for Tissue Engineering Scaffolds. *Biomaterials* **26,** 5221–5230 (2005).

138. Akay, G., Birch, M. A. & Bokhari, M. A. Microcellular polyHIPE polymer supports osteoblast growth and bone formation in vitro. *Biomaterials* **25,** 3991–4000 (2004).

139. Hua, Y. *et al.* Switchable Release and Recovery of Nanoparticles via a Pickering-Emulsion-Templated Porous Carrier. *J. Mater. Chem. A* **1,** 13970–13977 (2013).

10 APPENDIX

Cirrus GPC Sample Injection Report

Generated by: Cirrus 06 February 2015 15:42
Workbook: C:\Cirrus Workbooks\DRI MixedC Chloroform\DRI MixedC Chloroform.plw

Sample Details
Sample Name: AM01
Acquired: 06/02/2015 14:51:25 By Analyst: Cirrus
Batch Name: AM06022015
Filename: C:\Cirrus Workbooks\DRI MixedC Chloroform\am06022015-0002.cgrm
Concentration: 0.10 mg/ml K of Sample: 14.1000
Injection Volume: 100.0 ul Alpha of Sample: 0.7000
LIMS ID: Bottle ID:

Workbook Details
Eluent: Chloroform Flow Rate: 1.00 ml/min
Column Set: PLgel 5um Mixed C Column Set Length: 650 mm
Detector: Differential Refractive Index Temperature: 40

Analysis Using Method: Analyse
Comments: Set for Manual Analysis. Peak Detection parameters may need fine tuning

Results File: C:\Cirrus Workbooks\DRI MixedC Chloroform\am06022015-0002.rst

Calibration Used: 03/07/2014 16:51:52
Calibration Type: Narrow Standard Curve Fit Used: 3
Calibration Curve: y = 19.230454 - 2.213387x^1 + 0.122350x^2 - 0.002836x^3

High Limit MW RT: 10.68 mins Low Limit MW RT: 17.50 mins
High Limit MW: 1231807 Low Limit MW: 585
K: 14.1000 FRM Name: Toluene
Alpha: 0.7000 Flow Marker RT: 19.97 mins
FRCF: 1.0050

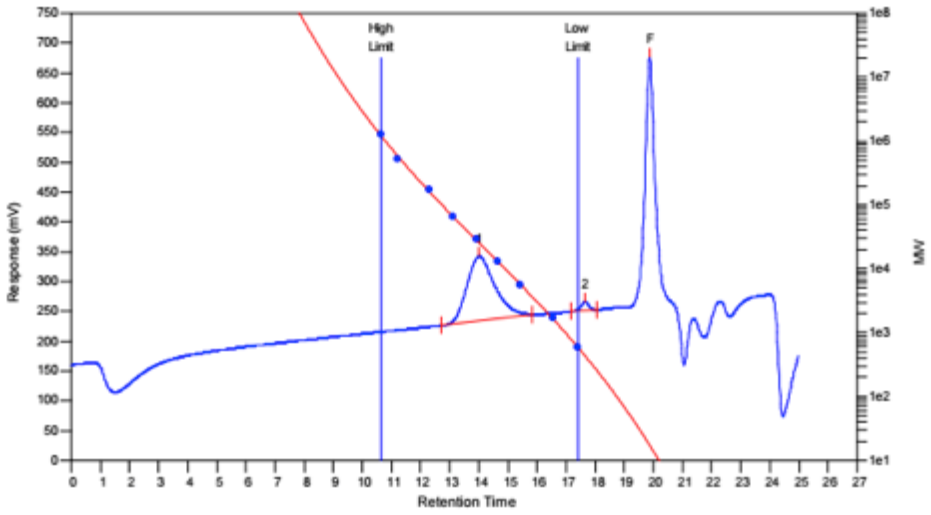

Sample Injection Report

MW Averages

Peak No	Mp	Mn	Mw	Mz	Mz+1	Mv	PD
1	25259	19808	25178	30559	35818	24391	1.2711
2	434	437	450	463	477	448	1.02975
3	17	16	17	19	20	17	1.0625

Processed Peaks

Peak No	Start RT (mins)	Max RT (mins)	End RT (mins)	Pk Height (mV)	Area (mV.secs)
1	12.70	14.02	15.82	108.467	7170.14
2	17.17	17.65	18.05	14.6308	269.441
3	19.20	19.87	20.37	403.699	9213.46

Peak Detection

Peak No	Type	St Detect Code	End Detect Code	Is St Mod	Is Max Mod	Is End Mod
1	0	1	1	No	No	No
2	0	1	1	No	No	No
3	0	1	1	No	No	No

Baseline Detection

No	Start RT (mins)	End RT (mins)	Start Height	End Height	Is St Mod	Is End Mod
1	12.70	15.82	226.20	245.10	No	No
2	17.17	18.05	249.70	253.01	No	No
3	19.20	20.37	257.54	283.58	No	No